The Abdus Salam
International Centre
for Theoretical Physics

United Nations
Educational, Scientific and
Cultural Organization

IAEA
International Atomic Energy Agency

2512-4

Fundamentals of Ocean Climate Modelling at Global and Regional Scales (Hyderabad - India)

5 - 14 August 2013

Physical processes that impact the evolution of global mean sea level in ocean climate models

GRIFFIES Stephen
Princeton University
U.S. Department of Commerce N.O.A.A.
Geophysical Fluid Dynamics Laboratory, 201 Forrestal Road
Forrestal Campus, P.O. Box 308, 08542-6649 Princeton NJ
U.S.A.

Ocean Modelling 51 (2012) 37–72

Contents lists available at SciVerse ScienceDirect

Ocean Modelling

journal homepage: www.elsevier.com/locate/ocemod

Physical processes that impact the evolution of global mean sea level in ocean climate models

Stephen M. Griffies [a,*], Richard J. Greatbatch [b]

[a] NOAA Geophysical Fluid Dynamics Laboratory, Princeton, USA
[b] GEOMAR – Helmholtz-Zentrum für Ozeanforschung Kiel, Kiel, Germany

ARTICLE INFO

Article history:
Received 1 July 2011
Received in revised form 5 March 2012
Accepted 6 April 2012
Available online 25 April 2012

Keywords:
Global mean sea level
Non-Boussinesq steric effect
Physical ocean processes
Ocean climate models
Budget for global mean sea level

ABSTRACT

This paper develops an analysis framework to identify how physical processes, as represented in ocean climate models, impact the evolution of global mean sea level. The formulation utilizes the coarse grained equations appropriate for an ocean model, and starts from the vertically integrated mass conservation equation in its Lagrangian form. Global integration of this kinematic equation results in an evolution equation for global mean sea level that depends on two physical processes: boundary fluxes of mass and the non-Boussinesq steric effect. The non-Boussinesq steric effect itself contains contributions from boundary fluxes of buoyancy; interior buoyancy changes associated with parameterized subgrid scale processes; and motion across pressure surfaces. The non-Boussinesq steric effect can be diagnosed in either volume conserving Boussinesq or mass conserving non-Boussinesq ocean circulation models, with differences found to be negligible.

We find that surface heating is the dominant term affecting sea level arising from buoyancy fluxes, contributing to a net positive tendency to global mean sea level, largely due to low latitude heating and because the thermal expansion coefficient is much larger in the tropics than high latitudes. Subgrid scale effects from parameterized quasi-Stokes transport, vertical diffusion, cabbeling, and thermobaricity are also found to be significant, each resulting in a reduction of global mean sea level. Sea level rise through low latitude heating is largely compensated by a sea level drop from poleward eddy heat transport and ocean mixing. Spatial variations in the thermal expansion coefficient provide an essential modulation of how physical effects from mixing and eddy induced advective transport impact global mean sea level.

Published by Elsevier Ltd.

1. Introduction

Dynamic sea level refers to the sea level associated with the fluid dynamic state of the ocean. Ocean currents, density, and boundary fluxes of mass and buoyancy impact the dynamic sea level. Sea level also depends on geophysical factors such as the earth's gravity, deformation, and rotation, with these additional factors influencing the *static equilibrium sea level* (i.e., the geoid) (e.g.,Mitrovica et al., 2001; Kopp et al., 2010). Further factors include tectonic uplift, thermal subsidence, and the morphology of shorelines (e.g., Milne et al., 2009). There is presently no global numerical model that incorporates all of these effects impacting sea level. In particular, climate models presently provide an estimate just of dynamic sea level, with estimates subject to varying levels of approximation based on ocean model formulation.

1.1. Focus of this paper

The following question forms the focus of this paper:

HOW DO PHYSICAL OCEAN PROCESSES, INCLUDING BOUNDARY FLUXES, REGIONALLY IMPACT GLOBAL MEAN DYNAMIC SEA LEVEL IN OCEAN CLIMATE MODELS?

For example, where geographically do surface heat fluxes most impact global mean sea level? How do parameterizations of dianeutral mixing, neutral mixing (and associated effects from cabbeling and thermobaricity), and parameterized quasi-Stokes transport impact global mean sea level? Absent the impacts from surface water fluxes, what is required physically to realize a balanced global mean sea level budget?

To help answer these, and other, questions, we formulate an analysis framework to understand and to quantify how physical processes, including boundary fluxes, impact on the evolution of global mean sea level. We focus on the averaged or coarse grained equations appropriate for an ocean climate model, with averaging considered at least over the microscale, and typically over the mesoscale as well (see Appendix A). A similar analysis framework

* Corresponding author. Tel.: +1 609 452 6672; fax: +1 609 987 5063
E-mail addresses: Stephen.Griffies@noaa.gov (S.M. Griffies), rgreatbatch@geomar.de (R.J. Greatbatch).

1463-5003/$ - see front matter Published by Elsevier Ltd.
http://dx.doi.org/10.1016/j.ocemod.2012.04.003

can be developed from the perspective of the unaveraged ocean equations, in which mixing arises solely from molecular diffusion. However, the unaveraged perspective is beyond the scope of the present study, as it does not directly serve our aim to interpret global mean sea level evolution in ocean climate models.

Throughout our formulation, we make the following three assumptions:

- the static equilibrium sea level (i.e., geoid and ocean bottom) is constant in time;
- the horizontal ocean area is constant in time;
- the gravitational acceleration is constant in space and time.

These assumptions must be removed for more realistic analyses, such as occur when considering data from satellite altimeters or when including changes to the geoid and crustal rebound associated with massive melts of land ice (Kopp et al., 2010). However, these assumptions are sufficient for our focus on how physical ocean processes and boundary fluxes impact global sea level in state-of-science global ocean climate models.

Our analysis framework is developed by vertically integrating the mass continuity equation. The resulting kinematic equation partitions sea level evolution into contributions from surface mass fluxes, the convergence of vertically integrated currents, and the non-Boussinesq steric effect (defined below). Beyond the assumptions noted above, the kinematic sea level equation requires no ocean dynamical assumptions. This situation is both a strength and weakness of the kinematic method. It is a weakness since the kinematic sea level equation *by itself* is insufficient for understanding the forces impacting sea level patterns, with such understanding arrived at through analyses of the momentum equation (e.g., Lowe and Gregory, 2006). It is a strength since a kinematic approach offers a means to mechanistically understand and quantify how physical processes impact global mean sea level, independent of dynamical assumptions.

1.2. Three types of steric effect

Our focus on global mean sea level complements those studies aimed at understanding how sea level patterns are impacted by the movement of mass and density. This question of regional sea level is often addressed kinematically through partitioning sea level evolution into two processes: those associated with mass changes and those associated with the *local steric* effect. Gill and Niiler (1973) proposed this approach for hydrostatic fluids, and its use is exemplified in the modelling papers by Landerer et al. (2007), Yin et al. (2009), and Yin et al. (2010). As seen in Section 2.2, Version II of the kinematic sea level equation is a slightly different form of the (Gill and Niiler, 1973) partitioning, derived solely on the basis of mass conservation. However, the focus in the present paper is on the complementary question concerning regional patterns impacting global mean sea level. For this purpose, we focus on Version I of the kinematic sea level equation derived in Section 2.1.

Throughout this paper, it is useful to note the different contexts by which the term *steric effect* is used. All contexts refer to changes in sea level associated with temporal changes in density.

- *Local steric effect*: The local steric effect contributes to sea level changes through changes in the depth integrated local time tendency of *in situ* density. Gill and Niiler (1973) were the first to suggest partitioning sea level evolution into a mass tendency and local steric tendency, with their approach following from the hydrostatic balance (see Section 2.2). Additionally, the local steric effect has a generalization to non-hydrostatic fluids through its appearance in Version II of the sea level equation derived on the basis of mass conservation alone (Eq. (9) derived in Section 2.2).
- *Non-Boussinesq steric effect*: The *non-Boussinesq* steric effect arises from the vertical integral of the material or Lagrangian form of the mass conservation equation. It contributes to global mean sea level changes through changes in the depth integrated material time derivative of *in situ* density. There are numerous terms that contribute to the non-Boussinesq steric effect, with a discussion of these terms forming the focus of this paper.
- *Global steric effect*: The *global* steric effect arises from the time tendency of the global mean *in situ* density. It accounts for an expansion of the global ocean volume when the global mean density decreases, and vice versa when density increases. The global steric effect can be readily diagnosed from climate model output, as one merely needs to compute the global mean density. Hence, it has been the *de facto* means for diagnosing global mean sea level in volume conserving Boussinesq ocean model simulations (see Appendix D). As shown in Section 4.5, the global steric effect corresponds to, but is not the same as, the global mean of the non-Boussinesq steric effect.

Mass conserving non-Boussinesq ocean simulations incorporate each of these three steric effects into the model kinematics, which in turn impacts directly on the model sea level. However, as first explored by Greatbatch (1994), for large-scale ocean climate modelling, there is little practical importance whether one chooses to employ a volume conserving or a mass conserving ocean model. The reason is that the non-Boussinesq steric effect and global steric effect, both of which are missing from the prognostic sea level computed in volume conserving models, do not greatly impact low frequency regional patterns of sea level. Furthermore, a time dependent global adjustment is sufficient to "correct" the sea level in a volume conserving Boussinesq model so that is corresponds to the global mean sea level in a mass conserving non-Boussinesq model. Details of this adjustment are given in Appendix D. Furthermore, various forms of the non-Boussinesq steric effects identified in this paper can be diagnosed in either volume conserving or mass conserving simulations. Tests with the global model used in this paper (see Appendix B) reveal few distinctions between volume conserving Boussinesq and mass conserving non-Boussinesq simulations for these purposes.

1.3. Contents of this paper

Section 2 begins the formulation of the analysis framework by deriving two slightly different forms for the kinematic sea level equation, both starting from mass conservation. Section 3 unpacks the physics contained within the non-Boussinesq steric effect that appears in Version I of the kinematic sea level equation, including motion across pressure surfaces and boundary fluxes of heat and salt. Section 4 then derives evolution equations for global mean sea level. Sections 5–7 focus on how three canonical physical processes, as parameterized in ocean climate models, impact on the non-Boussinesq steric effect, and thus impact on global mean sea level: vertical diffusion, neutral diffusion, and eddy induced or quasi-Stokes advection. Section 8 closes the main body of the paper with summary and discussion. In particular, this section contains a synthesis of the global sea level budget from the ocean–ice simulation.

Five appendices support the main development by presenting various details. Appendix A summarizes salient points concerning

mass conservation in both an unaveraged and averaged description of the ocean fluid. We also consider the kinematic boundary conditions and introduce the quasi-Stokes transport as well as seawater thermodynamics. Results from Appendix A are referred to repeatedly in the main portion of the text, as they are fundamental to development and interpretation of the sea level equations. Appendix B summarizes the global model used to illustrate how certain processes affect sea level. Appendix C summarizes the inverse barometer response of sea level to an applied mass loading from the atmosphere or sea ice. Appendix D details the diagnostic corrections made to the sea level computed from volume conserving Boussinesq models to account for the missing non-Boussinesq and global steric effects, thus allowing volume conserving models to have a more accurate diagnostic sea level and bottom pressure. Appendix E presents mathematical details of how cabbeling and thermobaricity, as derived from mesoscale averaged equations, contribute to the non-Boussinesq steric effect.

2. Kinematic equations for sea level evolution

We formulate here the kinematic evolution equations for sea level, again under the assumptions of (A) fixed geoid and ocean bottom, (B) constant horizontal area of the ocean, (C) space–time independent gravitational acceleration. All mathematical symbols refer to the averaged quantities appropriate for an ocean model, with salient points of averaging summarized in Appendix A.

2.1. Kinematic sea level equation: Version I

Integrating the material or Lagrangian form of the mass continuity Eq. (181) over the depth of the ocean, using the kinematic boundary conditions (152) and (161) (see Appendix A for these equations), and Leibniz's rule for moving the derivative operator across an integral, yields Version I of the *kinematic sea level equation*

$$\frac{\partial \eta}{\partial t} = \frac{Q_m}{\rho(\eta)} - \nabla \cdot \mathbf{U} - \int_{-H}^{\eta} \frac{1}{\rho} \frac{d\rho}{dt} dz \tag{1}$$

with

$$\mathbf{U} = \int_{-H}^{\eta} \mathbf{u}\, dz, \tag{2}$$

the vertically integrated horizontal velocity, and

$$\rho(\eta) = \rho(x, y, z = \eta(x, y, t), t), \tag{3}$$

the ocean density at the free surface. Eq. (1) partitions the evolution of sea level into the following three physical processes, with Fig. 1 providing a schematic.

1. *Boundary mass fluxes*: The transport of mass across the ocean surface is converted to a volume flux through multiplication by the specific volume $\rho(\eta)^{-1}$ at the ocean surface. Transport of mass across the ocean surface in regions of relatively large surface specific volume $\rho(\eta)^{-1}$ (e.g., warm and freshwater) leads to greater sea level tendencies than the transport in regions of small surface specific volume (e.g., cold and salty regions).
2. *Dynamic*: The convergence of vertically integrated horizontal currents onto a fluid column redistributes ocean volume, and as such it imparts a sea level tendency. To help understand how flow convergence arises, decompose the vertically integrated velocity as $\mathbf{U} = d\bar{\mathbf{u}}^z$, where $d = H + \eta$ is the thickness of the fluid column, and $\bar{\mathbf{u}}^z$ is the vertically averaged horizontal velocity.[1] Converging flow in a flat bottom ocean is equivalent to convergence of the vertically averaged flow, so that $-\nabla \cdot \mathbf{U} = -d\nabla \cdot \bar{\mathbf{u}}^z > 0$. Flow convergence occurs also when the vertically averaged flow slows down when approaching a region in the fluid, or flow convergence occurs when vertically constant flow impinges on a shoaling bottom, so that $-\nabla \cdot \mathbf{U} = -\nabla(d) \cdot \bar{\mathbf{u}}^z > 0$. Globally integrating the sea level Eq. (1) eliminates the effects of ocean volume transport since $-\nabla \cdot \mathbf{U}$ integrates to zero. Hence, in this formulation of the sea level equation, ocean currents redistribute ocean volume, yet do not directly impact global mean sea level. This property of the sea level equation (1) is especially convenient for studying the evolution of global mean sea level.
3. *Non-Boussinesq* steric: Material time changes of the *in situ* density integrated over a column of seawater lead to the expansion or contraction of the fluid column. Material changes in density arise from buoyancy fluxes at the ocean boundaries, convergence of buoyancy fluxes in the ocean interior, and processes associated with the equilibrium thermodynamics of the ocean as embodied by the equation of state (Eq. (184)).

[1] This discussion is adopted from Fig. 3.7 of Kämpf (2009).

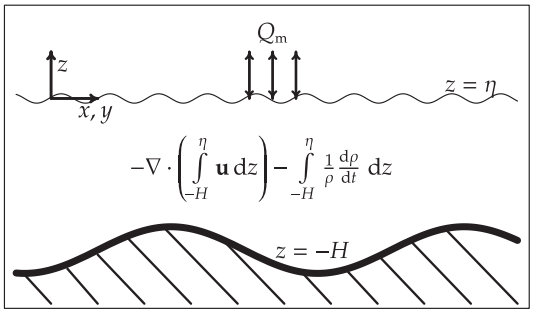

Fig. 1. Schematic ocean basin illustrating the ocean fluid dynamic and boundary processes that impact dynamic sea level according to the kinematic sea level equation (1). The surface mass flux Q_m arises from exchange of mass across the permeable sea surface $z = \eta(x, y, t)$ via precipitation, evaporation, runoff, and melt. This mass flux is converted to a volume flux through dividing by the surface ocean density $\rho(z = \eta)$. The non-Boussinesq steric effect, $-\int_{-H}^{\eta} \rho^{-1} (d\rho/dt) dz$, arises from material time changes in the *in situ* density, as integrated from the impermeable bottom at $z = -H(x, y)$ to the ocean surface. Both the surface mass flux and non-Boussinesq steric effect can change the net global mean sea level. The third process impacting sea level arises from the convergence of depth integrated currents, $-\nabla \cdot \mathbf{U}$, which redistributes volume without impacting global mean sea level.

2.2. Kinematic sea level equation: Version II

The second version of the kinematic sea level equation is formulated from the mass budget for a fluid column (Eq. (164) in Appendix A)

$$\partial_t \left(\int_{-H}^{\eta} \rho\, dz \right) = Q_m - \nabla \cdot \left(\int_{-H}^{\eta} \rho \mathbf{u}\, dz \right). \tag{4}$$

The left hand side of this equation expresses the time tendency for the mass per unit horizontal area in the column, with this tendency affected by mass transported across the ocean surface, and mass transported into the column by ocean currents. This mass budget can be written in a modified form by introducing the column averaged density

$$\bar{\rho}^z = \frac{1}{H + \eta} \left(\int_{-H}^{\eta} \rho\, dz \right), \tag{5}$$

and the column integrated horizontal mass transport

$$\mathbf{U}^{\rho} = \int_{-H}^{\eta} \rho \mathbf{u}\, dz, \tag{6}$$

in which case the mass budget becomes

$$\partial_t [(H + \eta) \bar{\rho}^z] = Q_m - \nabla \cdot \mathbf{U}^{\rho}. \tag{7}$$

Expanding the time derivative renders Version II of the sea level equation

$$\frac{\partial \eta}{\partial t} = \frac{Q_m - \nabla \cdot \mathbf{U}^\rho - (H+\eta)\partial \bar{\rho}^z/\partial t}{\bar{\rho}^z}. \tag{8}$$

Eq. (8) is mathematically equivalent to Version I of the sea level Eq. (1). However, there is a difference in emphasis that provides some complement to Version I. We thus find it useful to again discuss the three physical processes that impact sea level as revealed by Eq. (8).

1. *Boundary fluxes*: As for Version I, the boundary contribution arises from mass fluxes crossing the ocean boundaries. However, for Version II, the conversion of mass to volume flux occurs through the column mean density, $\bar{\rho}^z$, rather than the surface density $\rho(\eta)$.
2. *Dynamic*: Version I considers the dynamic effects from the transport of volume by the vertically integrated currents. Version II considers the transport of mass by the vertically integrated currents, which is then converted to a sea level tendency through dividing by the vertically averaged density. Since the mass flux must be converted to a volume flux through division by the spatially dependent depth mean density, $\bar{\rho}^z$, a global area integral of the sea level Eq. (8) does not identically remove the effects on sea level from mass transport by ocean currents. Instead, the effects are only approximately removed, to the extent that the vertical mean density is horizontally constant.
3. *Local steric*: Version II of the sea level Eq. (8) exposes an Eulerian time derivative acting on the vertically averaged density, rather than the vertical integral of the material time derivative present in Version I. In so doing, we see how sea level is directly affected through the local changes to the column mean density. As the column mean density decreases, the column expands and this in turn contributes a positive tendency to sea level evolution. We refer to this steric contribution as the *local steric effect* to contrast it with the non-Boussinesq steric term introduced in Section 2.1.

Although we focus in the remainder of this paper on Version I of the kinematic sea level Eq. (1), it is useful to here make a connection between the kinematic sea level Eq. (8) and the analogous sea level equation proposed by Gill and Niiler (1973) for a hydrostatic fluid. First, note that the sea level evolution in Eq. (8) can be partitioned into a contribution from mass changes and a contribution from local steric changes

$$\frac{\partial \eta}{\partial t} = \underbrace{\frac{Q_m - \nabla \cdot \mathbf{U}^\rho}{\bar{\rho}^z}}_{\text{mass}} - \underbrace{\frac{(H+\eta)\partial \bar{\rho}^z/\partial t}{\bar{\rho}^z}}_{\text{local steric}}. \tag{9}$$

A similar decomposition was promoted by Gill and Niiler (1973) for a hydrostatic fluid. Notably, Eq. (9) follows solely from the kinematics of a mass conserving fluid and so holds for both hydrostatic and non-hydrostatic fluids.

To further make the connection to Gill and Niiler (1973), introduce the hydrostatic approximation, in which the difference between hydrostatic pressure at the ocean bottom, p_b, and pressure applied to the ocean surface, p_a, is given by

$$p_b - p_a = g \int_{-H}^{\eta} \rho \, dz, \tag{10}$$

where g is the gravitational acceleration. Use of the column integrated mass balance (4) leads to the kinematic evolution equation

$$g^{-1} \partial_t (p_b - p_a) = Q_m - \nabla \cdot \mathbf{U}^\rho. \tag{11}$$

This equation says that mass per area within a column of seawater changes according to the surface mass flux and the convergence of the vertically integrated mass transport. Substituting this result into the sea level equation (8) leads to

$$\frac{\partial \eta}{\partial t} = \underbrace{\frac{\partial_t (p_b - p_a)}{g \bar{\rho}^z}}_{\text{mass}} - \underbrace{\frac{(H+\eta)\partial \bar{\rho}^z/\partial t}{\bar{\rho}^z}}_{\text{local steric}}. \tag{12}$$

As for the expression (9), we see that sea level experiences a positive tendency in those regions where mass locally increases and where the vertically averaged density decreases. As noted by Gill and Niiler (1973), and further supported by model analyses from Landerer et al. (2007), Yin et al. (2009), and Yin et al. (2010), there are many useful physical insights concerning regional sea level garnered when performing this kinematic partitioning of sea level evolution into mass and local steric changes, with local steric effects often further partitioned into thermal (thermosteric) and haline (halosteric) effects. The particular form of this partition as proposed by Gill and Niiler (1973) arises from taking the time derivative of the hydrostatic balance (10), which leads after rearrangement to

$$\frac{\partial \eta}{\partial t} = \underbrace{\frac{\partial_t (p_b - p_a)}{g \rho(\eta)}}_{\text{mass}} - \underbrace{\frac{\int_{-H}^{\eta} (\partial \rho / \partial t) dz}{\rho(\eta)}}_{\text{steric}}. \tag{13}$$

The two expressions (12) and (13) have the same physical content, though the terms on the right hand side slightly differ quantitatively.

2.3. Boundary mass fluxes and convergence of mass transport

In Version II of the sea level equation (8), a steady state is associated with a balance between the divergence of depth integrated mass transport and the mass transported across the ocean surface. An analogous balance also dominates for Version I of the sea level equation (1), with this balance consistent with the utility of Boussinesq fluids, whereby the non-Boussinesq steric effect is absent (Greatbatch, 1994). We illustrate this balance in Fig. 2, which shows the time mean mass flux crossing the ocean surface associated with freshwater transport (i.e., precipitation, evaporation, river runoff, and ice melt/formation), divided by the surface ocean density, and the time mean of $-\rho_o^{-1} \nabla \cdot \mathbf{U}^\rho$ where $\rho_o = 1035 \text{ kg m}^{-3}$ is a reference density. The maps are rough mirror image of each other, thus reflecting the near steady state nature of the large scale sea level forcing. Fig. 3 further supports this view by illustrating the sea level computed in a volume conserving Boussinesq model and one computed in a mass conserving non-Boussinesq model. Both patterns are quite similar at the large-scales, as we may expect since the oceanic Boussinesq approximation is accurate for many purposes.

2.4. How we make use of the kinematic sea level equations

The kinematic sea level equations (1) and (8) arise just from mass balance and the kinematic boundary conditions, which lends great generality to their applicability; e.g., they are valid for both hydrostatic and non-hydrostatic fluids. At each point in the ocean, sea level tendencies must respect these kinematic constraints. Hence, Eqs. (1) and (8) offer a means for partitioning the evolution of sea level into various physical processes.

Although sufficient for our purposes, there are questions that kinematics cannot answer absent dynamical principles (e.g.,Lowe and Gregory, 2006). That is, the kinematic approach provides a useful diagnostic framework, but it does not, alone, produce a complete predictive framework. For example, a kinematic approach alone cannot uncover how sea level adjusts in the presence

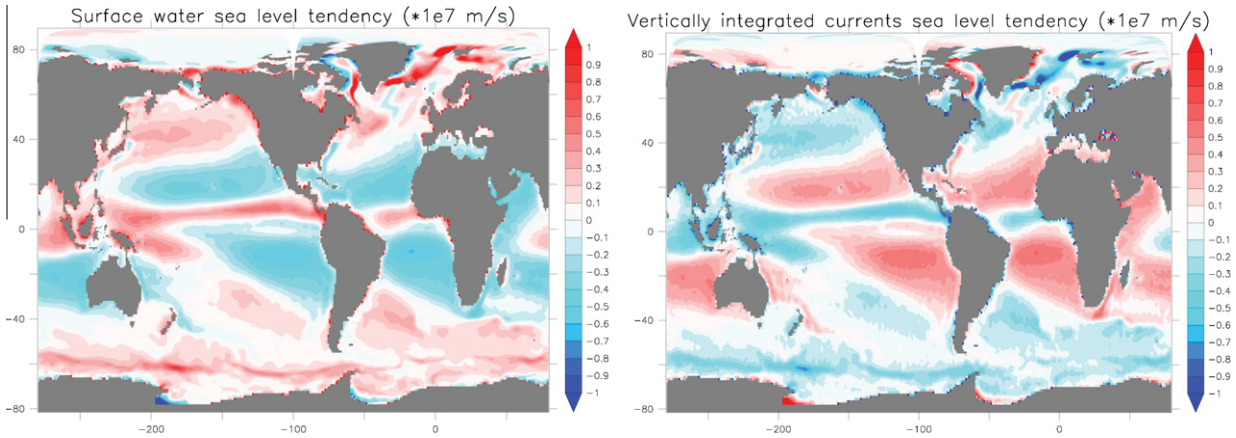

Fig. 2. A map of the 20 year mean net water transferred across the ocean surface, Q_m, divided by the surface ocean density, and the convergence of mass transported within and ocean column, $-\nabla \cdot \mathbf{U}^\rho$, divided by a reference density $\rho_o = 1035$ kg m^{-3}. The two patterns are near mirror-images, which reflects the near steady state nature of the time mean. However, note that the global integral of $-\nabla \cdot \mathbf{U}^\rho$ vanishes whereas that from $Q_m/\rho(\eta)$ generally does not vanish, even when the area integral of Q_m is zero. Some features characteristic of climatological water flux forcing includes large values around coastlines, associated with river runoff; large values in the Intertropical Convergence Zone; and evaporation in the subtropical gyres. The global ocean area means for these maps are 2.5×10^{-11} m s^{-1} = 8×10^{-4} m year^{-1} for the water forcing, and zero for the convergence of vertically integrated mass transport.

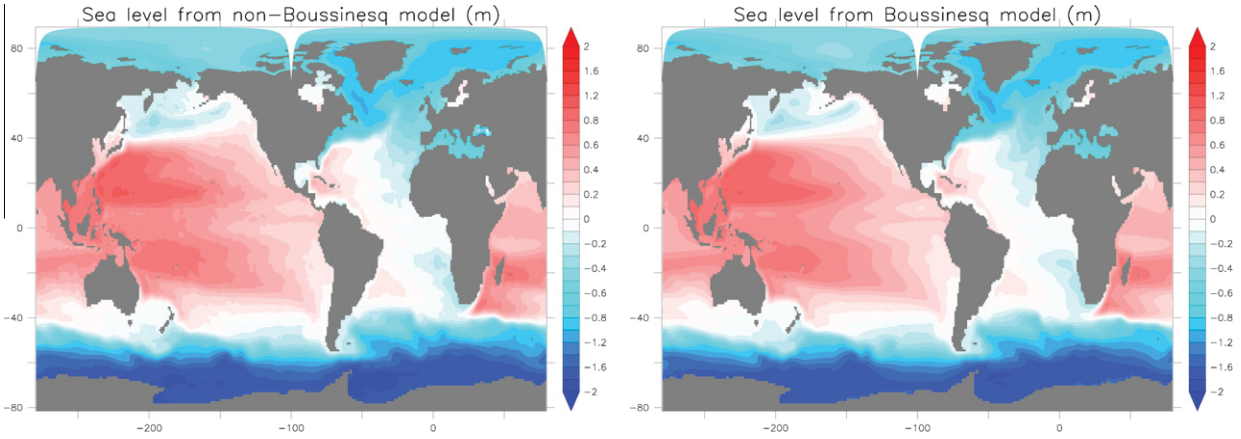

Fig. 3. Map of the 20 year mean sea level from non-Boussinesq and Boussinesq model simulations, using the model detailed in Appendix B. The area mean has been removed from both patterns to eliminate differences associated with the global steric effect. Note the very similar broad-scale features from the two simulations. Additionally, there are some enhanced smaller scale features in the non-Boussinesq simulation, which are conjectured to arise partly from the non-Boussinesq steric effect. The global root-mean-square difference for these patterns is 3.7×10^{-2} m, and the global correlation coefficient is >99%.

of forcing, or the time scales over which low frequency patterns emerge. In particular, should we expect low frequency (order monthly or longer) sea level patterns to exhibit high values under regions of net precipitation and low values under regions of net evaporation? At any instant of time, net precipitation will contribute a positive tendency to the sea level, and net evaporation will contribute a negative tendency, as revealed by the kinematic sea level equations (1) and (8). However, as seen by comparing Figs. 2 and 3, the low frequency sea level patterns are not generally correlated with patterns of evaporation minus precipitation.

The reason for the decorrelation is that there is a dynamical adjustment occurring on a barotropic time scale (a few days) that causes perturbations from boundary mass fluxes, as well as from surface buoyancy fluxes contained in the non-Boussinesq steric effect, to be transmitted globally through barotropic gravity wave adjustments (Greatbatch, 1994). That is, the perturbations can be considered barotropic wavemakers, with barotropic gravity waves rapidly impacting global mean sea level, but generally leaving little imprint on regional low frequency sea level patterns. Additional impacts from boundary and interior fluxes of mass and buoyancy alter regional sea level patterns through baroclinic adjustments. The far slower baroclinic adjustments associated with these perturbations are well captured in both volume conserving Boussinesq and mass conserving non-Boussinesq ocean models (see, e.g., Hsieh and Bryan, 1996; Bryan, 1996; Landerer et al., 2007; Stammer, 2008; Yin et al., 2009; Yin et al., 2010; Lorbacher et al., in revision). These points provide some perspective for how we interpret the patterns exhibited in this paper arising from surface mass and buoyancy fluxes, as well as other patterns from the non-Boussinesq steric effect.

3. The non-Boussinesq steric effect

The non-Boussinesq steric effect and the boundary mass flux are the only two means, within the kinematic sea level equation (1), to impact global mean sea level. Impacts from the convergence of vertically integrated ocean currents exactly vanish in the global mean and so are of no direct relevance to global sea level.

Certainly ocean currents are important for global mean sea level. In particular, they impact on turbulent mixing, which in turn modifies the way buoyancy irreversibly penetrates into the ocean.

So in that regard ocean dynamics is of fundamental importance for global sea level. But it is through the non-Boussinesq steric effect that ocean mixing of buoyancy impacts global mean sea level, and it is through the non-Boussinesq steric effect that boundary fluxes of buoyancy impact global mean sea level. Consequently, to understand mechanisms for changes to global mean sea level requires a framework to explore the non-Boussinesq steric effect.

3.1. Defining the non-Boussinesq steric effect

Version I of the sea level equation (1), repeated here for completeness,

$$\frac{\partial \eta}{\partial t} = \frac{Q_m}{\rho(\eta)} - \nabla \cdot \mathbf{U} - \int_{-H}^{\eta} \frac{1}{\rho} \frac{d\rho}{dt} dz \tag{14}$$

provides a means to kinematically partition various physical processes impacting sea level evolution. We are particularly interested in the time tendency

$$\left(\frac{\partial \eta}{\partial t}\right)_{\text{non-bouss steric}} \equiv -\left(\int_{-H}^{\eta} \frac{1}{\rho} \frac{d\rho}{dt} dz\right). \tag{15}$$

We refer to this term as the *non-Boussinesq steric effect*, since it is absent from the prognostic sea level equation in Boussinesq fluids (Greatbatch, 1994). The time derivative acting on *in situ* density in the non-Boussinesq steric effect (15) is a material or Lagrangian derivative, rather than an Eulerian tendency. This detail is fundamental to the formulation given in the following, and we return to its implications throughout this paper.

3.2. Vertical motion across pressure surfaces

To initiate a discussion of the non-Boussinesq steric effect, use the material evolution of *in situ* density in the form of Eq. (185) (see Appendix A) to write

$$-\frac{1}{\rho}\frac{d\rho}{dt} = \alpha \frac{d\Theta}{dt} - \beta \frac{dS}{dt} - \frac{1}{\rho c_{\text{sound}}^2} \frac{dp}{dt}. \tag{16}$$

The material evolution of *in situ* density is thus affected by the material evolution of buoyancy, through material changes in temperature and salinity, and by material evolution of pressure. We focus on the pressure evolution in this subsection.

To garner some exposure to the physics of dp/dt as it appears in Eq. (16), consider the special case of a hydrostatic fluid, where the volume per time per horizontal area of fluid crossing a surface of constant hydrostatic pressure is given by (see Section 6.7 of Griffies (2004))

$$w^{(p)} = \frac{\partial z}{\partial p}\frac{dp}{dt} = -(\rho g)^{-1}\frac{dp}{dt}. \tag{17}$$

The transport measured by $w^{(p)}$ is the pressure-coordinate analog of the vertical velocity component $w = dz/dt$ in a geopotential coordinate representation of the vertical direction. To the extent that pressure surfaces are well approximated by depth surfaces, $w^{(p)} \approx w$. Fluid moving into regions of increasing hydrostatic pressure ($dp/dt > 0$) represents downward movement of fluid, with $w^{(p)} < 0$ in this case. Conversely, motion into decreasing hydrostatic pressure represents upward motion, with $w^{(p)} > 0$.

We identify the following contribution to the non-Boussinesq steric effect associated with vertical motion across hydrostatic pressure surfaces

$$\left(\frac{\partial \eta}{\partial t}\right)_{dp/dt} \equiv -\int_{-H}^{\eta} \left(\frac{1}{\rho c_{\text{sound}}^2}\frac{dp}{dt}\right) dz = g\int_{-H}^{\eta}\left(\frac{w^{(p)}}{c_{\text{sound}}^2}\right) dz = g(H+\eta)\overline{\left(\frac{w^{(p)}}{c_{\text{sound}}^2}\right)}^{z}, \tag{18}$$

where we introduced the vertical average operator for an ocean column. In columns where the vertically averaged vertical motion is upward, the column stretches, thus imparting a positive sea level tendency. The opposite occurs for vertically averaged downward fluid motion. Both effects are enhanced in regions of smaller sound speed, such as in the high latitude upper 2000 m (see Fig. 4).

Fluid generally moves across pressure surfaces under adiabatic and isohaline parcel motions, as in the presence of gravity or planetary waves. Additionally, dianeutral mixing generally gives rise to vertical transport, for example as seen in the case of a horizontally unstratified fluid in the presence of vertical diffusion. Diagnosing the term (18) does not identify the cause of the dia-pressure motion; it merely quantifies the effects of this motion on global mean sea level.

To gain a sense for the scale of the term (18), approximate the shallow water gravity wave speed as

$$c_{\text{grav}}^2 \approx g(H+\eta), \tag{19}$$

thus leading to

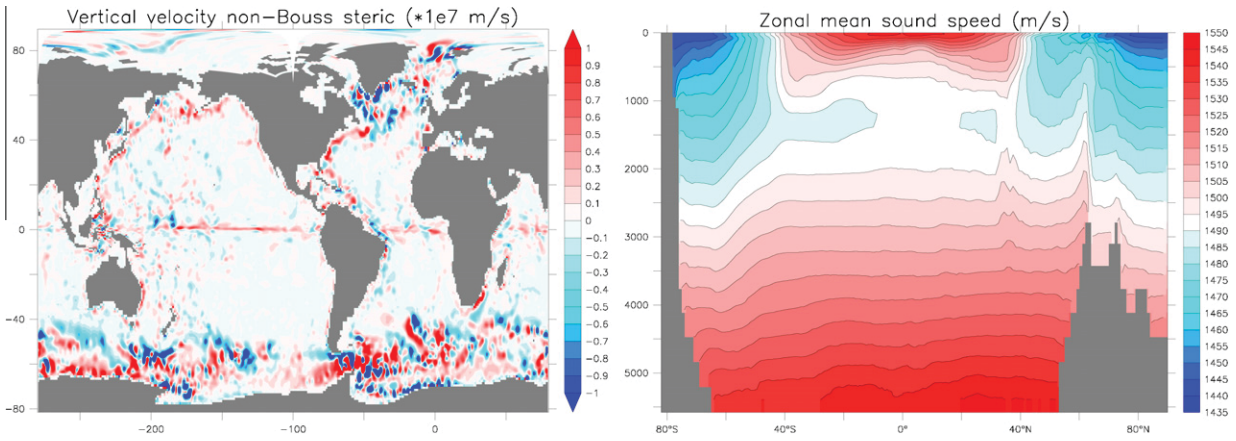

Fig. 4. A map of the non-Boussinesq steric effect (see Eq. (20)) arising from motion across pressure surfaces, as time averaged for 20 years from the global model detailed in Appendix B. Note the larger values in the boundary currents as well as in regions where currents strongly interact with the bottom, such as the Southern Ocean and the North Atlantic subpolar gyre. The global ocean mean for this map is 2×10^{-11} m s^{-1} = 7×10^{-4} m year^{-1}. Also shown is the corresponding zonal mean sound speed (Eq. (188)), with the squared inverse sound speed modulating the impact on sea level from vertical motion. Relatively small values in the upper 2000 m of the high latitude oceans helps to amplify the impacts from deep currents feeling topography and so initiating strong vertical motions.

$$\left(\frac{\partial \eta}{\partial t}\right)_{\mathrm{dp/dt}} \approx \overline{w^{(p)} (c_{\mathrm{grav}}/c_{\mathrm{sound}})^2}^{z}, \tag{20}$$

where $(c_{\mathrm{grav}}/c_{\mathrm{sound}})^2 \leqslant 10^{-2}$. Fig. 4 shows this contribution to the non-Boussinesq steric effect, as averaged over 20 years from the global model detailed in Appendix B. Larger values appear in regions with strong vertical motions, such as near boundaries and where currents reach towards the bottom such as the Southern Ocean. It is here that sizable ocean currents impinge on topography, with the no-normal flow boundary condition (Eq. (152) in Appendix A) inducing sizable vertical motion. Additionally, the Southern Ocean patterns suggest the presence of gravity wave motions, again likely initiated by interactions between the Antarctic Circumpolar Current and the bottom (Nikurashin and Ferrari, 2010). There is also a signature from equatorial upwelling in the Pacific.

The contribution (Eq. (18)) to the non-Boussinesq steric effect possesses a higher wave number structure and larger magnitude locally than contributions from surface water fluxes and from the convergence of column integrated mass transport (see Fig. 2). We expect the high wave number power to increase in simulations with refined resolutions and realistic astronomical (tidal) forcing (absent in this simulation), such that internal gravity wave activity is further promoted (through conversion from barotropic to baroclinic tides through interactions with topography). In this way, dynamically active regions, such as the Southern Ocean, act as a barotropic and baroclinic wavemaker through vertical motion. As explained in Section 2.4 and Greatbatch (1994), contributions to the non-Boussinesq steric effect act dynamically in a manner analogous to mass forcing, leaving a regional low frequency field that is smoother than forcing from the non-Boussinesq steric effect. We thus do not generally see an imprint of the non-Boussinesq steric effect on low frequency (i.e., longer than monthly) regional sea level. Such is revealed in the simulation shown in Fig. 3, where there is no signature in the time mean sea level of the pattern from Fig. 4.

The global mean for the pattern shown in Fig. 4 contributes to the tendency for global mean sea level (Section 4.2). As there are a number of positive and negative regions, cancellation occurs when performing the global area integral. Indeed, as summarized in Table 1 presented later in Section 8.1, the contribution to global mean sea level from vertical motion across pressure surfaces becomes comparable in magnitude to that from certain subgrid scale processes, such as cabbeling, thermobaricity, and the submesoscale parameterization of Fox-Kemper et al. (2008), yet it is smaller than the effects from vertical diffusion and the (Gent and McWilliams, 1990) mesoscale eddy parameterization.

3.3. An expanded form of the kinematic sea level equation

We now focus on how material changes in temperature and salinity contribute to the non-Boussinesq steric effect. To do so, assume that the material evolution of conservative temperature and salinity is given by the convergence of a subgrid scale flux plus a source/sink term

$$\rho \frac{d\Theta}{dt} = -\nabla \cdot \mathbf{J}^{(\Theta)} + \rho \mathcal{S}^{(\Theta)}, \tag{21}$$

$$\rho \frac{dS}{dt} = -\nabla \cdot \mathbf{J}^{(S)} + \rho \mathcal{S}^{(S)}. \tag{22}$$

The conservative temperature flux $\mathbf{J}^{(\Theta)}$ and the salt flux $\mathbf{J}^{(S)}$ include their respective diffusive and skew fluxes, as formulated by Eq. (176) in Appendix A (see also Eq. (125) of Section 8.1). Note that the temperature flux $\mathbf{J}^{(\Theta)}$ may also include the effects from penetrative shortwave radiation (e.g.,Iudicone et al., 2008). The source terms $\mathcal{S}^{(\Theta)}$ and $\mathcal{S}^{(S)}$ may include non-local mixing processes such as those parameterized by Large et al. (1994), or the non-local cross-land or downslope processes such as those parameterized by Griffies et al. (2005) and Danabasoglu et al. (2010). For brevity, we omit the source terms $\mathcal{S}^{(\Theta)}$ and $\mathcal{S}^{(S)}$ in the following manipulations, but reintroduce them for the final result in Eq. (41).

Temporarily dropping the source terms in the conservative temperature and salinity equations (21) and (22) lead to (see Eq. (16))

$$\begin{aligned} -\alpha \frac{d\Theta}{dt} + \beta \frac{dS}{dt} &= \left(\frac{\partial v}{\partial \Theta}\right) \nabla \cdot \mathbf{J}^{(\Theta)} + \left(\frac{\partial v}{\partial S}\right) \nabla \cdot \mathbf{J}^{(S)} \\ &= \nabla \cdot \left(\frac{\partial v}{\partial \Theta} \mathbf{J}^{(\Theta)} + \frac{\partial v}{\partial S} \mathbf{J}^{(S)} \right) - \mathbf{J}^{(\Theta)} \cdot \nabla \left(\frac{\partial v}{\partial \Theta} \right) \\ &\quad - \mathbf{J}^{(S)} \cdot \nabla \left(\frac{\partial v}{\partial S} \right), \end{aligned} \tag{23}$$

where

$$v = \rho^{-1} \tag{24}$$

is the specific volume, and its derivatives are given by

$$\frac{\partial v}{\partial \Theta} = \frac{\alpha}{\rho}, \tag{25}$$

$$\frac{\partial v}{\partial S} = -\frac{\beta}{\rho}, \tag{26}$$

where $\alpha = -\rho^{-1} \partial \rho / \partial \Theta$ and $\beta = \rho^{-1} \partial \rho / \partial S$ are the thermal expansion and haline contraction coefficients introduced in Section A.4 in Appendix A. Bringing these results together leads to

$$\begin{aligned} \left(\frac{\partial \eta}{\partial t}\right)_{\text{non-bouss steric}} &= -\int_{-H}^{\eta} \nabla \cdot \left[(\alpha/\rho) \mathbf{J}^{(\Theta)} - (\beta/\rho) \mathbf{J}^{(S)} \right] dz \\ &\quad + \int_{-H}^{\eta} \left(\mathbf{J}^{(\Theta)} \cdot \nabla(\alpha/\rho) - \mathbf{J}^{(S)} \cdot \nabla(\beta/\rho) - \frac{1}{\rho c_{\mathrm{sound}}^2} \frac{dp}{dt} \right) dz. \end{aligned} \tag{27}$$

3.3.1. Exposing the boundary fluxes of temperature and salinity

We expose the surface and bottom boundary fluxes through use of the following identity

$$\begin{aligned} &\int_{-H}^{\eta} \nabla \cdot ((\alpha/\rho) \mathbf{J}^{(\Theta)} - (\beta/\rho) \mathbf{J}^{(S)}) dz = \nabla_z \cdot \left(\int_{-H}^{\eta} [(\alpha/\rho) \mathbf{J}^{(\Theta)} - (\beta/\rho) \mathbf{J}^{(S)}] dz \right) \\ &+ \nabla(z-\eta) \cdot [(\alpha/\rho) \mathbf{J}^{(\Theta)} - (\beta/\rho) \mathbf{J}^{(S)}]_{z=\eta} - \nabla(z+H) \cdot [(\alpha/\rho) \mathbf{J}^{(\Theta)} - (\beta/\rho) \mathbf{J}^{(S)}]_{z=-H}. \end{aligned} \tag{28}$$

Tracer fluxes through the ocean bottom $z = -H(x,y)$ are written as

$$Q^{(C)} = \mathbf{J}^{(C)} \cdot \hat{\mathbf{n}} \left(\frac{dA_{\hat{\mathbf{n}}}}{dA} \right) = \mathbf{J}^{(C)} \cdot \nabla(z+H), \tag{29}$$

where $\hat{\mathbf{n}} = -\nabla(z+H)/|\nabla(z+H)|$ is the bottom normal vector, and we used the relation (see Section 20.13.2 of Griffies (2004))

$$dA_{\hat{\mathbf{n}}} = |\nabla(z+H)| dA \quad \text{at } z = -H(x,y) \tag{30}$$

between the area element $dA_{\hat{\mathbf{n}}}$ on the ocean bottom, and its horizontal projection dA. Hence, the conservative temperature and salt fluxes through the ocean bottom are given by

$$Q^{(\Theta)} = \mathbf{J}^{(\Theta)} \cdot \nabla(z+H) \quad \text{at } z = -H, \tag{31}$$

$$Q^{(S)} = \mathbf{J}^{(S)} \cdot \nabla(z+H) \quad \text{at } z = -H. \tag{32}$$

The flux

$$\text{enthalpyflux} = c_p Q^{(\Theta)} \tag{33}$$

is the heat, or more precisely the enthalpy, per time per horizontal area entering the ocean through the bottom, with

$$c_p \approx 3992.1 \text{ J kg}^{-1} \text{ K}^{-1} \tag{34}$$

the heat capacity for seawater at constant pressure, with the value given by IOC et al. (2010) the most precise. Geothermal heating is quite small relative to surface heat fluxes (e.g., see Fig. 8 discussed in Section 3.4.1). However, the work of Adcroft et al. (2001) and Emile-Geay and Madec (2009) motivate retaining this contribution to the temperature equation, as there are some systematic impacts from geothermal heating over long periods. For climatological purposes, the introduction of salt to the ocean through the sea floor is negligible, in which case

$$Q^{(S)} \approx 0 \quad \text{at } z = -H. \tag{35}$$

Likewise, water may enter through the sea floor, but this contribution is generally quite negligible

$$Q^{(m)} \approx 0 \quad \text{at } z = -H. \tag{36}$$

As for the ocean bottom, tracer fluxes through the ocean surface $z = \eta(x,y,t)$ are written as

$$Q^{(C)} = -\mathbf{J}^{(C)} \cdot \hat{\mathbf{n}} \left(\frac{dA_{\hat{\mathbf{n}}}}{dA} \right) = -\mathbf{J}^{(C)} \cdot \nabla(z-\eta), \tag{37}$$

where $\hat{\mathbf{n}} = \nabla(z-\eta)/|\nabla(z-\eta)|$ is the surface outward normal vector, and we used the relation (see Section 20.13.2 of Griffies (2004))

$$dA_{\hat{\mathbf{n}}} = |\nabla(z-\eta)| dA \quad \text{at } z = \eta \tag{38}$$

between the area element $dA_{\hat{\mathbf{n}}}$ on the ocean surface, and its horizontal projection dA. Hence, the conservative temperature and salt fluxes through the ocean surface take the form

$$Q^{(\Theta)} = -\mathbf{J}^{(\Theta)} \cdot \nabla(z-\eta) \quad \text{at } z = \eta, \tag{39}$$

$$Q^{(S)} = -\mathbf{J}^{(S)} \cdot \nabla(z-\eta) \quad \text{at } z = \eta, \tag{40}$$

where the sign convention is chosen so that positive flux $Q^{(\Theta)}$ adds heat to the ocean, and positive flux $Q^{(S)}$ adds salt to the ocean. There is near zero salt flux through the ocean surface, except for the small exchange during the formation and melt of sea ice. We further discuss surface fluxes in Section 3.4.

3.3.2. Expanded form of the kinematic sea level equation

Bringing these results together leads to an expanded form of the kinematic sea level equation

$$\begin{aligned} \frac{\partial \eta}{\partial t} = & -\nabla_z \cdot \left(\int_{-H}^{\eta} \left(\frac{(\alpha \mathbf{J}^{(\Theta)} - \beta \mathbf{J}^{(S)} + \rho \mathbf{u})}{\rho} \right) dz \right) \\ & + \int_{-H}^{\eta} \left(\mathbf{J}^{(\Theta)} \cdot \nabla(\alpha/\rho) - \mathbf{J}^{(S)} \cdot \nabla(\beta/\rho) \right. \\ & \left. - \frac{1}{\rho c_{\text{sound}}^2} \frac{dp}{dt} + \alpha \mathcal{S}^{(\Theta)} - \beta \mathcal{S}^{(S)} \right) dz \\ & + \left(\frac{\alpha Q^{(\Theta)} - \beta Q^{(S)} + Q_m}{\rho} \right)_{z=\eta} + \left(\frac{\alpha Q^{(\Theta)} - \beta Q^{(S)} + Q_m}{\rho} \right)_{z=-H}, \end{aligned} \tag{41}$$

where we reintroduced the buoyancy source term $\alpha \mathcal{S}^{(\Theta)} - \beta \mathcal{S}^{(S)}$. This expression yields a precise measure for how physical processes and boundary fluxes determine the kinematic evolution of sea level, with Fig. 5 providing a schematic. We retain the bottom fluxes for salt and mass merely for completeness, but note that these two terms are generally set to zero for climate studies.

3.3.3. Buoyancy fluxes and mass fluxes

The first integral in the kinematic sea level equation (41) is the convergence of vertically integrated lateral subgrid scale flux of buoyancy (arising from the non-Boussinesq steric effect), along with the lateral advective flux of mass. When integrated over the global ocean, this convergence vanishes exactly. Hence, this term moves mass and buoyancy around in the ocean without altering the global mean sea level.

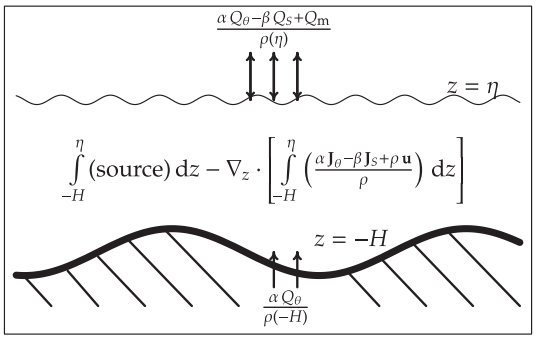

Fig. 5. A schematic ocean basin as in Fig. 1, but now illustrating the various boundary and internal processes that impact sea level according to the unpacked kinematic sea level equation (41). The surface mass flux, Q_m, is combined here with a surface buoyancy flux to yield the surface boundary forcing $\rho(\eta)^{-1}(\alpha Q^{(\Theta)} - \beta Q^{(S)} + Q_m)$. Likewise, the bottom boundary forcing arises from geothermal heating in the form $\alpha Q^{(\Theta)}/\rho(-H)$, which is a small, but always positive, contribution to global mean sea level evolution. This schematic neglects the bottom fluxes of salt and mass, since they are quite small in general. In the ocean interior, the convergence of mass and buoyancy, along with a source term (Eq. (42)), yield the forcing $\int_{-H}^{\eta} (\text{source}) dz - \nabla_z \cdot \int_{-H}^{\eta} \rho^{-1} (\alpha \mathbf{J}^{(\Theta)} - \beta \mathbf{J}^{(S)} + \rho \mathbf{u}) dz$.

The combination $\alpha Q^{(\Theta)} - \beta Q^{(S)}$ represents the buoyancy flux crossing the ocean boundary. Boundary fluxes that increase buoyancy also increase global mean sea level. In particular, it is precisely through this effect that surface ocean warming acts to increase global mean sea level. These boundary buoyancy fluxes act in concert with the boundary mass flux Q_m to impact sea level through interactions at the ocean surface.

3.3.4. Interior source

The second integral in Eq. (41) (arising from the non-Boussinesq steric effect) takes the form of a *source* term, since it does not occur as a flux divergence

$$\text{source} = \mathbf{J}^{(\Theta)} \cdot \nabla(\alpha/\rho) - \mathbf{J}^{(S)} \cdot \nabla(\beta/\rho) - \frac{1}{\rho c_{\text{sound}}^2} \frac{dp}{dt} + (\alpha \mathcal{S}^{(\Theta)} - \beta \mathcal{S}^{(S)}) \tag{42}$$

with the source having units of inverse time. There are four terms contributing to the source, the third of which we discussed in Section 3.2 relates to vertical motion across pressure surfaces. The fourth term arises from interior buoyancy sources that can be present in a simulation due to non-local parameterization of unresolved mixing and/or transport processes (e.g., Large et al., 1994; Griffies et al., 2005; Danabasoglu et al., 2010). The first and second terms relate to the orientation of temperature and salinity subgrid scale fluxes in relation to thermodynamic properties of the fluid and geometric properties of the density surface. We consider special cases of subgrid scale flux terms in Section 5 for dianeutral diffusion, approximated as vertical diffusion; Section 6 for neutral diffusion, where it is shown how cabbeling and thermobaricity, arising from parameterized mixing effects from mesoscale eddies along neutral directions, impact global mean sea level; and Section 7 for quasi-Stokes transport from mesoscale eddies as parameterized according to Gent and McWilliams (1990) as well as submesoscale eddies as parameterized by Fox-Kemper et al. (2008) and Fox-Kemper et al. (2011).

3.3.5. Complementary patterns from subgrid fluxes and the predominance for sea level reduction

We primary focus in this paper is on processes impacting global mean sea level, so it is the global integral of the source terms appearing in Eq. (42) that are of concern (to be discussed in Section 4.2). Consequently, when examining the impacts on global mean

sea level from parameterized subgrid scale (SGS) processes, we may choose to examine patterns from either of the following forms of the source term

$$\text{sgs source : flux projection form} = \mathbf{J}^{(\Theta)} \cdot \nabla(\alpha/\rho) - \mathbf{J}^{(S)} \cdot \nabla(\beta/\rho), \tag{43}$$

$$\text{sgs source : weighted flux divergence form} = -(\alpha/\rho)\nabla \cdot \mathbf{J}^{(\Theta)} + (\beta/\rho)\nabla \cdot \mathbf{J}^{(S)}. \tag{44}$$

These two forms differ by a total divergence. For those subgrid scale processes that have zero boundary fluxes, the divergence vanishes upon taking a global integral, so both Eqs. (43) and (44) have the same impact on global mean sea level. The weighted flux divergence form (44) is readily diagnosed since the model computes the flux divergence to update temperature and salinity during a model time step. This form generally has more spatial structure given the derivative acting on the flux components, and since variations of α/ρ and β/ρ typically appear on a much larger spatial scale than subgrid scale fluxes (see Fig. 6).

The patterns exhibited by the flux projection form (43) expose the geometric orientation of the flux components relative to gradients in (α/ρ) and (β/ρ). Since (β/ρ) exhibits far less spatial variation than (α/ρ) (see Fig. 6), the form (43) is typically dominated by the temperature term $\mathbf{J}^{(\Theta)} \cdot \nabla(\alpha/\rho)$. Though there are notable exceptions, the subgrid scale temperature flux is generally found in Sections 5–7 to be down the gradient of the thermal expansion coefficient (α/ρ variations are dominated by α variations)

$$\mathbf{J}^{(\Theta)} \cdot \nabla\alpha < 0. \tag{45}$$

That is, heat is transferred preferentially by subgrid scale processes in a direction where the thermal expansion coefficient gets smaller. For sea level, this result means that heat moves from regions where its impact on thermosteric sea level rise is relatively large (e.g., lower latitudes) to where its impact is smaller (e.g., higher latitudes). Specifically, the poleward heat transport by quasi-Stokes parameterizations, or downward heat diffusion within the upper 1000–1500 m of the ocean, both lead towards a net reduction in global mean sea level. Additional impacts by cabbeling and thermobaricity also play a role (Section 6).

3.3.6. Concerning the absence of advective temperature and salt fluxes

It is notable that the expanded kinematic sea level equation (41) only involves the subgrid scale fluxes of temperature and salt, as well as their non-advective boundary fluxes. There are no interior nor boundary advective fluxes of buoyancy that directly impact sea level. This absence relates to our choice to focus on Version I of the sea level equation (1), in which the time derivative acting on *in situ* density is a material or Lagrangian derivative, not an Eulerian derivative. This point is of fundamental importance to how we identify physical processes impacting global mean sea level in Section 4 and further considered in Sections 5–7. Hence, buoyancy

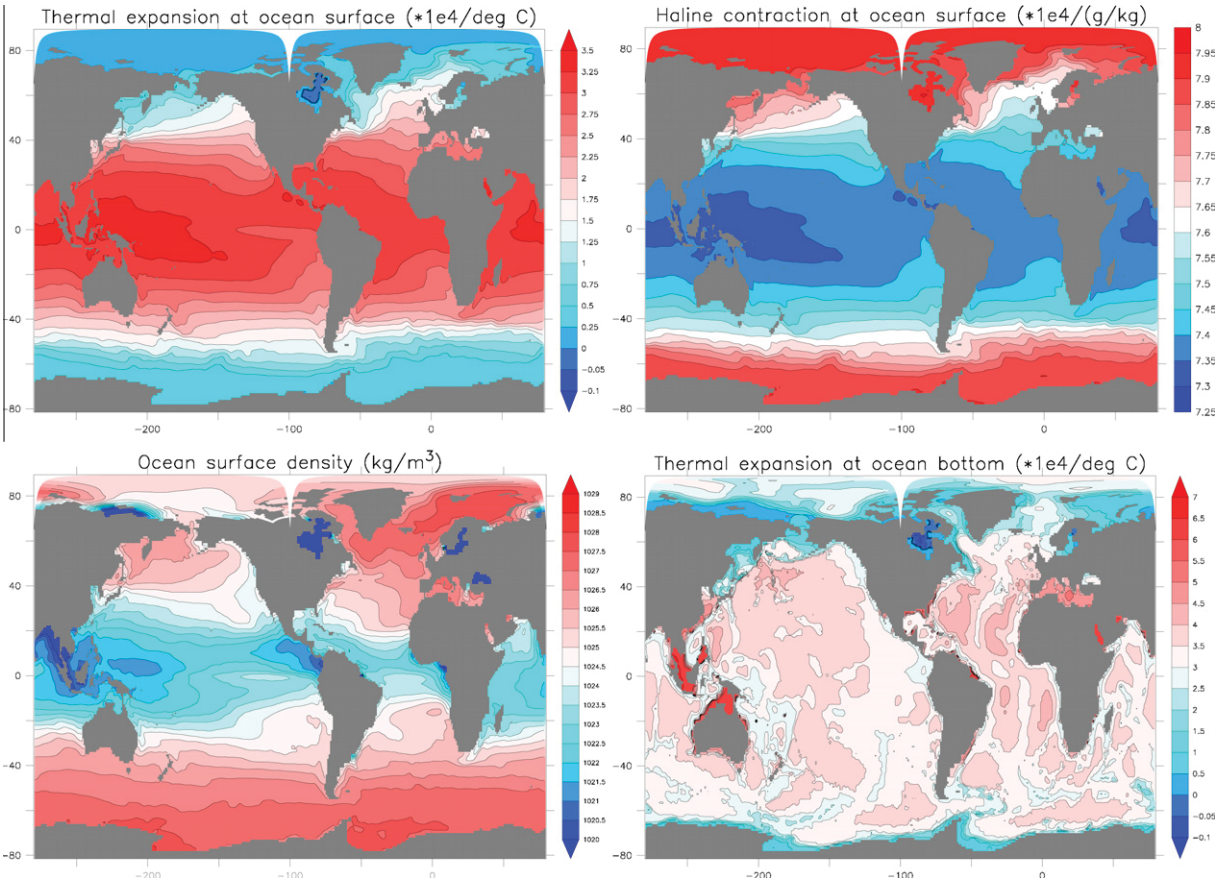

Fig. 6. Map of the 20 year mean simulated surface ocean values for the following fields: thermal expansion coefficient $\alpha = -\rho^{-1}\partial\rho/\partial\Theta$ (Eq. (186)); haline contraction coefficient $\beta = \rho^{-1}\partial\rho/\partial S$ (Eq. (187)); and *in situ* density. Also shown is the ocean bottom value for α. Note the distinct colour range for each of the figures, particularly the distinct range for surface and bottom α. Note that $\alpha < 0$ in regions of very cold and freshwater, such as the Hudson Bay. There is generally a wide range of values for α, being about a factor of 10 larger in the tropics than in high latitudes, whereas β and ρ deviate only a few percent from their respective global means. The wide range for the thermal expansion coefficient arises largely from its temperature dependence. The wide range of variations for α relative to the far smaller variations in β plays a fundamental role in determining how surface boundary conditions and subgrid scale processes impact on sea level.

changes impact global mean sea level only through processes that render a nonzero material change to *in situ* density, with such changes occurring through boundary buoyancy fluxes, interior mixing, nonlinear equation of state effects, and subgrid scale eddy induced advection.

3.4. Boundary fluxes of heat and salt

We now detail how boundary fluxes of heat, salt, and freshwater impact the non-Boussinesq steric effect appearing in Eq. (41). The global integral of these fluxes impact on the global mean sea level (Section 4). Start by noting that the contribution from the surface buoyancy flux,

$$\left(\frac{\partial \eta}{\partial t}\right)_{\text{surfacebuoyancy}} = \frac{\alpha Q^{(\Theta)} - \beta Q^{(S)}}{\rho(\eta)} \tag{46}$$

is determined both by the boundary fluxes of heat and salt, as well as the boundary values for the thermal expansion coefficient, haline contraction coefficient, and density. The contribution from the bottom geothermal heating is likewise affected by the bottom value for the thermal expansion coefficient. Boundary fluxes of buoyancy impact sea level upon mixing the boundary buoyancy into the liquid seawater. Such mixing is implicit in the bulk formulae used to compute boundary fluxes, with these fluxes directly input to the top model grid cell.

Fig. 6 shows the 20 year mean for the sea surface α, β, and ρ from the model configuration detailed in Appendix B, and the bottom value for α. We make the following observations.

- The thermal expansion coefficient, α, is about 10 times smaller in the high latitudes than low latitudes. This rather large range greatly modulates how heat fluxes impact the non-Boussinesq steric effect, with tropical surface heating impacting global mean sea level far more than high latitude surface cooling. Likewise, tropical geothermal heating has more impact than high latitude heating.
- At the ocean surface, the haline contraction coefficient, β, is about 5% larger in the high latitudes than low latitudes, which means for many cases one may assume β is horizontally constant.
- Surface *in situ* density, ρ, is smallest in regions impacted by freshwater input from river runoff, and largest in the high latitude North Atlantic and Southern Ocean, with a range of values being only about 3%.

3.4.1. Boundary heat fluxes

The non-advective heat flux crossing the surface ocean boundary consists of the following contributions (in units of W m^{-2}),

$$Q_{\text{surface}} = Q_{\text{SW}} + Q_{\text{LW}} + Q_{\text{sens}} + Q_{\text{lat}} + Q_{\text{frazil}} \tag{47}$$

with a sign convention chosen so that positive fluxes add heat to the liquid seawater. What appears in the sea level Eq. (41) is actually the surface flux of temperature, not heat. So it is necessary to convert between heat and temperature fluxes when considering the impacts on sea level. As noted by McDougall (2003), to convert from heat fluxes to fluxes of potential temperature requires the use of a non-constant specific heat capacity, which varies by roughly 5% over the globe. In contrast, converting between heat fluxes and conservative temperature fluxes is done with a constant specific heat capacity

$$Q_{\text{surface}} = c_{\text{p}} Q^{(\Theta)}_{\text{surface}}, \tag{48}$$

thus serving to further promote the use of conservative temperature.

We now summarize the various contributions to surface ocean heating.

- *Shortwave*: The dominant heating occurs through the shortwave contribution $Q_{\text{SW}} > 0$. Shortwave radiation penetrates on the order of 10 m to 100 m into the ocean interior, with the distance depending on optical properties of seawater (see, e.g., Sweeney et al., 2005 and cited references).
- *Longwave*: The longwave contribution Q_{LW} represents the net longwave energy that is re-radiated back to the atmosphere. Even though there are many occasions for backscattering, the net effect of longwave radiation is to cool the ocean.
- *Sensible*: Sensible heating Q_{sens} arises from turbulent exchange with the atmosphere, and is generally parameterized by turbulent bulk formula. The sensible heat term typically cools the ocean surface.
- *Latent*: Latent heating Q_{lat} cools the ocean, as it is the energy extracted from the ocean to vaporize liquid water that enters the atmosphere. Additionally, the latent heating term includes heat extracted from the ocean to melt solid runoff (i.e., calving land ice) or snow entering the liquid ocean. These latent heat terms are thus related to mass transport across the ocean surface according to

$$Q^{\text{vapor}}_{\text{lat}} = H^{\text{vapor}} Q^{\text{evap}}_{\text{m}}, \tag{49}$$

$$Q^{\text{melt}}_{\text{lat}} = H^{\text{fusion}} \left(Q^{\text{calving}}_{\text{m}} + Q^{\text{snow}}_{\text{m}} \right), \tag{50}$$

where $H^{\text{vapor}} \approx 2.5 \times 10^6$ J kg^{-1} is the latent heat of vaporization, $Q^{\text{evap}}_{\text{m}}$ is the evaporative mass flux in units of kgm^{-2} s^{-1}, $H^{\text{fusion}} \approx 3.34 \times 10^5$ J kg^{-1} is the latent heat of fusion, $Q^{\text{calving}}_{\text{m}}$ is the mass flux of calving land ice entering the ocean, and $Q^{\text{snow}}_{\text{m}}$ is the mass flux of frozen precipitation falling on the ocean surface. Note that sea ice and frozen precipitation may enter the ocean at a temperature below the freezing point, in which case additional heat needs to be extracted from the liquid ocean to raise the frozen water to the melting point.
- *Frazil*: As the temperature of seawater cools to the freezing point, sea ice is formed, initially through the production of frazil. Operationally in an ocean model, liquid water can be supercooled at any particular time step through surface fluxes and transport. An adjustment process heats the liquid water back to the freezing point, with this positive heat flux Q_{frazil} extracted from the ice model as frazil sea ice is formed.

In addition to the above listed heat fluxes, there is a heat flux, or more generally a buoyancy flux, associated with the buoyancy contained in water transferred across the ocean surface. This buoyancy flux is associated with mass transport and so it is contained in the advective term in the material time derivative. Mass transfer across the ocean surface impacts sea level through $Q_{\text{m}} > 0$. Additionally, there is a contribution to the non-Boussinesq steric effect upon mixing of heat and salt contained in the transported fluid (i.e., density is materially changed), with such mixing impacting sea level. We return to this point in Section 4.3.

Fig. 7 shows the 20 year mean contribution to the non-Boussinesq steric effect from the surface ocean heating in the global model described in Appendix B. The dominant regions for steric expansion include the equatorial regions, especially in the Pacific. Additionally, as seen in Fig. 6, the tropics are where the thermal expansion coefficient is largest, so heating of tropical surface waters impacts global mean sea level far more than cooling in the higher latitudes. As noted in the review by Fu (2001), the seasonal cycle in sea level is largest in the tropics, with the larger expansion coefficient part of the reason. The key regions for negative non-Boussinesq steric effect include the western boundary currents in the Atlantic and Pacific, as well as the warm Agulhas current flowing

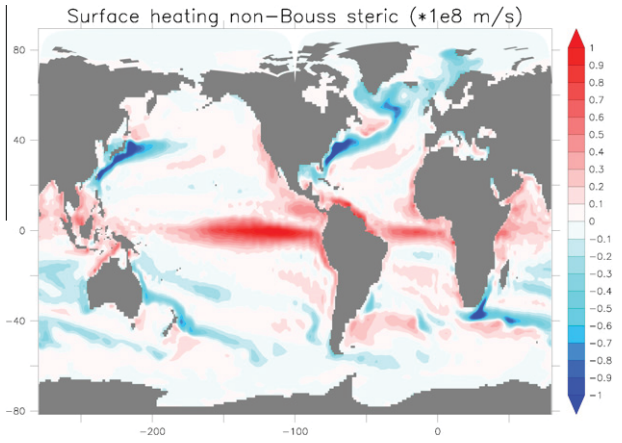

Fig. 7. Map of the 20 year mean contribution from ocean surface heating to the non-Boussinesq steric effect (see Eq. (41)). This map includes heating from shortwave, longwave, sensible, and latent effects, as well as the impacts from frazil ice formation. Note the large positive values in the tropics, especially in the Pacific, and the large negative values in the western boundary currents of the Atlantic and Pacific, as well as the Agulhas region of South Africa. The global ocean mean for this map is 3.3×10^{-10} m s^{-1} = 1×10^{-2} m year^{-1}.

into the Atlantic and being cooled around South Africa. These are regions of strong land-sea temperature contrasts, with warmer ocean waters encountering cooler continental air, thus creating large sensible and latent heat exchanges. Note the absence of a significant non-Boussinesq steric heating/cooling effect in the Southern Ocean, which is largely due to the absence of strong land-sea contrasts and the smaller thermal expansion coefficient.

The total non-advective boundary flux of heat affecting ocean heat content is the sum of the surface flux detailed above, and the bottom flux arising from geothermal heating

$$Q_{\text{heat}} = Q_{\text{surface}} + Q_{\text{geothermal}}. \tag{51}$$

The geothermal contribution to heating is quite small (less than 0.1 W m^{-2} locally), and so contributes only a very small amount to the global sea level evolution. Fig. 8 shows the pattern for this contribution. It is seen to be 1000 times smaller locally than the net surface heating shown in Fig. 7. However, as it is single signed, when globally averaged it is only 100 times smaller than the global mean net surface heating (see Table 1 in Section 8.1).

Although not considered in our simulation, it is interesting to compare the sea level rise from geothermal heating to that from Joule heating arising from the dissipation of kinetic energy due to molecular viscosity. Assuming the rate of Joule heating to be $H_{\text{Joule}} \approx 10^{-9}$ W kg^{-1} (McDougall, 2003), and for this heating to be uniformly distributed throughout the ocean, leads to a contribution to sea level rise

$$\left(\frac{\partial \eta}{\partial t}\right)_{\text{Joule heating}} = \frac{\langle \alpha \rangle H_{\text{Joule}} \mathcal{V}}{\mathcal{A} c_p} \approx 4 \times 10^{-6} \text{m year}^{-1}, \tag{52}$$

where we took $\langle \alpha \rangle = 1.5 \times 10^{-4}$ K^{-1} as a global mean thermal expansion coefficient, $\mathcal{V} \approx 1.3 \times 10^{18}$ m^3 as the global ocean volume, and $\mathcal{A} \approx 3.6 \times 10^{14}$ m^2 as the global ocean surface area. Based on the global mean of 6×10^{-5} m year^{-1} for geothermal heating given in Fig. 8, we conclude that geothermal heating contributes roughly 15 times more to global mean sea level rise than Joule heating.

3.4.2. Boundary salt fluxes and sea ice

For most purposes of ocean climate modelling, the mass flux of salt into the liquid ocean is limited to exchanges associated with the formation and melt of sea ice

$$Q^{(S)} = Q_{\text{ice-ocean salt exchange}}, \tag{53}$$

which arises since the salinity of sea ice is nonzero (on the order of 5 parts per thousand). Hence, as sea ice forms, it extracts a small amount of salt from the liquid ocean, and a larger amount of liquid freshwater. The converse happens upon melting sea ice.

So how does the formation and melt of sea ice impact global mean sea level? First, there is a transfer of mass between the solid and liquid phases. In particular, salt and freshwater transfer affect the mass of the liquid ocean through the mass flux Q_m appearing in Eq. (41) in the form

$$\left(\frac{\partial \eta}{\partial t}\right)_{\text{sea ice mass exchange}} = \frac{Q^{(S)} + Q_w}{\rho(\eta)} \tag{54}$$

with Q_w the mass flux from freshwater. As salt and freshwater are added to the ocean through sea ice melt, they raise the global mean liquid sea level according to this expression. However, the transfer of mass from the solid to liquid phase leads to near zero net change in the effective sea level, since the liquid ocean response to sea ice loading is consistent with an inverse barometer (see Appendix C). This mass transfer includes the transfer of both freshwater and salt. Most ocean and sea ice models used for climate studies ignore the mass of salt when computing the liquid ocean mass and solid sea ice mass. So in practice, the mass transfer referred to here occurs only through the transfer of freshwater.

In addition to exchanging mass, there is an exchange of buoyancy as salt is moved between the solid and liquid phases. Changing buoyancy at the ocean surface impacts the non-Boussinesq steric effect according to

$$\left(\frac{\partial \eta}{\partial t}\right)_{\text{surface salt buoyancy}} \equiv -\left(\frac{\beta Q^{(S)}}{\rho}\right). \tag{55}$$

As salt is added to the upper ocean through ice melt, this process removes buoyancy. Fig. 9 illustrates this effect. The lower latitude boundary of sea ice is where most of the ice melts over the course of a year, and it is here that the non-Boussinesq steric effect is negative due to the introduction of salt back into the liquid ocean (thus reducing buoyancy) upon melting sea ice. The converse occurs in the regions where sea ice tends to form. Additionally, mixing processes will modify ocean salinity and impact sea level through halosteric effects. Such mixing processes are represented in the sea level equation (41) by the salt flux terms where $\mathbf{J}^{(S)}$ appears.

The magnitude of the non-Boussinesq steric effect from salt induced buoyancy fluxes in Fig. 9 is locally about 100 times smaller than that from the net surface heat fluxes shown in Fig. 7. We are therefore justified, for quantitative purposes, ignoring the surface salt flux contribution when concerned with global sea level evolution. This point is further supported by noting that the bulk of the ocean is ice-free, so the salt mass in the global ocean is very close to constant in time. Correspondingly, changes in the mean ocean salinity arise mostly through changes in the global ocean volume. When computing global means for quantities such as salinity and temperature, ocean volume changes are tiny relative to the volume associated with a resting ocean. Hence, a constant salt mass for the World Ocean implies a nearly constant mean salinity. Correspondingly, as discussed further in Section 4.5, changes in global mean sea level during the 20th century are dominated by changes in global mean temperature and increases in land ice melt, whereas contributions from changes in global mean salinity are tiny by comparison.

The above statement regarding the tiny contribution of salt fluxes in the real ocean are contrasted by the sometimes nontrivial contribution of salt fluxes associated with salinity restoring used in ocean–ice simulations. As detailed in Griffies et al. (2009), global

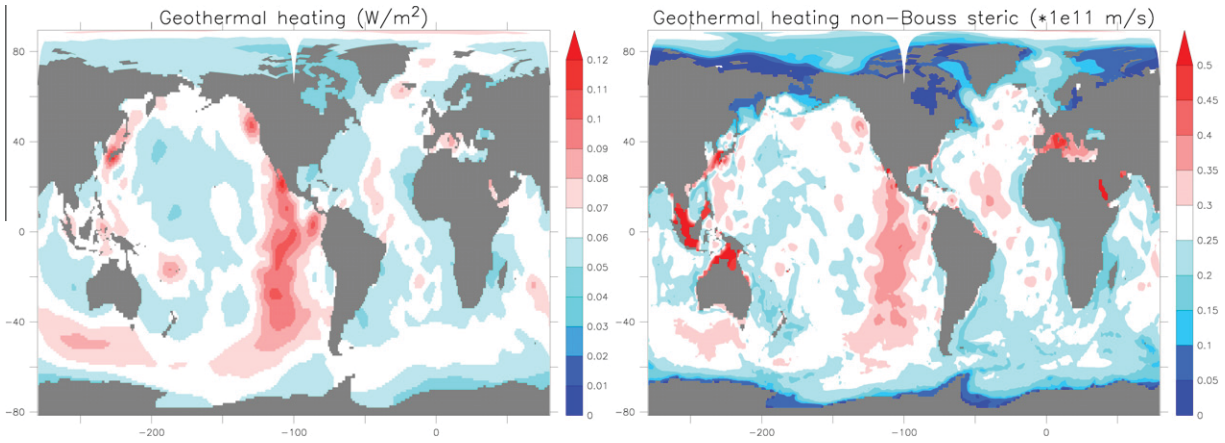

Fig. 8. Map of the geothermal heating used in the simulations, with details of this field given in Appendix B. Also shown is the associated map of the 20 year mean contribution from ocean geothermal heating to the non-Boussinesq steric effect (see Eq. (41)). Note that all values are greater than zero. The relatively large positive values in the shallow seas, such as the Indonesian Archipelago and Red Sea, arise from the relatively large thermal expansion coefficient (Fig. 6) in these regions that multiply the modest values of geothermal heating. The opposite occurs in the high latitudes, where the thermal expansion coefficient is relatively small. The global ocean mean for this map is 2.6×10^{-12} m s^{-1} = 8×10^{-5} m year^{-1}.

ocean–ice models often use salinity restoring to retain stability of the large-scale overturning circulation. The simulation used in this paper sets the global mean of the salt flux to zero on each time step. However, the slight spatial dependence of the haline contraction coefficient and sea surface density give rise to a modest nonzero value for the sea level contribution (Fig. 9).

4. Evolution of global mean sea level

We present in this section two versions of the evolution equation for global mean sea level.

4.1. Preliminaries

We begin by establishing some notation and restating assumptions. For this purpose, write the volume of liquid seawater in the global ocean in the following equivalent manners

$$\mathcal{V} = \int_{\text{globe}} dA \int_{-H}^{\eta} dz = \int_{\text{globe}} (\eta + H) dA = \mathcal{A}(\overline{H} + \overline{\eta}). \tag{56}$$

In the final step, we introduced the global ocean surface area

$$\mathcal{A} = \int_{\text{globe}} dA = \int_{\text{globe}} dx\, dy, \tag{57}$$

the global mean sea level

$$\bar{\eta} = \mathcal{A}^{-1} \int_{\text{globe}} \eta\, dA, \tag{58}$$

and the global mean ocean depth beneath a resting sea surface at $z = 0$

$$\overline{H} = \mathcal{A}^{-1} \int_{\text{globe}} H\, dA. \tag{59}$$

We assume throughout this paper that the ocean surface area remains constant in time. That is, we do not consider changes in sea level associated with shoreline changes. We also assume that the ocean depth $z = -H(x,y)$ remains constant in time. An evolution equation for the global ocean volume is therefore equivalent to an evolution equation for global mean sea level

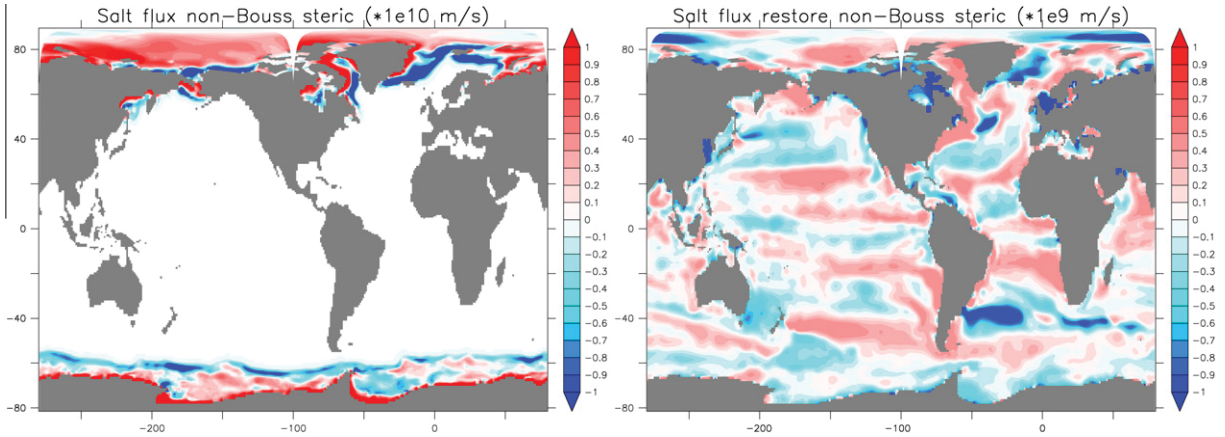

Fig. 9. Map of the 20 year mean contribution to the non-Boussinesq steric effect from salt fluxes. The first panel arises just from salt exchanged with sea ice (see Eq. (41)), according to the surface ocean buoyancy flux term $-\beta Q^{(S)}/\rho$. The sea ice in this simulation is assumed to contain a uniform salinity of five parts per thousand. The global ocean area mean for this map is 2×10^{-14} m s^{-1} = 6×10^{-7} m year^{-1}. The second panel arises from the salinity restoring term applied to the ocean–ice simulation according to the discussion in Griffies et al. (2009). Note the different scalings applied to these two patterns (noted on figure title). The global net salt flux from this restoring is set to zero on each time step, so the impact on global mean sea level arises solely from the spatial dependence of the haline contraction coefficient and the surface density. The global ocean area mean for this map is -1×10^{-12} m s^{-1} = -3×10^{-5} m year^{-1}.

$$\partial_t \mathcal{V} = \mathcal{A} \partial_t \bar{\eta}. \tag{60}$$

4.2. Global mean sea level and the non-Boussinesq steric effect

The first version of the global mean sea level equation is formulated starting from Version I of the kinematic sea level equation (1), rewritten here for completeness

$$\frac{\partial \eta}{\partial t} = \frac{Q_m}{\rho(\eta)} - \nabla \cdot \mathbf{U} - \int_{-H}^{\eta} \left(\frac{1}{\rho} \frac{d\rho}{dt} \right) dz. \tag{61}$$

A global integration, with no-flux side walls or periodic domains, leads to

$$\partial_t \bar{\eta} = \overline{\left(\frac{Q_m}{\rho(\eta)} \right)} - \frac{\mathcal{V}}{\mathcal{A}} \left\langle \frac{1}{\rho} \frac{d\rho}{dt} \right\rangle, \tag{62}$$

where

$$\langle \psi \rangle = \mathcal{V}^{-1} \int_{\text{globe}} dA \int_{-H}^{\eta} \psi \, dz \tag{63}$$

is the global volume mean of a field. The relation (62) says that the global mean sea level changes in time according to (A) the area mean of the mass flux multiplied by the specific volume of seawater at the ocean surface, and (B) the global mean of the non-Boussinesq steric effect. To uncover some of the physical processes that impact global sea level, consider the unpacked version of Eq. (62), obtained by taking a global area integral of the sea level equation (41)

$$\begin{aligned} \mathcal{A} \partial_t \bar{\eta} = & \int_{\text{globe}(z=\eta)} \left(\frac{Q_m + \alpha Q^{(\Theta)} - \beta Q^{(S)}}{\rho} \right) dA \\ & + \int_{\text{globe}(z=-H)} \left(\frac{Q_m + \alpha Q^{(\Theta)} - \beta Q^{(S)}}{\rho} \right) dA \\ & + \int_{\text{globe}} \Big(\mathbf{J}^{(\Theta)} \cdot \nabla(\alpha/\rho) - \mathbf{J}^{(S)} \cdot \nabla(\beta/\rho) \\ & - \frac{1}{\rho c_{\text{sound}}^2} \frac{dp}{dt} + \alpha \mathcal{S}^{(\Theta)} - \beta \mathcal{S}^{(S)} \Big) dV. \end{aligned} \tag{64}$$

There are two typical assumptions made in regards to the bottom boundary fluxes.

1. Zero water fluxes enter the ocean through the solid earth boundary.
2. There may be nonzero boundary heat or salt fluxes. However, as noted in Section 3.4.2, salt exchanged through ocean boundaries is generally limited to a small exchange associated with sea ice formation and melt, with negligible amounts transferred across the ocean bottom.

4.3. Boundary mass fluxes and global mean sea level

The boundary mass flux term $Q_m/\rho(\eta)$ appearing in the global mean sea level equation (64) provides for a rise of sea level upon adding mass to the ocean through Q_m, with a conversion to a volume flux made through multiplication by the surface specific volume $1/\rho(\eta)$. In principle there is not much more to discuss in regards to how this boundary term impacts the global mean sea level. As highlighted by the appendix to Lowe and Gregory (2006) (see also Munk (2003)), there are subtleties that warrant further discussion. These subtleties related to how ocean properties are modified when the boundary mass mixes with the ambient seawater, with such mixing impacting the non-Boussinesq steric effect through material changes in ρ.

Consider the case of a freshwater boundary flux. Mixing of this water with the ambient seawater is facilitated through turbulent processes and/or transport by large scale currents. Mixing of freshwater dilutes the seawater (i.e., it becomes fresher), and dilution causes seawater density to decrease. Conversely, the freshwater that entered the ocean becomes saltier as it mixes with seawater, so that its density increases. A similar story holds when, for example, cold precipitating water is added to a warm surface ocean. Upon mixing, the seawater cools, which increases seawater density, with this process complemented by a warming of the fresh precipitating water and the consequent reduction of its density.

The question arises: will there be an exact compensation, so that the global mean sea level is only modified by the added mass from freshwater? Or is there an additional contribution from changes in density as through mixing, with such impacting the non-Boussinesq steric effect? It is unlikely that exact compensation will be the norm, since much depends on specifics of the mixing processes, the temperature and salinity distributions, and the equation of state for seawater. However, we can make some approximate statements in regards to salinity.

For this purpose, return to the global mean sea level Eq. (64). As stated above, there are two terms that impact global mean sea level when freshwater is transferred across the ocean boundary: (A) the boundary flux term $Q_m/\rho(\eta)$ which changes the volume of seawater through changes in seawater mass; (B) the source term defined by Eq. (42), with the source term a function of the equation of state, ocean dynamics, and subgrid scale processes. In many circumstances, we may ignore salinity contributions to the source term, since the magnitude of horizontal gradients in β/ρ are far smaller than gradients in α/ρ (see Fig. 6). In such cases, we are led to the conclusion that the dilution effect upon adding freshwater to the ocean is smaller than the effect of adding or subtracting volume to the ocean through the boundary term $Q_m/\rho(\eta)$. This is yet another reason that for global sea level studies it is often a good approximation to ignore the impact of salinity changes. That is, besides having far smaller surface boundary contributions due to there being a regional limitation to areas with sea ice, salt contributions to global mean sea level through the halosteric effect are smaller than thermosteric contributions. In Section 4.5, we reach a similar conclusion through alternative means.

4.4. Raising sea level with a given amount of heat

Where is heat most effective at raising global sea level? Is it more effective if used to melt land ice and allow the melt water to enter the ocean? Or should the heat go directly into warming the ocean, thus impacting a thermosteric sea level rise? The answer to this question is determined by fundamental properties of water, with the global mean sea level equation (64) providing details (see also Trenberth (2009)).

Assume that the heating, Q_{heat}, is spatially constant and for it to heat the upper ocean boundary layer. The tendency for thermosteric sea level rise, given from Eq. (64), takes the form

$$\left(\frac{\partial \bar{\eta}}{\partial t} \right)_{\text{thermosteric}} \approx \frac{Q_{\text{heat}} \langle \alpha \rangle}{\rho_o c_p}, \tag{65}$$

where $c_p \approx 3992.1 \text{ J kg}^{-1} \text{ K}^{-1}$ is the seawater specific heat capacity, and $\langle \alpha \rangle$ is the averaged thermal expansion coefficient for the region where heating is applied. If the same heating Q_{heat} is instead used to melt land ice, and we assume the land ice is at the freezing point and the resulting water mass enters the ocean, then the associated tendency in global sea level is given by

$$\left(\frac{\partial \bar{\eta}}{\partial t} \right)_{\text{melt}} \approx \frac{Q_m}{\rho_o} = \frac{Q_{\text{heat}}}{\rho_o H^{\text{fusion}}}, \tag{66}$$

where $H^{\text{fusion}} \approx 3.34 \times 10^5 \text{J kg}^{-1}$ is the latent heat of fusion. The ratio of the two sea level tendencies (66) and (65) is given by

$$\frac{(\partial\bar{\eta}/\partial t)_{\text{melt}}}{(\partial\bar{\eta}/\partial t)_{\text{thermosteric}}} = \frac{c_{\text{p}}}{\langle\alpha\rangle H^{\text{fusion}}}, \tag{67}$$

which is a function of thermodynamic properties of seawater. This ratio varies by roughly a factor of ten between the tropics, where α is relatively large and seawater thus relatively compressible, and the high latitudes, where α is smaller and seawater correspondingly less compressible (see Fig. 6). For melting low latitude land ice (e.g., tropical mountain glaciers), we set $\langle\alpha\rangle = 10^{-4}\,\text{K}^{-1}$, in which case

$$\frac{(\partial\bar{\eta}/\partial t)_{\text{melt}}}{(\partial\bar{\eta}/\partial t)_{\text{thermosteric}}} \approx 100. \tag{68}$$

Higher latitude melt is another factor of ten more efficient due to the smaller thermal expansion. A similar picture applies if calving land ice enters the ocean, in which case the added mass raises sea level 100–1000 times more than the reduction of sea level associated with the latent heat loss to melt the ice.

In summary, the use of heat to melt land ice is roughly 100–1000 times more efficient at raising global mean sea level than using the same heat to raise sea level through thermosteric effects. The huge ratio reflects the largely incompressible nature of seawater. However, even with this large difference in efficiency, thermosteric effects remain important for global mean sea level due to the far larger area encompassed by the liquid ocean than regions with land ice.

4.5. Global mean sea level and the global steric effect

Eq. (62), and its unpacked version (64), help us to understand how physical processes and boundary effects impact the global mean sea level. However, if one is only interested in the net effect on sea level, then an alternative formulation is appropriate. This second version of the evolution equation for global mean sea level is developed by introducing the following relation between the total mass of liquid seawater, total volume of seawater, and global mean seawater density,

$$\mathcal{M} = \mathcal{V}\langle\rho\rangle. \tag{69}$$

In this relation,

$$\mathcal{M} = \int_{\text{globe}} \text{d}A \int_{-H}^{\eta} \rho\, \text{d}z \tag{70}$$

is the global liquid seawater mass, and $\mathcal{V}$ is the global volume of seawater (Eq. (56)). It follows that

$$\partial_t\mathcal{M} = \mathcal{V}\partial_t\langle\rho\rangle + \langle\rho\rangle\partial_t\mathcal{V}. \tag{71}$$

An area integration of the mass budget (4) indicates that total seawater mass changes if there is a nonzero mass flux across the ocean surface

$$\partial_t\mathcal{M} = \mathcal{A}\overline{\text{Q}_{\text{m}}}, \tag{72}$$

where

$$\overline{\text{Q}_{\text{m}}} = \mathcal{A}^{-1}\int_{\text{globe}} \text{Q}_{\text{m}}\, \text{d}A \tag{73}$$

is the global mean mass per horizontal area per time crossing the ocean boundaries. Bringing these results together, and recalling that $\partial_t\mathcal{V} = \mathcal{A}\partial_t\bar{\eta}$ (Eq. (60)) leads to the second evolution equation for the global mean sea level

$$\partial_t\bar{\eta} = \frac{\overline{\text{Q}_{\text{m}}}}{\langle\rho\rangle} - \left(\frac{\mathcal{V}}{\mathcal{A}}\right)\frac{\partial_t\langle\rho\rangle}{\langle\rho\rangle}. \tag{74}$$

As in the formulation given in Section 4.2, there is no direct contribution from ocean currents, since they act to redistribute volume without changing the total volume. The first term on the right hand side of Eq. (74) alters sea level by adding or subtracting volume from the ocean through the surface boundary. This term vanishes when the net mass flux is zero. The second term on the right hand side of Eq. (74) arises from temporal changes in the global mean density. We refer to the second term as the *global steric effect* to make a distinction from the global mean of the non-Boussinesq steric effect discussed in Section 4.2. Both terms on the right hand side of Eq. (74) are readily diagnosed from a model simulation, thus providing a means to partition the change in global mean sea level into a contribution from boundary fluxes and one from global steric changes.

Following on the arguments in Section 4.3, we comment here on the dominance of changes in global mean temperature on the global steric effect in Eq. (74). For this purpose, write the time tendency of global mean density in the form

$$\partial_t \ln\langle\rho\rangle = -\alpha_{\text{bulk}}\partial_t\langle\Theta\rangle + \beta_{\text{bulk}}\partial_t\langle S\rangle + \frac{1}{(\rho c^2_{\text{sound}})_{\text{bulk}}}\partial_t\langle p\rangle. \tag{75}$$

This equation defines α_{bulk} as a bulk, or *effective*, thermal expansion coefficient, β_{bulk} as a bulk haline contraction coefficient, and $(\rho c^2_{\text{sound}})_{\text{bulk}}$ as a bulk density times the squared sound speed. These coefficients can be thought of as best fit parameters for the linear relation (75) connecting changes in global mean sea level to global mean temperature, salinity, and pressure. The global mean salinity remains nearly constant for most climate purposes (see Section 3.4.2), in which case the salinity term vanishes. Likewise, changes in global mean pressure are quite small. Consequently, when both salt and pressure effects are sub-dominant, as they generally are, then global mean density changes are dominated by global mean temperature changes. Hence, the global mean sea level Eq. (74) takes on the approximate form

$$\partial_t\bar{\eta} \approx \frac{\overline{\text{Q}_{\text{m}}}}{\langle\rho\rangle} + \left(\frac{\mathcal{V}\alpha_{\text{bulk}}}{\mathcal{A}}\right)\partial_t\langle\Theta\rangle. \tag{76}$$

This approximate result provides a very good indicator of the 20th century global mean sea level rise associated with ocean warming (Church and Gregory, 2001; Nicholls and Cazenave, 2010).

4.6. Relating global steric to non-Boussinesq steric

Equating the two Eqs. (62) and (74) for global mean sea level yields the identity

$$\overline{\left(\frac{\text{Q}_{\text{m}}}{\rho(\eta)}\right)} - \frac{\mathcal{V}}{\mathcal{A}}\left\langle\frac{1}{\rho}\frac{\text{d}\rho}{\text{d}t}\right\rangle = \frac{\overline{\text{Q}_{\text{m}}}}{\langle\rho\rangle} - \left(\frac{\mathcal{V}}{\mathcal{A}}\right)\frac{\partial_t\langle\rho\rangle}{\langle\rho\rangle}. \tag{77}$$

Consider two special cases related to the water flux term. First, let $\overline{\text{Q}_{\text{m}}} = 0$, so there is no net change in ocean mass. In this case, the global steric effect balances the non-Boussinesq steric effect and the volume flux

$$\overline{\left(\frac{\text{Q}_{\text{m}}}{\rho(\eta)}\right)} - \frac{\mathcal{V}}{\mathcal{A}}\left\langle\frac{1}{\rho}\frac{\text{d}\rho}{\text{d}t}\right\rangle = -\left(\frac{\mathcal{V}}{\mathcal{A}}\right)\frac{\partial_t\langle\rho\rangle}{\langle\rho\rangle} \quad \text{if } \overline{\text{Q}_{\text{m}}} = 0. \tag{78}$$

Note that $\overline{(\text{Q}_{\text{m}}/\rho(\eta))}$ generally does not vanish since $\rho(\eta)$ is non-constant. This result emphasizes the distinction between the global steric and non-Boussinesq steric terms. Only if we specialize to the case of identically zero mass flux can we identify the global mean of the non-Boussinesq steric effect to the global steric effect

$$\left\langle\frac{1}{\rho}\frac{\text{d}\rho}{\text{d}t}\right\rangle = \frac{\partial_t\langle\rho\rangle}{\langle\rho\rangle} \quad \text{if } \text{Q}_{\text{m}} = 0. \tag{79}$$

As explored in Section D.3 of Appendix D, this result motivates a commonly used method to adjust the sea level in Boussinesq models, even in the presence of nonzero boundary fluxes of mass.

5. Vertical mixing and global mean sea level

This section is the first of three to further explore the non-Boussinesq steric effect discussed in Sections 3 and 4. The focus here is on how subgrid scale fluxes of conservative temperature and salinity arising from vertical mixing in the ocean interior determine patterns of the non-Boussinesq steric effect. Vertical diffusion is the traditional method used by global ocean climate models to parameterize the impacts from dianeutral mixing processes. Additional non-local mixing effects are prescribed by the KPP scheme of Large et al. (1994) used in our numerical model. We consider both of these mixing processes in this section.

5.1. Contributions from vertical diffusion

Recall that we have already discussed in Sections 3.3 and 3.4 those contributions from boundary fluxes of buoyancy. Hence, the impacts of concern here from vertical diffusion involve just contributions to the source term (Eq. (42))

$$(\mathbf{J}^{(\Theta)} \cdot \nabla(\alpha/\rho) - \mathbf{J}^{(S)} \cdot \nabla(\beta/\rho))_{\text{vertical diffusion}} = -\rho[D^{(\Theta)}\partial_z\Theta\partial_z(\alpha/\rho) - D^{(S)}\partial_z S\partial_z(\beta/\rho)]. \tag{80}$$

Here, we consider the tracer flux to equal that arising from downgradient vertical diffusion

$$\mathbf{J}^{(\Theta)} = -\rho D^{(\Theta)}\partial_z\Theta\hat{\mathbf{z}}, \tag{81}$$

$$\mathbf{J}^{(S)} = -\rho D^{(S)}\partial_z S\hat{\mathbf{z}} \tag{82}$$

with eddy diffusivities for conservative temperature and salinity, $D^{(\Theta)} > 0$ and $D^{(S)} > 0$. This flux is meant to parameterize mixing arising from dianeutral processes (see Section 7.4.3 of Griffies (2004) for discussion). In the ocean interior, the diffusivities have values $D \approx 10^{-6}\ \text{m}^2\ \text{s}^{-1}$ at the equator, beneath the regions of strong vertical shears associated with the equatorial undercurrent (Gregg et al., 2003), and $D \approx 10^{-5}\ \text{m}^2\ \text{s}^{-1}$ in the middle latitudes (Ledwell et al., 1993, 2011), with far larger values near rough topography and other boundary regions (Polzin et al., 1997; Naveira-Garabato et al., 2004). Additionally, D can be set to a very large value in gravitationally unstable regions, as is done for the model simulation used here. Finally, differences in the temperature and salinity diffusivities arise from double diffusive processes (Schmitt, 1994).

Fig. 10 shows the contribution (80) to the non-Boussinesq steric effect arising from vertical diffusion in the model simulation detailed in Appendix B. The contribution is negative in most regions, with the exception of a few locations in the subpolar North Atlantic. That is, vertical diffusion predominantly acts to reduce global mean sea level through the non-Boussinesq steric effect. The dominant regions contributing to this reduction are those associated with strong deep mixing, such as near the sea ice edge in the North Atlantic.

To help understand why the non-Boussinesq steric effect associated with vertical diffusion is predominantly negative, we further unpack the contribution (80). For simplicity, assume $D^{(\Theta)} = D^{(S)} = D$ so to eliminate double diffusive processes. Start by performing the partial derivatives on the specific volume

$$\partial_z(\alpha/\rho) = \rho^{-1}(\partial_z\alpha - \alpha\rho^{-1}\partial_z\rho), \tag{83}$$

$$\partial_z(\beta/\rho) = \rho^{-1}(\partial_z\beta - \beta\rho^{-1}\partial_z\rho), \tag{84}$$

and substitute into Eq. (80) to find

$$-\rho D[\partial_z\Theta\partial_z(\alpha/\rho) - \partial_z S\partial_z(\beta/\rho)] = -D(\partial_z\alpha\partial_z\Theta - \partial_z\beta\partial_z S) - D\rho^{-1}\partial_z\rho(-\alpha\partial_z\Theta + \beta\partial_z S). \tag{85}$$

Next, write

$$\partial_z\rho(-\alpha\partial_z\Theta + \beta\partial_z S) = \left(\frac{N\rho}{g}\right)^2 (N^2 + (g/c_{\text{sound}})^2), \tag{86}$$

where $c_{\text{sound}}^{-2} = \partial\rho/\partial p$ is the inverse squared sound speed,

$$N^2 = g(\alpha\partial_z\Theta - \beta\partial_z S) \tag{87}$$

is the squared buoyancy frequency, and we assumed a hydrostatic fluid so that $\partial_z p = -\rho g$. Bringing these results together renders (again, assuming $D^{(\Theta)} = D^{(S)} = D$)

$$(\mathbf{J}^{(\Theta)} \cdot \nabla(\alpha/\rho) - \mathbf{J}^{(S)} \cdot \nabla(\beta/\rho))_{\text{vertical diffusion}} = -DN^2((N/g)^2 + c_{\text{sound}}^{-2}) - D(\partial_z\alpha\partial_z\Theta - \partial_z\beta\partial_z S). \tag{88}$$

The first term in Eq. (88) is negative, so long as the vertical stratification is stable ($N^2 > 0$). This term is present even for a fluid with a constant thermal expansion and haline contraction coefficient. The second term arises from the depth dependence of α and β, scaled by the vertical derivative of conservative temperature and salinity, respectively. For the World Ocean, the salinity term, $\partial_z\beta\partial_z S$, is generally far smaller in magnitude than the temperature term, $\partial_z\alpha\partial_z\Theta$. Indeed, all terms appearing in Eq. (88) are dominated by the temperature term, which is generally positive throughout the upper 1500 m of the ocean, with largest values in the lower latitudes where vertical gradients are strongest. It is in this depth range that both $\partial_z\Theta$ and $\partial_z\alpha$ are positive and relatively large, so that the generally positive nature of the temperature term $\partial_z\alpha\partial_z\Theta$ is the key contributor to the predominantly negative sea level tendency seen in Fig. 10 arising from vertical diffusion. This result represents an example in which the dominance of the inequality (45) provides the reason why sea level falls as the result of a subgrid scale process.

So in summary, sea level drops through the effects from vertical diffusion of heat in the upper 1500 m of ocean, where diffusion moves heat from a region of large thermal expansion (upper ocean) to a region of small thermal expansion (mid-depth ocean around 1000–1500 m). Downward vertical diffusion in the ocean deeper than 1500 m acts to raise sea level, since the thermal expansion coefficient gets larger below roughly 1500 m. However, the vertical temperature gradients are relatively small below 1500 m, making the deep ocean diffusion far subdominant to vertical heat diffusion in the upper ocean. Regions in the North Atlantic where mixing penetrates deeper than 1500 m are exceptions, in which case such deep vertical mixing of heat contributes to sea level rise.

5.2. Contributions from KPP non-local mixing

Fig. 10 shows the contribution to the non-Boussinesq steric effect from the non-local aspect of KPP. Note the generally negative tendencies appearing in the deep water and mode water formation regions. There is a very slight positive tendency appearing in the lower latitudes. As for vertical diffusive mixing, the net impact from the KPP nonlocal mixing scheme is to reduce global mean sea level, with physical interpretation largely as for vertical diffusion and its relation to the thermal expansion coefficient. That is, so long as heat is moved from warm to cold, this process will reduce sea level since it means heat is moved from regions of large thermal expansion to smaller.

6. Neutral diffusion and global mean sea level

Mesoscale eddy motions impact the large-scale ocean temperature and salinity distributions in important and nontrivial ways, with their parameterization in coarsely resolved climate models a longstanding focus of theoretical physical oceanography. Amongst the common means for parameterizing these effects is to prescribe a diffusion of temperature and salinity oriented according to the

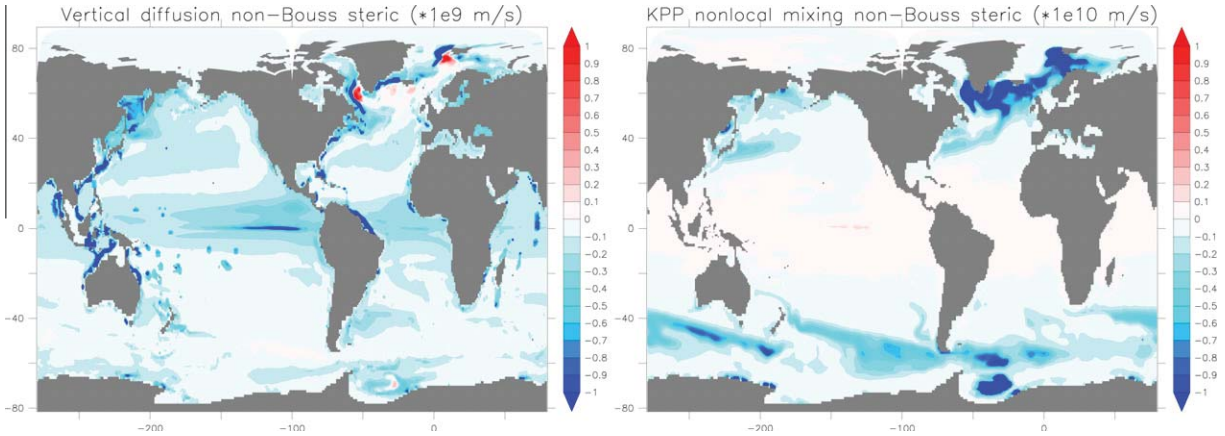

Fig. 10. The first panel shows the contribution (43) to the non-Boussinesq steric effect from vertical diffusion from the model simulation described in Appendix B. Note the patchy regions in the West Pacific arise from areas of enhanced vertical diffusion associated with the ocean model's tide mixing parameterizations (Simmons et al., 2004; Lee et al., 2006). The large values in the North Atlantic arise from mixing in deep water formation regions. Positive contributions to sea level typically occur in regions that mix into depths where $\partial_z \alpha < 0$ (deeper than roughly 1500 m) and negative sea level tendencies elsewhere. The global ocean mean for this map is -1.6×10^{-10} m s^{-1} = -5×10^{-3} m year^{-1}. The second panel shows the contribution (44) from the KPP nonlocal mixing process (Large et al., 1994). There are large values in the deep water and mode water formation regions, with the global mean impact a reduction in sea level. The global ocean mean for this map is -9×10^{-12} m s^{-1} = -3×10^{-4} m year^{-1}. Note the different scalings applied to the two patterns (noted on figure titles).

planes tangent to locally referenced potential density surfaces (Solomon, 1971; Redi, 1982; Olbers et al., 1985; McDougall and Church, 1986; Cox, 1987; Gent and McWilliams, 1990; Griffies et al., 1998). To expose how this neutral diffusion process impacts sea level first requires the establishment of its salient physical and mathematical properties. Thereafter, we describe how the physical processes of cabbeling and thermobaricity impact global mean sea level. Note that following McDougall (1987b) (see also Klocker and McDougall, 2010a; Klocker and McDougall, 2010b; IOC et al., 2010), we are concerned with cabbeling and thermobaricity as dianeutral transport processes that arise from a coarse-grained perspective of the mixing of fluid parcels by mesoscale eddies along neutral directions. We are not concerned with how molecular diffusion or vertical diffusion can be formulated in terms of micro-scale cabbeling and thermobaricity processes.

6.1. Neutral directions and neutral tangent plane

Following McDougall (1987a), we introduce the notion of a neutral direction by considering an infinitesimal displacement d $\mathbf{x}$, in which the *in situ* density changes according to

$$\mathrm{d}\rho = \rho\, \mathrm{d}\mathbf{x} \cdot \left(-\alpha \nabla \Theta + \beta \nabla S + \frac{1}{\rho c_s^2} \nabla p \right). \tag{89}$$

Under adiabatic and isohaline motions, the density change is associated just with pressure changes

$$(\mathrm{d}\rho)_{\text{adiabic/isohaline}} = \rho\, \mathrm{d}\mathbf{x} \cdot \left(\frac{1}{\rho c_s^2} \nabla p \right). \tag{90}$$

Therefore, if we consider an adiabatic and isohaline displacement, the difference in density between the parcel and the surrounding environment is given by

$$\begin{aligned} \mathrm{d}\rho - (\mathrm{d}\rho)_{\text{adiabatic/isohaline}} &= \rho \mathrm{d}\mathbf{x} \cdot (-\alpha \nabla \Theta + \beta \nabla S) \\ &= \rho \mathrm{d}\mathbf{x} \cdot \hat{\boldsymbol{\gamma}} | - \alpha \nabla \Theta + \beta \nabla S |, \end{aligned} \tag{91}$$

where the *dianeutral unit vector* is defined by

$$\hat{\boldsymbol{\gamma}} = \frac{-\alpha \nabla \Theta + \beta \nabla S}{|-\alpha \nabla \Theta + \beta \nabla S|}. \tag{92}$$

At each point in the fluid, displacements orthogonal to $\hat{\boldsymbol{\gamma}}$ define neutral directions, and the accumulation of such displacements define a *neutral tangent plane*.

6.2. Fluxes computed with locally orthogonal coordinates

There are two means to write the neutral diffusion fluxes for a tracer. The first follows from Redi (1982), who considers the three dimensional fluxes computed parallel to the local neutral direction. This is an approach that arises naturally if working in local orthogonal coordinates (Griffies et al., 1998; Griffies, 2004)

$$\mathbf{J}^{(\Theta)} = -\rho A_n [\nabla \Theta - \hat{\boldsymbol{\gamma}} (\hat{\boldsymbol{\gamma}} \cdot \nabla \Theta)], \tag{93}$$

$$\mathbf{J}^{(S)} = -\rho A_n [\nabla S - \hat{\boldsymbol{\gamma}} (\hat{\boldsymbol{\gamma}} \cdot \nabla S)]. \tag{94}$$

In this equation, $A_n > 0$ is a diffusivity (units of squared length per time) setting the magnitude of the neutral diffusive fluxes. Geometrically, the neutral diffusive fluxes of conservative temperature, $\mathbf{J}^{(\Theta)}$, and salinity, $\mathbf{J}^{(S)}$, are proportional to that portion of the tracer gradient parallel to the neutral directions. Hence, by construction,

$$\mathbf{J}^{(\Theta)} \cdot \hat{\boldsymbol{\gamma}} = 0, \tag{95}$$

$$\mathbf{J}^{(S)} \cdot \hat{\boldsymbol{\gamma}} = 0. \tag{96}$$

6.3. Fluxes computed with projected neutral coordinates

The second means for computing neutral diffusive fluxes follows from Gent and McWilliams (1990), whereby we employ the projected coordinates used in generalized vertical coordinate models (see Starr, 1945; Bleck, 1978; McDougall, 1995, or Chapter 6 of Griffies (2004)), here applied to the locally defined neutral tangent plane as in McDougall (1987a). To use this framework requires a vertically stable stratification. Here, lateral gradients of a tracer are computed along the neutral direction, but the lateral distance used to compute the gradient is taken as the distance on the horizontal plane resulting from projecting the neutral slope onto the constant depth surfaces (see, for example, Fig. 6.4 in Griffies, 2004). For this case, the horizontal and vertical components of the neutral diffusion tracer fluxes take the form

$$\mathbf{J}^h = -A_n \rho \nabla_n C, \tag{97}$$

$$J^z = -A_n \rho \boldsymbol{S} \cdot \nabla_n C, \tag{98}$$

where the projected lateral gradient operator is given by

$$\nabla_n = \nabla_z + \boldsymbol{S} \partial_z. \tag{99}$$

Just as for the fluxes associated with orthogonal coordinates, we have $\mathbf{J} \cdot \hat{\boldsymbol{\gamma}} = 0$, which ensures that the fluxes are indeed aligned with neutral directions. Furthermore, these flux components are equal to the Redi (1982) flux components in the limit that the magnitude of the neutral slope

$$\boldsymbol{S} = -\left(\frac{-\alpha \nabla_z \Theta + \beta \nabla_z S}{-\alpha \partial_z \Theta + \beta \partial_z S}\right) \tag{100}$$

becomes small. Because of this connection, the neutral diffusion fluxes associated with projected neutral coordinates are known as the *small slope* fluxes. However, there is no approximation involved with using the small slope fluxes, so long as the vertical stratification is stable. Rather, their use represents a choice associated with how we measure lateral distances when computing gradients. Since the small slope fluxes are directly related to those along-isopycnal fluxes used in isopycnal models, they are more commonly used in level models than the fluxes of Redi (1982). The small slope fluxes are also simpler to compute, as they involve fewer terms.

6.4. Compensating neutral diffusive fluxes of temperature and salinity

It is straightforward to show that either of the neutral diffusive fluxes defined in Section 6.2 or Section 6.3 satisfy the identity

$$\alpha \mathbf{J}^{(\Theta)} - \beta \mathbf{J}^{(S)} = 0. \tag{101}$$

That is, each component of the neutral diffusive flux of buoyancy vanishes, by definition. This is a key property of neutral diffusion, which in particular means that neutral diffusion directly contributes to the non-Boussinesq steric effect only through the source term defined by Eq. (42).

6.5. The cabbeling and thermobaricity parameters

To help further elucidate how neutral diffusion impacts the non-Boussinesq steric effect, and hence global mean sea level, we manipulate the source term (42) for the case of neutral diffusive fluxes. The steps are presented in Appendix E, with the final result being

$$\begin{aligned}&(\mathbf{J}^{(\Theta)} \cdot \nabla(\alpha/\rho) - \mathbf{J}^{(S)} \cdot \nabla(\beta/\rho))_{\text{neutral diffusion}} \\ &\quad = \rho^{-1} \mathbf{J}^{(\Theta)} \cdot (\mathcal{T} \nabla p + \mathcal{C} \nabla \Theta).\end{aligned} \tag{102}$$

The cabbeling parameter $\mathcal{C}$ and thermobaricity parameter $\mathcal{T}$ are given by Eqs. (103) and (108) discussed in the following. We now consider some of the physical implications of this result.

6.6. Physical aspects of cabbeling

Consider the mixing of two water parcels along a neutral direction through the action of mesoscale eddies. Let the parcels separately have distinct conservative temperature and/or salinity, but equal locally referenced potential density. If the equation of state were linear (Section A.5), then the resulting mixed parcel would have the same density as the unmixed separate parcels. Due to the more general equilibrium thermodynamics in the ocean, in which there is a dependence of density on temperature, salinity, and pressure, the mixed parcel actually has a different density. Furthermore, the density of the mixed parcel is greater than the unmixed parcels. This densification upon mixing is a physical process known as *cabbeling* (McDougall, 1987b). The upper two panels of Fig. 11 shows the cabbeling parameter (103) from the ocean model described in Appendix B. Note how the parameter is largest in the higher latitudes, and smaller in the upper ocean midlatitudes and tropics.

The sign definite nature of cabbeling (i.e., cabbeling always results in denser parcels after mixing) is a direct result of the geometry of the locally referenced potential density surface when viewed in conservative temperature and salinity space. This property in turn manifests with the following inequality for the cabbeling parameter

$$\mathcal{C} = \frac{\partial \alpha}{\partial \Theta} + 2 \frac{\alpha}{\beta} \frac{\partial \alpha}{\partial S} - \left(\frac{\alpha}{\beta}\right)^2 \frac{\partial \beta}{\partial S} \geqslant 0, \tag{103}$$

which is an empirical property of the ocean's equilibrium thermodynamics (IOC et al., 2010).

Downgradient neutral diffusion is meant to parameterize the mesoscale eddy induced mixing of tracers along neutral directions. We verify that the neutral diffusive flux considered thus far is indeed downgradient by considering the small slope neutral diffusive flux (Eqs. (97) and (98)) to render

$$\nabla \Theta \cdot \mathbf{J}^{(\Theta)} = -A_{\mathrm{n}} \rho (\nabla_{\mathrm{n}} \Theta)^2 \leqslant 0. \tag{104}$$

Likewise, the neutral diffusive flux (93) from Redi (1982) yields

$$\nabla \Theta \cdot \mathbf{J}^{(\Theta)} = -A_{\mathrm{n}} \rho [(\nabla \Theta)^2 - (\hat{\boldsymbol{\gamma}} \cdot \nabla \Theta)^2] \leqslant 0. \tag{105}$$

Given this downgradient nature of the neutral diffusive fluxes, we have

$$\rho^{-1} \mathcal{C}\, \mathbf{J}^{(\Theta)} \cdot \nabla \Theta \leqslant 0, \tag{106}$$

thus providing a mathematical expression for the cabbeling process. That is, cabbeling results in a positive material evolution of density; i.e., density increases due to cabbeling, and this process can be interpreted as a downward or negative dianeutral transport (McDougall, 1987b).

An increase in density through cabbeling results in a reduction of sea level due to the compression of the fluid column as manifest in the non-Boussinesq steric effect

$$\left(\frac{\partial \eta}{\partial t}\right)_{\text{cab}} = -\int_{-H}^{\eta} (\mathcal{C} A_{\mathrm{n}} (\nabla_{\mathrm{n}} \Theta)^2) \mathrm{d}z < 0. \tag{107}$$

Fig. 12 illustrates the time mean impact of cabbeling on the non-Boussinesq steric effect for the global model detailed in Appendix B. To produce this figure, we chose the projected form of the neutral diffusion flux according to Section 6.3, and used the identity (104). The contribution of cabbeling is largest in the western boundary currents and the Southern Ocean. Additionaly, note the feature in the equatorial Pacific, which is associated with the equatorial undercurrent. In general, strong temperature gradients that, in the presence of salinity, can be slightly misaligned from the locally referenced potential density gradient, give rise to a nontrivial $\nabla_{\mathrm{n}} \Theta$ and thus to a contribution from cabbeling to global mean sea level evolution.

6.7. Physical aspects of thermobaricity

The thermobaricity parameter

$$\mathcal{T} = \beta \partial_p \left(\frac{\alpha}{\beta}\right) \tag{108}$$

is nonzero due to pressure dependence of the ratio of thermal expansion coefficient to haline contraction coefficient. As both thermal and haline effects are present, the parameter $\mathcal{T}$ is more precisely split into two terms

$$\mathcal{T} = \frac{\partial \alpha}{\partial p} - \frac{\alpha}{\beta} \frac{\partial \beta}{\partial p}. \tag{109}$$

Thermobaricity is the common name for the sum, since pressure variations in the thermal expansion coefficient dominate those of the haline contraction coefficient. Fig. 11 shows the thermobaricity parameter (108) from the ocean model described in Appendix B. Since the thermal expansion coefficient generally increases as pressure increases, the thermobaricity parameter is typically positive.

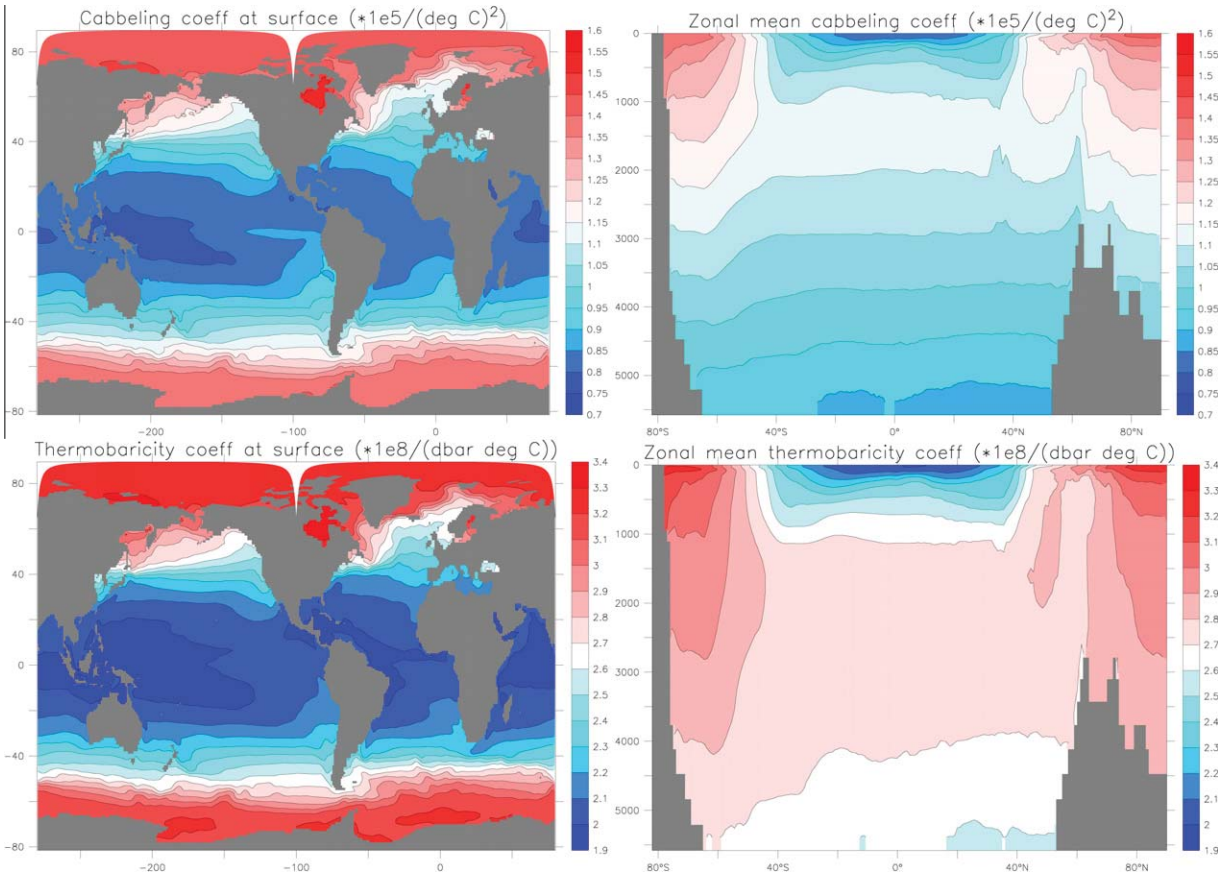

Fig. 11. Cabbeling coefficient (103) and thermobaricity coefficient (Eq. (108)) at the ocean surface and for the zonal mean, all taken from a 20 year mean in the model simulation detailed in Appendix B.

Note the larger values in the higher latitudes for the thermobaricity parameter, analogous to the situation with the cabbeling parameter. Since neutral diffusive fluxes need not be oriented in a special manner relative to the pressure gradient, there is no sign-definite nature to the thermobaricity source term

$$\begin{aligned}\rho^{-1}\mathbf{J}^{(\Theta)}\cdot\mathcal{T}\nabla p &= -A_{\mathrm{n}}\mathcal{T}(\nabla_{\mathrm{n}}\Theta+\hat{\mathbf{z}}\,\boldsymbol{S}\cdot\nabla_{\mathrm{n}}\Theta)\cdot\nabla p\\ &= -A_{\mathrm{n}}\mathcal{T}\nabla_{\mathrm{n}}\Theta\cdot\nabla_{\mathrm{n}}p.\end{aligned}\tag{110}$$

Thus, thermobaricity can either increase or decrease density. However, for the bulk of the ocean, thermobaricity tends to increase density, just as cabbeling.

Fig. 12 shows the diagnosed tendency for the non-Boussinesq steric effect from thermobaricity in the global model of Appendix B, as determined according to

$$\left(\frac{\partial\eta}{\partial t}\right)_{\text{thermob}} = -\int_{-H}^{\eta}(\mathcal{T}A_{\mathrm{n}}\nabla_{\mathrm{n}}p\cdot\nabla_{\mathrm{n}}\Theta)\mathrm{d}z.\tag{111}$$

The contribution of thermobaricity to the non-Boussinesq steric effect is generally a bit smaller than that from cabbeling (Fig. 12), though it displays some distinctive features in the Southern Ocean and western boundary currents. The global mean tendency is negative, though there are some regions with positive impact.

6.8. Horizontal diffusion in boundary regions

Following the recommendations from Treguier et al. (1997), Ferrari et al. (2008), and Ferrari et al. (2010), neutral diffusion is exponentially transitioned to horizontal diffusion in those regions where the surface boundary layer is encountered. Furthermore, following from the recommendations of Gerdes et al. (1991), neutral diffusive fluxes are converted to horizontal diffusion next to solid walls. Such boundary horizontal diffusion contributes a nontrivial level of buoyancy transformation, which in turn impacts on global mean sea level. Fig. 12 shows the contribution to the non-Boussinesq steric effect from the full rotated diffusion operator, including the effects from cabbeling, thermobaricity, and horizontal diffusion in boundary regions. As for vertical diffusion (Section 5.1), the net impact from horizontal diffusion is to reduce sea level, with a magnitude in this simulation that is comparable to that from cabbeling. Again, the reason for a sea level reduction is that the downgradient horizontal temperature fluxes are generally oriented in a direction down the gradient of the thermal expansion coefficient as per the inequality (45).

7. Parameterized quasi-Stokes transport and global mean sea level

We now consider how the parameterization of quasi-Stokes transport impacts on the non-Boussinesq steric effect with a focus on its contribution to global mean sea level.

7.1. Sea level reduction from mesoscale and submesoscale parameterizations

Fig. 13 shows the contribution to the non-Boussinesq steric effect from the Ferrari et al. (2010) mesoscale eddy parameterization, which acts physically in a manner directly analogous to the

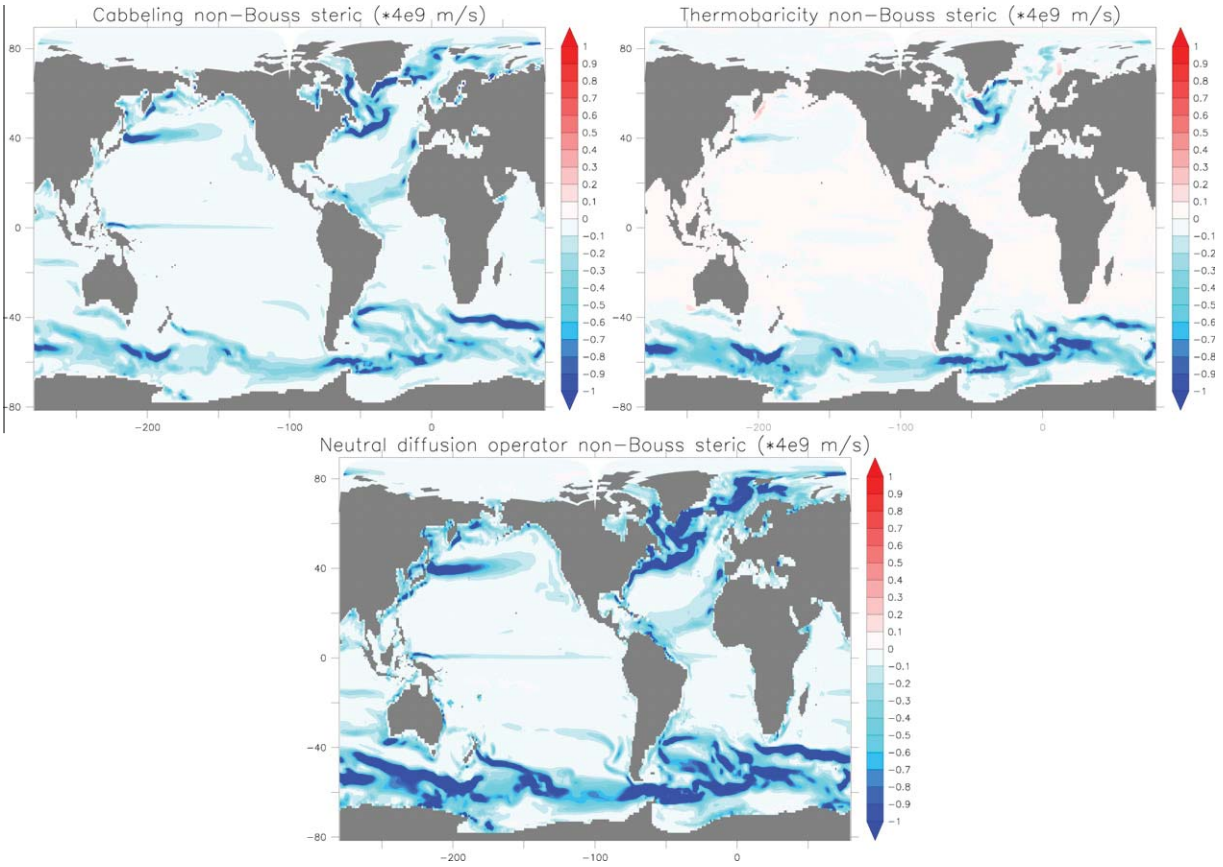

Fig. 12. A 20 year simulated mean for contributions to the non-Boussinesq steric effect from cabbeling (Eq. (107)); thermobaricity (Eq. (111)); and the full neutral diffusion operator in the form of Eq. (44), including horizontal diffusion within boundary regions. The global ocean area mean of the cabbeling contribution is -2.7×10^{-11} m s^{-1} = -8×10^{-4} m year^{-1}; the global area mean for thermobaricity is -1.5×10^{-11} m s^{-1} = -5×10^{-4} m year^{-1}; and the global mean from the horizontal boundary diffusion operator is -6.5×10^{-11} m s^{-1} = -7×10^{-4} m year^{-1}.

Gent et al. (1995) parameterization. This figure also shows the non-Boussinesq steric effect from the Fox-Kemper et al. (2008) submesoscale eddy parameterization. We exhibit both the forms (43), written as a flux projected onto gradients of α/ρ and β/ρ, as well as the weighted flux divergence form (44). Furthermore, we choose the skew flux form for both schemes (Griffies, 1998), so that the horizontal and vertical flux components are written

$$\mathbf{J}^h = -\rho \boldsymbol{\Upsilon} \partial_z C, \tag{112}$$
$$J^z = \rho \boldsymbol{\Upsilon} \cdot \nabla_z C, \tag{113}$$

where C is temperature or salinity, and the eddy induced transport, $\boldsymbol{\Upsilon}$, is given according to Ferrari et al. (2010) and Fox-Kemper et al. (2008) (see also Section A.3.2).

Fig. 13 is dominated by structure in the mode and deep water formation regions, as well as in western boundary currents, consistent with our understanding that both schemes have the most impact in regions with large baroclinicity. The submesoscale scheme has somewhat finer scale features since it acts over just the mixed layer, which experiences a strong seasonal cycle. When viewed in the form (44) as a weighted flux divergence, both the mesoscale and submesoscale schemes exhibit characteristic features of sea level rise adjacent to fall, with this behaviour expected as the schemes act to dissipate buoyancy fronts (see Section 7.2). The alternative form (43) highlights the tendency for both schemes to transport heat down the gradient of α (as per the inequality (45)), thus leading to a negative tendency for global mean sea level.

7.2. Interpretation of non-Boussinesq steric patterns from parameterized quasi-Stokes transport

We provide here some further interpretation of the patterns shown in Fig. 13. For this purpose, follow the treatment of Greatbatch and McDougall (2003) for quasi-Stokes transport in non-Boussinesq fluids, in which we make use of the non-divergent condition

$$\nabla \cdot (\rho \mathbf{v}^*) = 0 \tag{114}$$

(see also Eq. (173) in Appendix A satisfied by the parameterized eddy-induced velocity $\mathbf{v}^*$, to write the contribution to the non-Boussinesq steric effect from quasi-Stokes advection

$$\begin{aligned} -\left(\frac{1}{\rho}\frac{\mathrm{d}\rho}{\mathrm{d}t}\right)_{\text{quasi-Stokes}} &= \left(\alpha \frac{\mathrm{d}\Theta}{\mathrm{d}t} - \beta \frac{\mathrm{d}S}{\mathrm{d}t}\right)_{\text{quasi-Stokes}} \\ &= \frac{1}{\rho}\left(-\alpha \nabla \cdot (\rho \mathbf{v}^* \Theta) + \beta \nabla \cdot (\rho \mathbf{v}^* S)\right) \\ &= \mathbf{v}^* \cdot (-\alpha \nabla \Theta + \beta \nabla S) \end{aligned} \tag{115}$$

with the final expression in the form of an advection of buoyancy by the quasi-Stokes velocity. We now introduce the vector streamfunction for the quasi-Stokes mass transport

$$\rho \mathbf{v}^* = \nabla \wedge \rho \boldsymbol{\Psi} = \partial_z (\rho \boldsymbol{\Upsilon}) - \hat{\mathbf{z}} \nabla_z \cdot (\rho \boldsymbol{\Upsilon}), \tag{116}$$

where $\boldsymbol{\Psi} = \boldsymbol{\Upsilon} \wedge \hat{\mathbf{z}}$ is the quasi-Stokes vector streamfunction, and $\boldsymbol{\Upsilon}$ is the eddy induced transport (see Section A.3.2), which then leads to

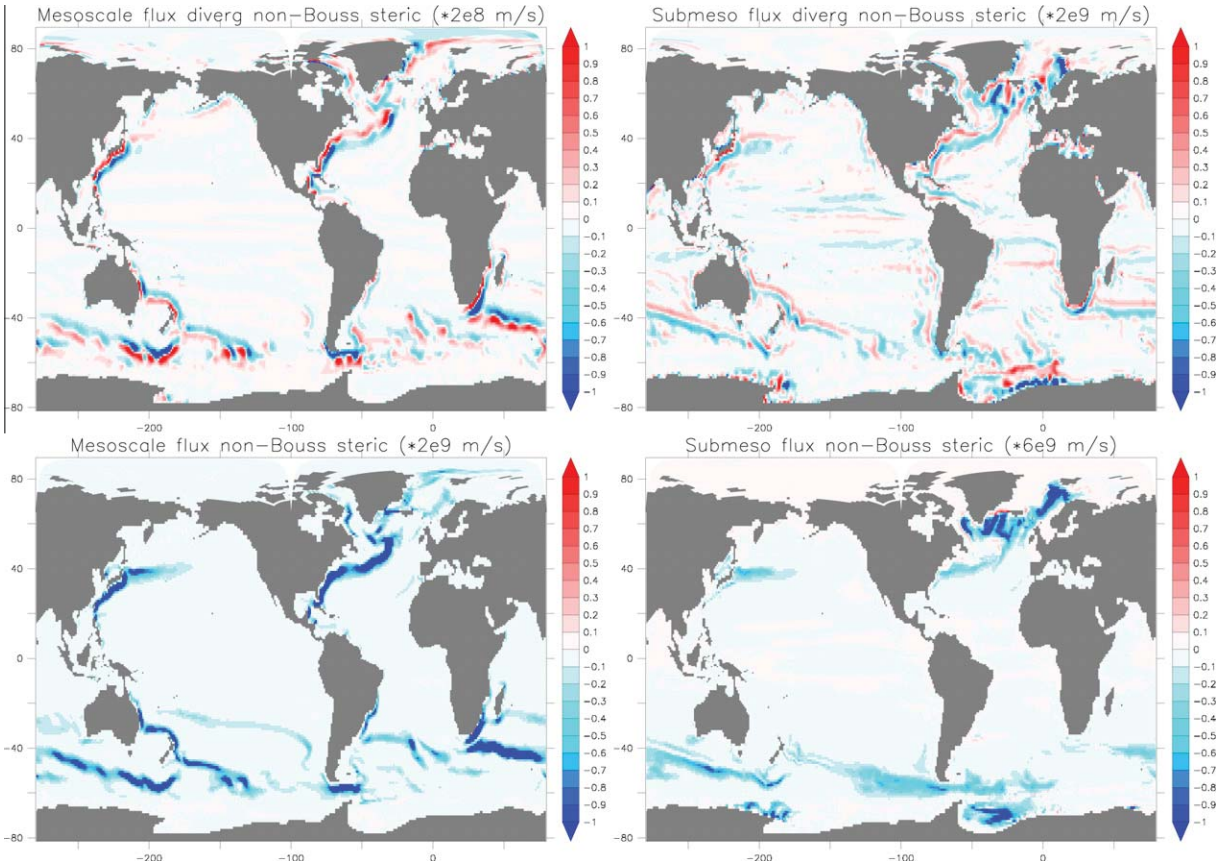

Fig. 13. Map of the 20 year mean contribution to the non-Boussinesq steric effect from the quasi-Stokes transport as parameterized for mesoscale eddies by Ferrari et al. (2010) (which acts physically in a manner directly analogous to the Gent et al., 1995 parameterization), and the submesoscale scheme of Fox-Kemper et al. (2008). The upper panels are based on computing weighted flux divergences (Eq. (44)), whereas the lower panels are based on the form (43). Of note are the large values near western boundaries and mode and deep water formation regions of the Atlantic and Southern Oceans. Poleward heat transport in the presence of a spatially dependent thermal expansion coefficient is the key reason for the negative sea level tendency from these two schemes. The global ocean mean from the mesoscale parameterization is -5×10^{-11} m s^{-1} = -2×10^{-3} m year^{-1}; the mean for the submesoscale parameterization is -7×10^{-12} m s^{-1} = -2×10^{-4} m year^{-1}. Note the different scalings for the figures (noted on the figure titles), with values chosen to help emphasize patterns.

$$-\left(\frac{1}{\rho}\frac{\mathrm{d}\rho}{\mathrm{d}t}\right)_{\text{quasi-Stokes}} = \partial_z(\rho \boldsymbol{\Upsilon}) \cdot \left(\frac{-\alpha \nabla_z \Theta + \beta \nabla_z S}{\rho}\right) - \nabla_z \cdot (\rho \boldsymbol{\Upsilon}) \left(\frac{-\alpha \partial_z \Theta + \beta \partial_z S}{\rho}\right). \tag{117}$$

We specialize this result to the case of a stable vertical stratification (i.e., the buoyancy frequency $N^2 > 0$), in which case

$$-\left(\frac{1}{\rho}\frac{\mathrm{d}\rho}{\mathrm{d}t}\right)_{\text{quasi-Stokes}} = \left(\frac{N^2}{\rho g}\right) \nabla_{\mathrm{n}} \cdot (\rho \boldsymbol{\Upsilon}), \tag{118}$$

where $\nabla_{\mathrm{n}} = \nabla_z + \boldsymbol{S}\partial_z$ is the projected neutral gradient operator introduced by Eq. (99), N^2 is the squared buoyancy frequency given by Eq. (87), and $\boldsymbol{S}$ is the neutral slope given by Eq. (100).

The next step introduces the Gent et al. (1995) form, in which the quasi-Stokes transport is given by

$$\boldsymbol{\Upsilon}^{\mathrm{gm}} = -A_{\mathrm{gm}} \boldsymbol{S} = -A_{\mathrm{gm}} \nabla_{\mathrm{n}} z, \tag{119}$$

where $A_{\mathrm{gm}} > 0$ is a diffusivity, and $\boldsymbol{S} = \nabla_{\mathrm{n}} z$ is an expression for the neutral slope, written here in terms of the projected lateral gradient of the depth of the neutral tangent plane (e.g., Eq. (6.6) of Griffies, 2004). These expressions for the parameterized quasi-Stokes transport yield

$$-\left(\frac{1}{\rho}\frac{\mathrm{d}\rho}{\mathrm{d}t}\right)_{\mathrm{gm}} = -\left(\frac{N^2}{\rho g}\right) \nabla_{\mathrm{n}} \cdot (\rho A_{\mathrm{gm}} \nabla_{\mathrm{n}} z). \tag{120}$$

The operator on the right hand side represents a neutral diffusion of the depth of a neutral tangent plane. We can make this correspondence precise through introducing the inverse infinitesimal thickness between two neutral tangent planes[2]

$$h = \mathrm{d}z = \left(\frac{\rho N^2}{g}\right)^{-1} \mathrm{d}\gamma, \tag{121}$$

where $\mathrm{d}\gamma$ is the density increment between the two tangent planes. This substitution leads to

$$-\left(\frac{1}{\rho}\frac{\mathrm{d}\rho}{\mathrm{d}t}\right)_{\mathrm{gm}} = -\left(\frac{1}{\rho^2 h g}\right) \nabla_{\mathrm{n}} \cdot \left(N^2 A_{\mathrm{gm}} \rho^2 h \nabla_{\mathrm{n}} z\right). \tag{122}$$

When surfaces of constant buoyancy bow downwards, as in a body of warm water (see Fig. 14), this configuration represents a local minimum in the height of the buoyancy surface (or maximum in the depth). The curvature of this surface is negative, so that the diffusion operator (120) is positive. The Gent et al. (1995) scheme acts to dissipate the negative curvature by transporting light water away from the anomalously light region, thus raising the depth maxima. That is, heat is transported away from a body of warm water. This physical interpretation of Gent et al. (1995) accords with its implementation in isopycnal coordinate ocean models,

[2] For example, see Eq. (9.70) in Griffies (2004) for the isopycnal diffusion operator in isopycnal coordinates.

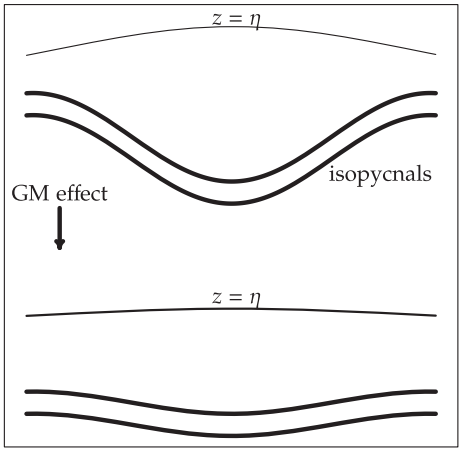

Fig. 14. Schematic to illustrate the impact of the (Gent et al., 1995) parameterization on isopycnals (dark curves) and sea level, assuming the idealized case of a 1.5 layer ocean. As the (Gent et al., 1995) scheme shoals the depth of the depressed pycnocline (moving from the top portion of the panel to the lower portion), warm water is transported from the core of a warm pool to the flanks. We may extrapolate this two-layer schematic to represent the global ocean, whereby higher latitude outcropping regions are relaxed through the effects of eddies. The tendency to move warm water poleward, from regions of large thermal expansion (low latitudes) to small thermal expansion (high latitudes) leads to a net drop in global mean sea level through the non-Boussinesq steric effect.

where it appears as an isopycnal layer depth diffusion rather than an isopycnal layer thickness diffusion (see Section 11.3.2 of Griffies et al. (2000)). The common interpretation as a thickness diffusion is *only* valid when the diffusivity is depth independent (see Section 9.5.4 of Griffies, 2004), and the ocean bottom is flat (see Section 11.3.2 of Griffies et al. (2000)).

A vertical integral of the GM effect in Eq. (120) leads to the following tendency for sea level through the non-Boussinesq steric effect

$$\left(\frac{\partial \eta}{\partial t}\right)_{\rm gm} = -\int_{-H}^{\eta} \left(\frac{N^2}{\rho g}\right) \nabla_{\rm n} \cdot (\rho A_{\rm gm} \nabla_{\rm n} z) \, {\rm d}z. \tag{123}$$

Hence, the parameterized quasi-Stokes transport of buoyancy according to Gent et al. (1995) acts to erode depth maxima by raising buoyancy surfaces, which in turn renders a negative local tendency to sea level through the non-Boussinesq steric effect in the regions shown in blue in the left upper panel of Fig. 13. The opposite effect occurs in the regions shown in red where the parameterised quasi-Stokes transport acts to erode depth minima by lowering buoyancy surfaces. The tendency for the quasi-Stokes transport to move heat from regions of relatively high to relatively low values of the thermal expansion coefficient, illustrated by the prodominently negative values plotted in the lower left panel of Fig. 13, is the reason the quasi-Stokes transport leads to a net lowering of global mean sea level.

7.3. Equivalent formulations of quasi-Stokes transport acting on global mean sea level

In diagnosing contributions from subgrid scale parameterizations, we assumed the governing equations to be first averaged over the microscale and then over the mesoscale (as in DeSzoeke and Bennett (1993) and DeSzoeke (2009)), with the effect of cabbeling and thermobaricity arising from parameterized neutral diffusive mixing from mesoscale eddies, and quasi-Stokes transport also arising from mesoscale and submesoscale eddies (e.g., Section A.3.3 in Appendix A for more comments on averaging). In simulations that resolve the mesoscale, there is no neutral diffusion to parameterize mixing along neutral directions, nor a parameterized quasi-Stokes transport. We explore here some points about the correspondence of the global mean sea level evolution between the averaged/parameterized system and the unaveraged/resolved system. Note that we continue to assume an average over the microscale.

There are two methods to derive the global mean sea level equation (64). The first was already utilized in this paper, and it starts from mass conservation in the form

$$-\frac{1}{\rho}\frac{{\rm d}\rho}{{\rm d}t} = \nabla \cdot \mathbf{v}. \tag{124}$$

As in Section 3, we expand the material time derivative (ignoring the source terms $\mathcal{S}^{(\Theta)}$ and $\mathcal{S}^{(S)}$ for brevity) to render

$$-\frac{1}{\rho}\frac{{\rm d}\rho}{{\rm d}t} = -\frac{\alpha}{\rho}\nabla \cdot \left(\mathbf{J}^{(\Theta)}_{\rm diffuse} + \rho \mathbf{v}^* \Theta\right) + \frac{\beta}{\rho}\nabla \cdot \left(\mathbf{J}^{(S)}_{\rm diffuse} + \rho \mathbf{v}^* S\right) + \frac{g w^{(p)}}{c^2_{\rm sound}}, \tag{125}$$

where we assumed a hydrostatic balance to introduce the vertical velocity component $w^{(p)}$ (Eq. (17)). The subgrid scale fluxes $\mathbf{J}^{(\Theta)}_{\rm diffuse}$ and $\mathbf{J}^{(S)}_{\rm diffuse}$ are diffusive fluxes that parameterize both small scale mixing processes (Section 5), and neutral diffusive mixing from mesoscale eddies (Section 6). The eddy induced transport velocity $\mathbf{v}^*$ parameterizes the quasi-Stokes transport from mesoscale and submesoscale eddies. The net contribution to the global mean sea level Eq. (64) from the subgrid-scale processes plus vertical motion thus takes the form

$$\mathcal{A}\left(\frac{\partial \bar{\eta}}{\partial t}\right)_{\rm sgs+vertical} = \int_{\rm globe} \Big[\left(\mathbf{J}^{(\Theta)}_{\rm diffuse} + \rho \mathbf{v}^* \Theta\right) \cdot \nabla(\alpha/\rho) - \left(\mathbf{J}^{(S)}_{\rm diffuse} + \rho \mathbf{v}^* S\right) \cdot \nabla(\beta/\rho) + \frac{g w^{(p)}}{c^2_{\rm sound}}\Big] {\rm d}V. \tag{126}$$

The second method to derive the impact on global mean sea level is to start from mass conservation written in the form (169) derived in Appendix A

$$\frac{1}{\rho}\frac{{\rm d}^\dagger \rho}{{\rm d}t} = -\nabla \cdot \mathbf{v}^\dagger, \tag{127}$$

where

$$\frac{{\rm d}^\dagger}{{\rm d}t} = \frac{\partial}{\partial t} + (\mathbf{v} + \mathbf{v}^*) \cdot \nabla \tag{128}$$

is the material time derivative with advection provided by the residual mean velocity

$$\mathbf{v}^\dagger = \mathbf{v} + \mathbf{v}^*, \tag{129}$$

where $\mathbf{v}^*$ is the quasi-Stokes velocity. Our ability to start from either form of mass conservation is detailed in Section A.3.2 of Appendix A, and arises from properties of the parameterized quasi-Stokes transport. Expanding the material time derivative in Eq. (127) leads to

$$-\frac{1}{\rho}\frac{{\rm d}^\dagger \rho}{{\rm d}t} = \frac{1}{\rho}\left(-\alpha \nabla \cdot \mathbf{J}^{(\Theta)}_{\rm diffuse} + \beta \nabla \cdot \mathbf{J}^{(S)}_{\rm diffuse}\right) + \frac{g}{c^2_{\rm sound}}(w^{(p)} + w^{(p)*}), \tag{130}$$

where

$$w^{(p)*} = \left(\frac{\partial z}{\partial p}\right)\mathbf{v}^* \cdot \nabla p \tag{131}$$

is the component of the eddy induced velocity normal to the pressure surfaces, $w^{(p)} = (\partial z/\partial p)\,{\rm d}p/{\rm d}t$ is the vertical velocity component for pressure coordinates introduced by Eq. (17), and we assumed hydrostatic balance. With this formulation, the subgrid scale plus

vertical motion contribute in the following manner to the global mean sea level equation (64)

$$\mathcal{A}\left(\frac{\partial\bar{\eta}}{\partial t}\right)_{\text{sgs+vertical}} = \int_{\text{globe}} \Big[\mathbf{J}^{(\Theta)}_{\text{diffuse}} \cdot \nabla(\alpha/\rho) - \mathbf{J}^{(S)}_{\text{diffuse}} \cdot \nabla(\beta/\rho) + \frac{g}{c^2_{\text{sound}}}(w^{(p)} + w^{(p)*})\Big] dV. \tag{132}$$

The quasi-Stokes transport thus appears as an extra vertical velocity component, $w^{(p)*}$, acting in concert with the resolved velocity component $w^{(p)}$, whereas subgrid scale buoyancy fluxes arise only from diffusion. From this perspective, we see that it is through the integrated effects from $w^{(p)*}$ that eddies contribute to global mean sea level.

Expressions (126) and (132) yield identical impacts on global mean sea level. We focused on the form (126) as it places the quasi-Stokes transport on buoyancy, and that facilitated an interpretation of its impacts in Section 7.1 following from studies such as Gent et al. (1995) and Fox-Kemper et al. (2011). Additionally, the vertical velocity component from Gent et al. (1995) can be quite noisy in simulations, thus compromising its diagnosis. Indeed, this numerical behaviour provides a motivation for reformulating the parameterization in terms of a skew flux by Griffies (1998).

It is useful to note how the form (132) exposing $w^{(p)*}$ also tends to reduce global mean sea level in a manner equivalant to the alternative form (126). For this purpse, let the warm body of water shown in Fig. 14 represent an idealized pole-to-pole ocean, with outcropping dense waters in the high latitudes. Both the mesoscale and submesoscale parameterizations act to reduce baroclinicity, in which case $w^{(p)*}$ will generally downwell on the poleward flank of the outcrop regions and upwell on the equatorial flank. In the upper 2000 m of ocean, the sound speed generally gets smaller towards the poles (Fig. 4), and it is in this region that the eddy parameterizations have their largest impact. Hence, $w^{(p)*}$ downwelling impacts on sea level more than upwelling, with the net effect acting to reduce global mean sea level.

The two equivalent expressions (126) and (132) facilitate correspondences between the averaged equations and the unaveraged equations. Namely, a simulation that resolves the mesoscale includes the explicit effects from eddy transport, which is parameterized through $\mathbf{v}^*$ in the non-eddying simulations. This transport impacts global mean sea level equivalently through a modification to the buoyancy transport (Eq. (126)), or as a modification to the column integrated vertical transport (Eq. (132)). A faithful parameterization of eddy effects will lead to similar net effects on global mean sea level for the averaged equations as for the eddy transport resolved in an eddying simulation.

The correspondence between averaged and unaveraged equations for cabbeling and thermobaricity follows similarly. We take the perspective following from McDougall (1987b), in which averaging is performed over the mesoscales, with temperature and salinity directly impacted by neutral diffusion. Cabbeling and thermobaricity are thus an effective large-scale dianeutral transport process arising from mesoscale eddy mixing along neutral directions. To describe the effects from cabbeling and thermobaricity in a simulation that resolves the mesoscale requires a coarse grained analysis, leading to expressions for the neutral diffusive fluxes in terms of eddy correlations of velocity and tracer computed along neutral directions.

8. Summary and discussion

Sea level reflects nearly all physical processes impacting the ocean, from surface boundary fluxes of mass and buoyancy, to bottom geothermal heating, and dynamical and physical processes in the ocean interior. A kinematic perspective on sea level evolution (Section 2) reveals that sea level emerges from balances between the convergence of depth integrated ocean currents; surface mass fluxes arising from precipitation, evaporation, and river runoff; and non-Boussinesq steric effects (Section 3) associated with boundary and interior fluxes of buoyancy, including those from subgrid scale physical processes, as well as motion across pressure surfaces. The kinematic approach to sea level is insufficient to understand all aspects of sea level patterns and adjustments, which require additional information obtained from dynamical considerations. However, kinematics is sufficient for understanding how physical processes determine global mean sea level. It is from this perspective that we developed an analysis framework to quantify how physical processes and boundary fluxes impact the evolution of global mean sea level in ocean climate models.

In addition to surface mass fluxes, the non-Boussinesq steric effect plays a central role in global mean sea level evolution. In particular, it is through the non-Boussinesq steric effect that global mean sea level rises upon ocean warming, with an imbalance of warming in the present day ocean largely the result of human induced climate impacts (Church and Gregory, 2001; Nicholls and Cazenave, 2010). Furthermore, the non-Boussinesq steric effect is the avenue through which parameterized physical processes, such as subgrid scale mixing and quasi-Stokes transport of conservative temperature and salinity, directly impact global mean sea level through impacts on buoyancy. We therefore propose that the framework detailed in this paper is appropriate for addressing questions related to how physical ocean processes, including boundary fluxes, impact global sea level in global ocean climate models, and in particular how their impacts may change in a warming world.

8.1. Synthesis of the global mean sea level budget

The main mathematical result from this paper is the budget (64) for global mean sea level $\bar{\eta}$, repeated here for completeness

$$\mathcal{A}\partial_t\bar{\eta} = \int_{\text{globe}(z=\eta)} \left(\frac{Q_m + \alpha Q^{(\Theta)} - \beta Q^{(S)}}{\rho}\right) dA + \int_{\text{globe}(z=-H)} \left(\frac{Q_m + \alpha Q^{(\Theta)} - \beta Q^{(S)}}{\rho}\right) dA + \int_{\text{globe}} \Big(\mathbf{J}^{(\Theta)} \cdot \nabla(\alpha/\rho) - \mathbf{J}^{(S)} \cdot \nabla(\beta/\rho) - \frac{1}{\rho c^2_{\text{sound}}}\frac{dp}{dt} + \alpha\mathcal{S}^{(\Theta)} - \beta\mathcal{S}^{(S)}\Big) dV. \tag{133}$$

The boundary integrals arise from mass and buoyancy fluxes crossing the ocean interface that impact on global mean sea level, whereas the volume integral arises from parameterized subgrid scale transport and the material time derivative of pressure. As noted in Section 4.2, the bottom fluxes of water and salt mass are generally set to zero. The final term in this equation is associated with mixing and quasi-Stokes transport, as well as vertical motion and possible interior buoyancy source terms. All terms on the right hand side of Eq. (133), save the mass flux Q_m, contribute to the non-Boussinesq steric effect.

We illustrated terms contributing to the budget (133) from a global ocean–ice climate model (see Appendix B for model details). In addition to contributions already identified in previous sections, there are minor contributions to buoyancy mixing discussed in Appendix B. All impacts on global mean sea level are listed in Table 1. Note that our results are specific to an ocean–ice model simulation with a fixed climate. In a global warming simulation using a more realistic coupled climate model, the relative importance of the different terms may change. In particular, we expect a modified

Table 1
Table of contributions to the global mean sea level; sections of the paper where they are detailed; figures where certain of the terms are mapped; and global ocean mean. Blanks indicate no corresponding section in the paper or figure. The global means are rounded to the nearest single significant digit, with more precision kept when performing sums and differences of global mean terms. The upper portion of the table presents contributions to sea level rise; the middle to sea level fall; and the bottom to sums and differences of terms. Net surface buoyancy is the sum shortwave + longwave + latent + sensible + frazil + geothermal heating, plus the salt fluxes from sea ice and restoring. The net subgrid scale term equals to river mixing + vertical diffusion + mesoscale + cabbeling + horizontal diffusion + thermobaricity + KPP non-local mixing + submesoscale + overflow + inland sea exchange. The net surface water flux equals to precipitation + evaporation + river runoff. Note that the drift in sea level arises largely from a warm drift associated with the unequilibrated ocean incurred upon switch from the 600 year spinup of the Boussinesq ocean switching to the non-Boussinesq ocean. Processes in this table that have no corresponding figure include the following: (A) river insertion/mixing occurs just near river mouths; (B) Joule heating: this term is assumed to be uniformly distributed throughout the ocean domain; (C) numerical smoothing operator applied to the bottom pressure, as required to suppress the B-grid computational mode; (D) parameterized overflow processes and inland–sea exchange processes, with these processes occurring only in a few regions.

Contribution	Section	Figure	Global ocean mean tendency (m year^{-1})
Precipitation	2.3	2	1×10^{0}
Surface shortwave + penetration	3.4.1	7	3×10^{-1}
River runoff	2.3	2	1×10^{-1}
Vertical motion	3.2	4	7×10^{-4}
River mixing	Section 3.4.1	-	6×10^{-4}
Geothermal heat	3.4.1	8	8×10^{-5}
Joule heat (not in model)	3.4.1	-	4×10^{-6}
Frazil sea ice	3.4.1	7	6×10^{-7}
Ice/ocean salt flux	3.4.2	9	6×10^{-7}
Evaporation	2.3	2	-1×10^{0}
Surface latent	Section 2.3	2	-2×10^{-1}
Surface longwave	2.3	2	-1×10^{-1}
Surface sensible	Section 2.3	2	-2×10^{-2}
Vertical diffusion	5.1	10	-5×10^{-3}
Meoscale param	7	13	-2×10^{-3}
Cabbeling	6.6	12	-8×10^{-4}
Boundary horiz diffusion	6.8	12	-7×10^{-4}
Thermobaricity	6.7	12	-5×10^{-4}
KPP non-local mixing	5.2	10	-3×10^{-4}
Numerical B-grid smoothing	Section B.2	-	-3×10^{-4}
Submesoscale	7	13	-2×10^{-4}
Overflow and exchange mixing	Section B.2	-	-1×10^{-4}
Salt restoring	B.1	9	-3×10^{-5}
Net surface buoyancy	3.4.1	7	9×10^{-3}
Net subgrid scale	–	–	-9×10^{-3}
Net surface water	3.4.1	2	8×10^{-4}
Vertical motion	3.2	4	7×10^{-4}
Sea level trend	–	–	3×10^{-4}
Residual = buoy + water + sgs + vert motion-trend	–	–	1×10^{-3}

impact on global mean sea level from both melting of land ice and a net surface heat input to the ocean, issues beyond the scope of this paper but which are are critical for projections of future sea level.

8.1.1. Limitations closing the diagnosed sea level budget

Mass conserving ocean models do not time step the sea level equation in the form (1). Instead, for hydrostatic models, sea level is diagnosed from the mass per area in a seawater column (found by time stepping the bottom pressure Eq. (11)), and the density of fluid within the column. The reason for this approach is that ocean volume is not a conserved scalar (see Section 8.2), so its budget is not determined by the sum of boundary fluxes. Our diagnostic calculations thus compute contributions from many large terms and small terms, with addition and subtraction required to compute net contributions and residuals. This approach is prone to truncation errors in a manner analogous to studies of ocean model energetics, where the diagnosed energy budget is rarely closed precisely since ocean models time step linear momentum and tracer, rather than mechanical and internal energy (e.g.,Treguier, 1992; Griffies and Adcroft, 2008).

To help reduce truncation errors in the budget diagnostic, we compute all terms online within the ocean model, sampling every time step. Nonetheless, there are numerical uncertainties for each term proportional to the magnitude of the term. Even so, it is notable that the unaccounted for residual in Table 1 is only about 0.1% of the contribution from the largest term (evaporation or precipitation), though it remains slightly larger than 10% of the net surface flux and subgrid scale contributions to sea level.

8.1.2. Terms contributing positively to global mean sea level

Surface heating dominates all buoyancy terms affecting global mean sea level. As seen from Fig. 7, surface heating is itself dominated by tropical shortwave radiation. Longwave, sensible, and latent heat fluxes cool the global ocean and thus reduce sea level, but their effects on sea level are overwhelmed by tropical shortwave heating. In addition to being the region of largest shortwave radiation, the tropics possess the largest thermal expansion coefficient (Fig. 6), which further focuses the sea level impacts to the tropics.

When gauging the degree that the surface mass flux contributes to global mean sea level in this simulation, recall that we remove the global mean water flux at each model time step (Section B.1) in order to reduce long term drift in the ocean–ice simulation. The nonzero positive contribution to global sea level arises from the tendency for precipitation and river runoff to occur in regions of low surface density, whereas evaporation generally occurs in regions of higher surface density. As discussed in Section 3.6 of Griffies et al. (2005), river runoff is mixed over the upper 40 m (four grid cells) of the ocean model. Such river mixing adds buoyancy to the ocean since runoff enters at zero salinity with the local sea surface temperature. Geothermal heating and frazil heating also add buoyancy, with the values quite small globally. The salt exchanged with sea ice contributes a very small amount to global mean sea level. Joule heating due to frictional dissipation, which is not included in the simulation, adds to sea level rise by an amount roughly 15 times smaller than geothermal heating.

The final positive contribution to global mean sea level is due to the motion of fluid crossing pressure surfaces. In Section 8.2, we

suggest that the positive sign for this term is partly in response to the negative contribution to sea level from mixing.

8.1.3. Terms contributing negatively to global mean sea level

The dominant surface buoyancy fluxes contributing to sea level reduction include surface longwave, sensible, and latent heat fluxes. Evaporation reduces global mean sea level, yet evaporation does not quite balance runoff plus precipitation, so the net mass fluxes add to global mean sea level in this simulation. The buoyancy flux associated with salt restoring reduces sea level by a small amount, with this term small since the net restoring salt flux is normalized to zero at each time step.

All subgrid scale parameterizations contribute to a reduction in global mean sea level. The dominant terms are from vertical diffusion and the mesoscale eddy parameterization. Cabbeling, thermobaricity, and horizontal boundary mixing are also important, with the impacts from cabbeling and thermobaricity consistent with their nontrivial roles in watermass transformation computed by Klocker and McDougall (2010a) and Klocker and McDougall (2010b), especially in the Southern Ocean. Contributions from the Fox-Kemper et al. (2008) submesoscale parameterization are smaller than the Gent and McWilliams (1990) mesoscale scheme, largely since the submesoscale scheme acts only in the surface boundary layer. Other subgrid scale processes listed in Table 1 are subdominant, yet they all act to reduce sea level.

The reason to expect mixing and poleward heat transport by eddies to reduce sea level is that both processes tend to move heat from warm regions, where the thermal expansion coefficient is large, to cooler regions, where the thermal expansion is smaller. Additionally, the processes of cabbeling and thermobaricity reduce sea level due to their tendency to increase density, and thus to compress fluid columns. It is notable that surface buoyancy input in the tropics is roughly balanced by sinks of buoyancy through parameterized subgrid scale mixing and poleward heat transport.

8.2. Regarding steady state budgets

The simulation presented in this paper, with global sea level budget shown in Table 1, is drifting warm, and so global mean sea level is rising. The question arises as to what is required to reach an equilibrium for global mean sea level or global ocean volume. Do the requirements provide some insight into the global mean budget, even for a budget that is not steady? To address this issue, consider the time dependent budgets for heat, salt, mass, and volume for the global ocean

$$\frac{\partial}{\partial t}\left(\int_{\text{globe}} \rho c_p \Theta \, dV\right) = \int_{\text{globe}(z=\eta)} Q_{\text{surface}} \, dA + \int_{\text{globe}(z=-H)} Q_{\text{geothermal}} \, dA, \tag{134}$$

$$\frac{\partial}{\partial t}\left(\int_{\text{globe}} \rho S \, dV\right) = \int_{\text{globe}(z=\eta)} Q_{\text{ice-ocean salt exchange}} \, dA, \tag{135}$$

$$\frac{\partial}{\partial t}\left(\int_{\text{globe}} \rho \, dV\right) = \int_{\text{globe}(z=\eta)} Q_m \, dA, \tag{136}$$

$$\frac{\partial}{\partial t}\left(\int_{\text{globe}} dV\right) = \int_{\text{globe}(z=\eta)} \left(\frac{Q_m}{\rho}\right) dA - \int_{\text{globe}} \left(\frac{1}{\rho}\frac{d\rho}{dt}\right) dV, \tag{137}$$

$$= \mathcal{A}\left(\frac{\overline{Q_m}}{\langle \rho \rangle}\right) - \mathcal{V}\left(\frac{\partial_t \langle \rho \rangle}{\langle \rho \rangle}\right). \tag{138}$$

The final identity follows from Eq. (77) relating the global steric effect to the non-Boussinesq steric effect.

Recall that the net transfer of salt across the ocean surface is tiny relative to the total amount of salt in the ocean. Hence, the total salt in the global ocean is nearly constant, even for those general cases where heat and mass are changing (Section 3.4.2). Furthermore, we can presumably realize a state where the net heat and mass fluxes vanish across the ocean boundaries, in which case the total heat and mass in the ocean are constant. This steady state ocean climate is generally realizable numerically through integrating a climate model for sufficiently long time (many thousands of years) to allow the deep ocean to reach equilibrium (Stouffer, 2004). Furthermore, in idealized situations, we can consider an ocean with no mass or buoyancy forcing at the surface, though retaining mechanical forcing.

In any case, a steady state for the global ocean heat, salt, and mass does *not* imply a steady state for ocean volume. The reason is that the liquid ocean volume is not a conserved scalar property of the ocean. Hence, there is no *a priori* reason to expect ocean volume to be constant, even with zero boundary fluxes of mass and buoyancy. We pursue various implications of this point, and consider what is required to in fact realize a steady state for seawater volume.

8.2.1. Considering the global steric effect

If there is zero net mass input to the ocean, the volume budget Eq. (138) says that the evolution of global mean sea level is determined by the evolution of global mean density

$$\partial_t \bar{\eta} = -\frac{\mathcal{V}}{\mathcal{A}}\left(\frac{\partial_t \langle \rho \rangle}{\langle \rho \rangle}\right) \quad \text{if } \overline{Q_m} = 0. \tag{139}$$

Global constant heat, salt, and mass need not imply a constant global mean density. Consequently, global mean sea level need not be constant. Indeed, even in the simplest case of *in situ* density a linear function of temperature, so that $\partial_t \ln\langle \rho \rangle = -\alpha_{\text{bulk}} \partial_t \langle \Theta \rangle$ (see Eq. (75)), a constant global ocean heat in an ocean with spatially varying density (Eq. (134)) is not equivalent to an ocean with constant volume mean temperature.

8.2.2. Considering the non-Boussinesq steric effect

Consider the alternative form of the volume budget given by Eq. (137). Here, the evolution of global ocean volume vanishes only when there is a balance between the boundary flux of mass and the non-Boussinesq steric effect

$$\int_{\text{globe}(z=\eta)} \left(\frac{Q_m}{\rho}\right) dA = \int_{\text{globe}} \left(\frac{1}{\rho}\frac{d\rho}{dt}\right) dV \quad \text{constant ocean volume.} \tag{140}$$

There is no *a priori* reason for this balance to be realized when global mean mass, heat, and salt are constant. Additionally, we do not expect that an ocean with a zero net surface mass flux to correspond to an ocean with a zero net surface volume flux, since the surface ocean specific volume $\rho^{-1}(x,y,z=\eta)$ is generally not a constant.

8.2.3. What is required to keep the ocean volume constant?

Given the above plausibility arguments for why global ocean volume may not remain steady even when mass and buoyancy are, we nonetheless examine what is implied by assuming global ocean volume is constant. Do the implications make sense physically? To help address this question, it is instructive to further consider the needs of a global steady state ocean volume by examining the unpacked global mean sea level equation (64) in the special case of identically zero boundary fluxes of mass, zero bottom fluxes, and zero interior sources. In this case, a steady state sea level requires the following balance of terms that all contribute to the non-Boussinesq steric effect

$$\int_{\text{globe}(z=\eta)} \left(\frac{\alpha Q^{(\Theta)} - \beta Q^{(S)}}{\rho} \right) dA$$
$$= - \int_{\text{globe}} \left(\mathbf{J}^{(\Theta)} \cdot \nabla(\alpha/\rho) - \mathbf{J}^{(S)} \cdot \nabla(\beta/\rho) - \frac{1}{\rho c_{\text{sound}}^2} \frac{dp}{dt} \right) dV. \quad (141)$$

Hence, a constant ocean volume is realized if there is a balance between boundary buoyancy fluxes (left hand side), which are dominated by sea level rise associated with tropical shortwave heating, and interior buoyancy fluxes and vertical motion (right hand side). In Section 7.1, we noted that poleward heat transport by ocean eddies indeed acts to partially maintain this balance, as does mixing discussed in Sections 5 and 6. Both poleward heat transport and mixing move heat from warm water, where the thermal expansion is large, to cool water, where the thermal expansion is smaller, which is a process that reduces the thermosteric sea level rise associated with shortwave heat input to the tropics. In effect, sea level rise from low latitude heating (Fig. 7) is partially compensated by sea level depression via ocean mixing and poleward mesoscale and submesoscale eddy heat transport.

Consider yet another idealized situation in which surface mass and buoyancy fluxes identically vanish, in which case a constant ocean volume is realized if the following balance is maintained between vertical motion (left hand side) and interior buoyancy transport

$$- \int_{\text{globe}} \left(\frac{1}{\rho c_{\text{sound}}^2} \frac{dp}{dt} \right) dV = - \int_{\text{globe}} (\mathbf{J}^{(\Theta)} \cdot \nabla(\alpha/\rho) - \mathbf{J}^{(S)} \cdot \nabla(\beta/\rho)) dV. \quad (142)$$

As seen by the budgets in Table 1, vertical motion does tend to increase global mean sea level, whereas mixing and eddy transport decrease it. Hence, in this special case, a balance between vertical motion and mixing leads to a steady state global mean sea level.

As a final idealized situation, consider zero boundary fluxes of mass and buoyancy for an ocean with uniform salinity (or equivalently a freshwater lake), yet in the presence of mechanical forcing by winds and tides. Furthermore, let the density equation of state be independent of pressure. In this case, the global mean sea level Eq. (133) reduces to

$$\partial_t \bar{\eta} = \mathcal{A}^{-1} \int_{\text{globe}} \mathbf{J}^{(\Theta)} \cdot \nabla(\alpha/\rho) dV. \quad (143)$$

Hence, so long as mechanical forcing leads to buoyancy transport and mixing, with fluxes oriented down the gradient of the thermal expansion coefficient, then global mean sea level will reduce until there is no more stratification on which the mixing and eddy stirring can act.

8.3. Closing comments

In this paper, we focused on how global mean sea level is affected by a suite of physical processes, both interior to the ocean and at the boundaries. Our motivation was largely taken from understanding sea level in ocean climate model simulations, though many aspects of our analysis are quite general. A possible application of the material presented here is to compare budgets for sea level between different model simulations. Such applications must be conditioned on difficulties obtaining a precise closure (Section 8.1). Nonetheless, we raise some potential avenues of further examination.

Model-model comparisons of boundary fluxes provide a means for understanding some basic differences in simulation features. Writing these boundary fluxes in terms of how they impact on global mean sea level renders one method to identify why simulated global mean sea level may differ between models. In particular, due to the strong latitudinal dependence of the thermal expansion coefficient (Fig. 6), differences in low latitude surface heating contribute far more to differences in global mean sea level than do differences in high latitude heat fluxes.

Further comparison of the interior subgrid scale processes and their impact on global mean sea level presents a novel means for comparing the behaviour of such parameterizations. Quite generally, these patterns provide a physically meaningful method to summarize, in two dimensions, the effects from three dimensional parameterizations. In addition to the particular patterns of buoyancy transport arising from the parameterizations, we identified the importance of spatial variations in the thermal expansion coefficient for modulating how boundary heat fluxes and parameterized physical process impact sea level. These spatial variations are particularly tied to watermass structure in the ocean, thus emphasizing the importance of a proper representation of watermasses for simulating sea level evolution.

Although encapsulating a wide suite of physical processes and boundary fluxes, it is notable that the non-Boussinesq steric effect does not impact sea level computed in volume conserving Boussinesq ocean models. This omission is in fact warranted for many purposes, since the sea level readily adjusts to impacts from the non-Boussinesq steric forcing, leaving a low frequency sea level pattern that differs little whether using a Boussinesq or non-Boussinesq model formulation (Figs. 2 and 3). Following from Greatbatch (1994), the net impacts on global mean sea level associated with the non-Boussinesq steric effect are readily added into the Boussinesq model sea level through the diagnostic calculation of a time dependent global adjustment (see Appendix D). Correspondingly, one may investigate terms contributing to the non-Boussinesq steric effect using the methods from this paper in either a volume conserving Boussinesq or mass conserving non-Boussinesq model, since the physical processes are represented in nearly the same manner. In particular, differences were found to be negligible in the global model used in this paper.

Acknowledgements

Many thanks go to Alistair Adcroft, Michael Bates, Gary Brassington, John Church, Stephanie Downes, Jonathan Gregory, Bob Hallberg, Andy Hogg, Tim Leslie, Trevor McDougall, Jaime Palter, Ron Stouffer, Mike Winton, and Jianjun Yin for discussions and comments that added much to the content and quality of this paper. Bonnie Samuels helped tremendously with the simulations. Anne Marie Treguier graciously edited the many revisions of this manuscript, with her patient insistance on quality much appreciated. Anonymous reviewers also provided valuable, and candidly critical, comments. We thank Daniele Bianchi for providing the geothermal heat flux used for the global ocean–ice model detailed in Appendix B. Some of the material in Sections 5–7 was completed during a visit by SMG in March 2009 to Universite catholique de Louvain in Louvain-la-Neuve, Belgium, with that visit graciously hosted by Professor Eric Deleersnijder. Further work occurred during a visit in January–June 2011 by SMG to CSIRO Marine and Atmospheric Research in Hobart, Australia, with that visit graciously hosted by Drs. John Church, Simon Marsland, and Trevor McDougall. RJG is grateful for support from GEOMAR.

Appendix A. Mass conservation for seawater and tracers

The purpose of this appendix is to formulate the equations for conservation of seawater mass and tracer mass from the perspective of the coarse-grained or averaged equations of an ocean model. The seawater mass conservation equation is the basis for the kinematic equations derived in Section 2 for sea level. The tracer mass conservation equation describes the evolution of scalar trace constituents in seawater such as salt and biogeochemical tracers.

Additionally, the evolution equation for conservative temperature satisfies the mathematically identical advection–diffusion equation (McDougall, 2003).

A.1. Unaveraged continuum fluid

Eulerian expressions for the conservation of seawater mass and tracer mass are given by

$$\frac{\partial \rho}{\partial t} = -\nabla \cdot (\rho \mathbf{v}), \tag{144}$$

$$\frac{\partial (\rho C)}{\partial t} = -\nabla \cdot (\rho \mathbf{v} C + \mathbf{J}_{\text{mdiff}}), \tag{145}$$

which have equivalent Lagrangian expressions

$$\frac{\mathrm{d}\rho}{\mathrm{d}t} = -\rho \nabla \cdot \mathbf{v}, \tag{146}$$

$$\rho \frac{\mathrm{d}C}{\mathrm{d}t} = -\nabla \cdot \mathbf{J}_{\text{mdiff}}. \tag{147}$$

In these equations,

$$\frac{\mathrm{d}}{\mathrm{d}t} = \frac{\partial}{\partial t} + \mathbf{v} \cdot \nabla \tag{148}$$

is the material time derivative computed by an observer moving with the fluid parcel's center of mass velocity $\mathbf{v}$, whereas ∂_t is the Eulerian time derivative computed at a fixed spatial point. The tracer concentration, C, is the mass of a trace constituent within a fluid parcel, per mass of seawater within the parcel. Consequently, the product ρC is the mass of tracer per volume of seawater, with ρ the *in situ* seawater mass density. The flux $\mathbf{J}_{\text{mdiff}}$ arises from local gradients in the tracer field being acted upon by a nonzero molecular diffusivity. For passive tracers (those tracers not impacting density), this molecular diffusion flux vanishes when the tracer concentration is uniform, in which case the expression for tracer mass conservation (145) reduces to the seawater mass conservation (144). This *compatibility condition* is fundamental to the continuum mass and tracer equations, and it follows since we choose to measure the motion of fluid parcels using the parcel's center of mass velocity $\mathbf{v}$ (e.g., see Section II.2 of DeGroot and Mazur (1984), Section 8.4 of Chaikin and Lubensky (1995), or Section 3.3 of Müller (2006)). For the active tracers temperature and salinity (those tracers impacting density), there is generally a nonzero molecular flux of each field arising from gradients in the other field, with this process known the Soret and Dufour effect (Landau and Lifshitz, 1987). We do not consider this cross-diffusion effect in the following (see McDougall, 1983 for an analysis of this effect with connection to the ocean).

A.2. Kinematic boundary conditions

Kinematic boundary conditions arise from the geometric constraints imposed by the ocean bottom and surface, with such constraints impacting the budgets of mass over a column of seawater. In formulating the kinematic boundary conditions, we assume the ocean bottom to be static and impermeable (i.e., closed to mass fluxes), whereas the ocean surface is dynamic and open to mass fluxes. We provide some detail regarding the derivation of these boundary conditions since they expose issues essential for understanding the evolution of global mean sea level.

A.2.1. Bottom kinematic boundary condition

At the rigid ocean bottom, the kinematic boundary condition states that the geometric expression for the ocean bottom

$$z + H(x,y) = 0 \quad \text{ocean bottom} \tag{149}$$

remains fixed in time for all parcels situated at the bottom, so that

$$\frac{\mathrm{d}(z+H)}{\mathrm{d}t} = 0 \quad \text{at } z = -H(x,y), \tag{150}$$

where the coordinates x, y denote the lateral position of a fluid parcel in the ocean. An equivalent statement is that there is no normal flow of fluid at the ocean bottom, so that $\mathbf{v} \cdot \hat{\mathbf{n}} = 0$, with the outward normal given by

$$\hat{\mathbf{n}} = -\left(\frac{\nabla(z+H)}{|\nabla(z+H)|} \right) \quad \text{at } z = -H(x,y). \tag{151}$$

In either case, we may write the bottom kinematic boundary condition as

$$w + \mathbf{u} \cdot \nabla H = 0 \quad \text{at } z = -H(x,y), \tag{152}$$

where

$$\mathbf{v} = (\mathbf{u}, w) \tag{153}$$

is the fluid velocity field, with $\mathbf{u}$ the horizontal velocity.

A.2.2. Surface kinematic boundary condition

We assume that the ocean surface can be written geometrically as

$$z - \eta(x,y,t) = 0 \quad \text{ocean surface}, \tag{154}$$

which means that there are no overturns; i.e., we filter out breaking surface waves. The mass per time of material crossing the surface is written as

$$\text{mass per time through surface} = \mathcal{Q}_{\text{m}} \, \mathrm{d}A_\eta, \tag{155}$$

where $\mathrm{d}A_\eta$ is the infinitesimal area element on the ocean surface, and $\mathcal{Q}_{\text{m}}$ is the mass per time per surface area of material crossing the surface. This mass flux can be equivalently written as the normal projection of the relative velocity at the ocean surface, multiplied by the surface density

$$\mathcal{Q}_{\text{m}} \mathrm{d}A_\eta = \rho (\mathbf{v} - \mathbf{v}_\eta) \cdot \hat{\mathbf{n}} \mathrm{d}A_\eta \quad \text{at } z = \eta, \tag{156}$$

where

$$\hat{\mathbf{n}} = \frac{\nabla(z-\eta)}{|\nabla(z-\eta)|} \quad \text{at } z = \eta \tag{157}$$

is the outward normal at the ocean surface, and

$$\mathbf{v}_\eta \cdot \hat{\mathbf{n}} = \frac{\partial_t \eta}{|\nabla(z-\eta)|} \quad \text{at } z = \eta \tag{158}$$

is the normal velocity of a material point fixed to the ocean surface. The surface kinematic boundary condition given by Eq. (156) says there is a nonzero projection of the relative velocity onto the surface outward normal, $(\mathbf{v} - \mathbf{v}_\eta) \cdot \hat{\mathbf{n}}$, only when there is a nonzero mass flux through the undulating surface.

Given our assumption of no overturns in the sea surface, we can equivalently write the surface mass flux as

$$\text{mass per time through surface} = Q_{\text{m}} \mathrm{d}A, \tag{159}$$

where $\mathrm{d}A$ is the horizontal area element obtained by projecting the surface area element $\mathrm{d}A_\eta$ onto the horizontal plane, and Q_{m} is the mass per time per horizontal area of material crossing the surface. The two area elements are related by the expression (see Section 20.13.2 of Griffies (2004))

$$\mathrm{d}A_\eta = |\nabla(z-\eta)| \mathrm{d}A. \tag{160}$$

We now return to the boundary condition (156), yet replace the mass flux $\mathcal{Q}_{\text{m}}$ with Q_{m}, use the area relation (160), and write the normal material velocity at the ocean surface in the form (158), with these steps yielding the kinematic boundary condition (e.g., Section 3.4 of Griffies (2004))

$$\rho(\partial_t + \mathbf{u}\cdot\nabla)\eta = Q_m + \rho w \quad \text{at } z = \eta \tag{161}$$

or the equivalent Lagrangian expression

$$\rho\left(\frac{d(z-\eta)}{dt}\right) = -Q_m \quad \text{at } z = \eta. \tag{162}$$

As a self-consistency check, note that the mass per horizontal area in a fluid column,

$$\text{mass per horizontal area} = \int_{-H}^{\eta} \rho\, dz \tag{163}$$

is altered by the convergence of mass to the column via ocean currents, and mass entering through the ocean surface, so that

$$\partial_t\left(\int_{-H}^{\eta}\rho dz\right) + \nabla\cdot\left(\int_{-H}^{\eta}\rho\mathbf{u}dz\right) = Q_m. \tag{164}$$

Leibniz's Rule can be used to move the time and space derivatives across the integral sign, with the bottom kinematic boundary condition (152) and Eulerian form of the mass continuity Eq. (144) recovering the surface kinematic boundary condition (161).

Matter entering the ocean is predominantly in the form of freshwater plus trace constituents, such as salt and biogeochemical matter,

$$Q_m = Q_w + Q^{(S)}, \tag{165}$$

where Q_w is the mass flux of freshwater, and $Q^{(S)}$ is the mass flux of salt or other trace constituents. A nonzero salt flux for climate purposes is generally limited to regions under sea ice. In general, the salt and trace constituent surface mass flux is far smaller than the mass flux from freshwater. Hence, the matter flux is often approximated just with the freshwater flux. In this way, the exchange of tracer mass across the ocean surface generally does not impact the ocean mass in climate models. More realistic river models, and sea ice models that carry the mass of tracers, will necessitate removing this assumption from ocean models.

The surface kinematic boundary condition can be rearranged into a prognostic equation for sea level

$$\partial_t\eta = Q_m/\rho + (\hat{\mathbf{n}}\cdot\mathbf{v})|\nabla(z-\eta)| \qquad \text{at} z = \eta. \tag{166}$$

Hence, mass entering through the free surface ($Q_m > 0$) contributes to a positive sea level tendency, as does a three dimensional velocity that has a nonzero projection "upwards" ($\hat{\mathbf{n}}\cdot\mathbf{v} > 0$). The expression (166), though useful geometrically, does not provide the necessary means for partitioning sea level evolution into physical processes. For this purpose, we pursue the development of alternative sea level equations in Section 2.

A.3. Coarse-grained or averaged mass and tracer equations

The seawater mass conservation equation (144), and the tracer mass conservation Eq. (145), arise from a continuum formulation of fluid mechanics (e.g., Batchelor (1967) and Landau and Lifshitz (1987)). The finite sized grid used in a numerical ocean model introduces a cutoff scale absent from the continuum. Formulating the equations discretized by an ocean model requires an averaging operation in which the continuum equations are averaged over scales smaller than the grid. A discrete ocean model then provides an approximation to the averaged equations by using various methods from computational physics. When averaging nonlinear products, such as $\rho\cdot\mathbf{v} > C$, correlations appear between space and time fluctuations that are unresolved by the grid. Ideally, these correlations can be organized into the form of a subgrid scale flux divergence. Parameterizing the subgrid scale flux divergence is nontrivial, with no universal approach available.

A.3.1. Form implied by mathematical correspondence

We only require general properties of subgrid scale fluxes, rather than formulations specific to a particular physical process. A very convenient property we desire is that the averaged mass and tracer equations are written in the same mathematical form as the corresponding continuum or unaveraged equations. More precisely, the terms appearing in the averaged equations correspond to, though are generally distinct from, their unaveraged analogs. In turn, we insist that the compatibility condition between the unaveraged continuum budgets for seawater mass and tracer mass be maintained for the averaged model equations. Maintaining this direct correspondence between unaveraged and averaged equations facilitates straightforward physical interpretations.

Maintenance of the same mathematical form as the continuum mass conservation equation (144) and tracer conservation equation (145) allows us to write the averaged mass and tracer conservation equations in the form

$$\frac{\partial\rho_a}{\partial t} = -\nabla\cdot(\rho_a\mathbf{v}^\dagger), \tag{167}$$

$$\frac{\partial(\rho_a C_a)}{\partial t} = -\nabla\cdot(\rho_a\mathbf{v}^\dagger C_a + \mathbf{J}_{\text{eddydiff}}), \tag{168}$$

or the equivalent Lagrangian expressions

$$\frac{d^\dagger\rho_a}{dt} = -\rho_a\nabla\cdot\mathbf{v}^\dagger, \tag{169}$$

$$\rho_a\frac{d^\dagger C_a}{dt} = -\nabla\cdot\mathbf{J}_{\text{eddydiff}}, \tag{170}$$

where the "a" subscript signifies an averaged quantity. In ocean circulation models, the subgrid scale eddy tracer diffusive flux, $\mathbf{J}_{\text{eddydiff}}$, is generally far larger than the corresponding molecular flux, $\mathbf{J}_{\text{mdiff}}$. Nonetheless, as for the molecular flux, compatibility between the averaged mass and tracer equations is maintained so long as the eddy flux vanishes when the tracer concentration, C_a, is spatially uniform. Compatibility is maintained by the commonly used flux-gradient relation for the parameterized subgrid scale tracer diffusive flux.

A.3.2. Residual mean velocity and quasi-Stokes velocity

Along with an eddy diffusive flux, $\mathbf{J}_{\text{eddydiff}}$, we introduced to the averaged equations the *residual mean* velocity, $\mathbf{v}^\dagger$, which advects seawater mass and tracer mass, thus bringing the material time derivative to the form

$$\frac{d^\dagger}{dt} = \frac{\partial}{\partial t} + \mathbf{v}^\dagger\cdot\nabla. \tag{171}$$

The residual mean velocity is generally partitioned into two pieces

$$\mathbf{v}^\dagger = \mathbf{v}_a + \mathbf{v}^*, \tag{172}$$

where $\mathbf{v}_a$ is the averaged velocity directly represented by the numerical model, and $\mathbf{v}^*$ is an eddy induced or quasi-Stokes velocity that requires a parameterization before being represented by the model. Proposed parameterizations of $\mathbf{v}^*$ used by ocean circulation models (e.g., Gent and McWilliams, 1990; Gent et al., 1995; McDougall and McIntosh, 2001; Fox-Kemper et al., 2008) all satisfy the non-divergence property in the ocean interior[3]

$$\nabla\cdot(\rho_a\mathbf{v}^*) = 0 \quad \text{ocean interior} \tag{173}$$

and the no-normal flow condition at ocean boundaries

$$\hat{\mathbf{n}}\cdot\mathbf{v}^* = 0 \quad \text{ocean boundaries}. \tag{174}$$

[3] Greatbatch and McDougall (2003) focus on quasi-Stokes transport in mass conserving non-Boussinesq fluids, and their formulation is consistent with that given here.

The non-divergence condition (173) means that the quasi-Stokes mass transport can be written as the curl of a vector streamfunction

$$\rho_a \mathbf{v}^* = \nabla \wedge \rho_a \boldsymbol{\Psi}, \tag{175}$$

so that the tracer equation (170) can be written as

$$\rho_a \frac{dC_a}{dt} = -\nabla \cdot (\mathbf{J}_{\text{eddydiff}} + \mathbf{J}_{\text{skew}}). \tag{176}$$

In this equation,

$$\mathbf{J}_{\text{skew}} = -\nabla C_a \wedge \rho_a \boldsymbol{\Psi} \tag{177}$$

is a skew tracer flux, which differs from the advective tracer flux through a non-divergent curl

$$\rho_a \mathbf{v}^* C_a = -\nabla C_a \wedge \rho_a \boldsymbol{\Psi} + \nabla \wedge (\rho_a \boldsymbol{\Psi} C_a), \tag{178}$$

thus making the divergence of the advective flux equal to the divergence of the skew flux

$$\nabla \cdot (\rho_a \mathbf{v}^* C_a) = -\nabla \cdot (\nabla C_a \wedge \rho_a \boldsymbol{\Psi}). \tag{179}$$

The following presents further implications of the non-divergence and no-normal flow properties (173) and (174) that are utilized in this paper.

- The non-divergence condition $\nabla \cdot (\rho_a \mathbf{v}^*) = 0$, satisfied in the ocean interior, and the no-normal flow condition $\hat{\mathbf{n}} \cdot \mathbf{v}^* = 0$, satisfied at the ocean boundaries, ensures that the quasi-Stokes transport associated with $\mathbf{v}^*$ acts to stir, rather than mix, tracer fields. That is, the quasi-Stokes transport is adiabatic. This property of the transport for mass conserving non-Boussinesq fluids follows from the formulation given by Greatbatch and McDougall (2003), which itself is a generalization of the volume conserving Boussinesq results of Gent et al. (1995) and McDougall and McIntosh (2001).
- The averaged seawater mass continuity equations hold whether one uses the residual mean velocity $\mathbf{v}^\dagger$, as in Eqs. (167) and (169), or the mean velocity $\mathbf{v}_a$

$$\frac{\partial \rho_a}{\partial t} = -\nabla \cdot (\rho_a \mathbf{v}_a), \tag{180}$$

$$\frac{d\rho_a}{dt} = -\rho_a \nabla \cdot \mathbf{v}_a. \tag{181}$$

- The kinematic boundary conditions from Section A.2 remain identical whether using $\mathbf{v}^\dagger$ or $\mathbf{v}_a$.
- Vertical integration of the non-divergence condition (173) over a seawater column, and use of the no-flux boundary condition (174), yields

$$\nabla \cdot \left(\int_{-H}^{\eta} \rho_a \mathbf{u}^* dz \right) = 0, \tag{182}$$

where $\mathbf{u}^*$ is the horizontal component to the eddy induced velocity. The Gent et al. (1995) mesoscale eddy parameterization and the (Fox-Kemper et al., 2008) submesoscale eddy parameterization achieve this property by satisfying

$$\int_{-H}^{\eta} dz \rho_a \mathbf{u}^* = 0 \quad \text{mesoscale and submesoscale parameterizations.}$$

The eddy induced mass transport for these parameterizations thus has zero vertically integrated component.

The above properties mean that it is a matter of convenience what form of the mass conservation equation we choose when formulating the kinematic sea level equations in Section 2. We prefer the starting point offered by equations (180) and (181). This choice then places impacts of the quasi-Stokes transport directly onto buoyancy, as detailed in Section 7, rather than on the material evolution of pressure (Section 3.2). We reconsider this decision in Section 7.3 and exhibit the two versions of how the quasi-Stokes transport appears in the sea level budget.

A.3.3. Comments on particular averaging methods

Although we are not concerned with details of the averaging required to reach Eqs. (167) and (168), it is important to note that methods exist to write the averaged scalar equations in precisely these forms. More generally, the theory required to produce *mean field* or averaged fluid equations is extensive and nontrivial. The variety of averaging methods amount to different mathematical approaches that are appropriate under differing physical regimes and functions of the vertical coordinates used to describe the fluid. A non-exhaustive list of examples specific to the ocean include the following (see also Olbers et al. (2012) and Eden (2012) for further discussion of even more averaging methods).

- The microscale or infra-grid averaging of DeSzoeke and Bennett (1993), Davis (1994a), Davis (1994b), and DeSzoeke (2009) focuses on scales smaller than a few tens of metres.
- The density weighted averaging of Hesselberg (1926) (see also McDougall et al., 2002 and Chapter 8 of Griffies (2004)), provides a framework to account for the mass conserving character of the non-Boussinesq ocean equations.
- The isopycnal thickness weighted methods of DeSzoeke and Bennett (1993), McDougall and McIntosh (2001), DeSzoeke (2009), and Young (2012) (see also Chapter 9 of Griffies (2004)) provide a framework to develop parameterizations of mesoscale eddy motions in the stratified ocean interior. See also the combined density and thickness weighted methods of Greatbatch and McDougall (2003).
- The approach of Eden et al. (2007) leads to different averaged mass and tracer equations than equations (167) and (168), since they introduce a different eddy induced velocity for each tracer. However, so long as the eddy induced velocity for each tracer satisfies the non-divergence condition (173) and the no-normal flow boundary condition (174), their approach should maintain the compatibility condition between mass and tracer equations, and thus it falls within the framework of the present considerations.

A.3.4. Notation convention for this paper

Now that we have introduced a convention for the model fields, which are the result of a particular averaging procedure, we dispense with the "a" subscript in order to reduce notational clutter. Unless otherwise noted, equations and fields in this paper refer to their averaged forms, as appropriate for an ocean model.

A.4. Material changes of in situ density

The *in situ* density, ρ, is a function of three intensive fluid properties

$$\rho = \rho(\Theta, S, p), \tag{184}$$

with Θ the conservative temperature (McDougall, 2003; IOC et al., 2010), S the salinity, and p the pressure. We prefer the conservative temperature as it reflects more accurately on the conservative nature of potential enthalpy transport in the ocean as compared to the alternative potential temperature.

The equation of state (184) leads to the material time evolution of *in situ* density

$$\frac{d\rho}{dt} = \frac{\partial\rho}{\partial\Theta}\frac{d\Theta}{dt} + \frac{\partial\rho}{\partial S}\frac{dS}{dt} + \frac{\partial\rho}{\partial p}\frac{dp}{dt} = -(\rho\alpha)\frac{d\Theta}{dt} + (\rho\beta)\frac{dS}{dt} + \frac{1}{c^2_{\text{sound}}}\frac{dp}{dt}. \tag{185}$$

These equations introduced the thermal expansion coefficient,

$$\alpha = -\frac{1}{\rho}\left(\frac{\partial\rho}{\partial\Theta}\right)_{p,S} \tag{186}$$

the haline contraction coefficient

$$\beta = \frac{1}{\rho}\left(\frac{\partial\rho}{\partial S}\right)_{p,\Theta} \tag{187}$$

and the squared speed of sound

$$c^2_{\text{sound}} = \left(\frac{\partial p}{\partial\rho}\right)_{S,\Theta}. \tag{188}$$

The material evolution of density is thus partitioned into the evolution of buoyancy (via changes in temperature and salinity) and the evolution of pressure. Buoyancy remains unchanged by processes that are both adiabatic and isohaline, as well as processes where diabatic and non-isohaline effects perfectly cancel. Pressure evolution arises from vertical motion across pressure surfaces which, in a hydrostatic fluid, is equivalent to the vertical motion of mass.

Mass conservation in the form of Eq. (146), along with material evolution of density (185), render the balance

$$-\rho\nabla\cdot\mathbf{v} = -(\rho\alpha)\frac{d\Theta}{dt} + (\rho\beta)\frac{dS}{dt} + \frac{1}{c^2_{\text{sound}}}\frac{dp}{dt}. \tag{189}$$

To help further develop our understanding of this result, consider the mass of a fluid parcel of volume δV written in the form $M = \rho\delta V$. Mass conservation for this parcel means that as the parcel volume increases, the density must decrease, so that

$$\frac{1}{\rho}\frac{d\rho}{dt} = -\frac{1}{\delta V}\frac{d\delta V}{dt}. \tag{190}$$

Correspondingly, from the mass continuity equation (146), the volume of a fluid parcel increases when moving through regions of fluid with a divergent velocity field

$$\frac{1}{\delta V}\frac{d\delta V}{dt} = \nabla\cdot\mathbf{v}. \tag{191}$$

Substitution into Eq. (189) then yields

$$-\frac{\rho}{\delta V}\frac{d\delta V}{dt} = -(\rho\alpha)\frac{d\Theta}{dt} + (\rho\beta)\frac{dS}{dt} + \frac{1}{c^2_{\text{sound}}}\frac{dp}{dt}. \tag{192}$$

This balance states that the volume of a fluid parcel increases (negative left hand side) as the buoyancy of the parcel increases, such as occurs with heating in regions of $\alpha > 0$, or freshening in regions of $\beta > 0$. Volume also increases as the pressure of the parcel decreases ($dp/dt < 0$). We have many opportunities to return to this balance, and its relatives, when interpreting the sea level equations, which account for the accumulation of volume changes throughout a seawater column.

A.5. General and simplified forms of the ocean equilibrium thermodynamics

The thermal expansion coefficient α, haline contraction coefficient β, and squared speed of sound c^2_{sound} are properties of the equilibrium thermodynamics of seawater, with (IOC et al., 2010) summarizing the state of the science. In the ocean, these fields are nonlinear functions of the conservative temperature, salinity, and pressure. This functional dependence leads to the processes of cabbeling and thermobaricity, in which parcels move dianeutrally through mixing effects by mesoscale eddies acting along neutral directions (McDougall, 1987b). Elements of these processes are described in Section 6, where we illustrate how they impact on global mean sea level through the non-Boussinesq steric effect. Additionally, as shown in Section 3, the values for α, β, and c^2_{sound} introduce scales that further influence how physical processes and boundary fluxes impact global mean sea level through the non-Boussinesq steric effect.

Under certain idealized situations, we may approximate α, β, and ρc^2_{sound} to be constants independent of the ocean state. This approximation simplifies the equilibrium thermodynamics to help characterize where the more general ocean thermodynamics is fundamental. In particular, as shown in Section 6, the simplified thermodynamics associated with constant α, β, and ρc^2_{sound} eliminates the processes of cabbeling and thermobaricity. Furthermore, with constant α, β, and ρc^2_{sound}, mass conservation in the form of Eq. (192) indicates that the material evolution for the volume of a fluid parcel is a linear function of material changes in conservative temperature, salinity, and pressure. In the special case where density is a function just of conservative temperature, a constant $\alpha = -\rho^{-1}\partial\rho/\partial\Theta$ leads to $\rho(\Theta) = \rho_o e^{-\alpha(\Theta-\Theta_o)}$, where $\rho_o = \rho(\Theta_o)$. For conservative temperatures near to the reference value Θ_o, density is given by the linear equation of state

$$\rho(\Theta) \approx \rho_o[1 - \alpha(\Theta - \Theta_o)]. \tag{193}$$

In turn, a constant α with a linear equation of state corresponds to $\alpha = -\rho_o^{-1}\partial\rho/\partial\Theta$.

Appendix B. The global ocean–ice model

In this appendix we detail the global ocean–sea ice model configuration used in this paper, with particular attention given to processes impacting the buoyancy budget and thus the budget for sea level.

B.1. Model configuration

The global ocean–ice model used in this study is based on the ocean and sea ice components used in the ESM2M earth system model developed at GFDL for the IPCC AR5 assessement (Dunne et al., in revision). In particular, the ocean component in ESM2M is an evolutionary step from that used in CM2.1 for the AR4 assessment, as documented by Delworth et al. (2006), Griffies et al. (2005) and Gnanadesikan et al. (2006). The basic features of the ocean–ice model are listed here.

- The ocean and sea ice models use the same horizontal grid, which is one degree zonal and nominal one degree latitudinally. The latitudinal resolution is refined to 1/3 degree at the equator, thus leading to 200 latitude rows in total. The ocean has 50 vertical levels, with 22 levels in the upper 220 m.
- The ocean model uses the generalized level coordinates available in the Modular Ocean Model (MOM; Griffies (2009)). In particular, the mass conserving non-Boussinesq configuration uses a scaled pressure variable

$$p^* = p^o_b\left(\frac{p - p_a}{p_b - p_a}\right), \tag{194}$$

where p_a is the pressure applied at the ocean surface from the atmosphere and/or sea ice, p_b is the hydrostatic pressure at the ocean bottom, and p^o_b is a time independent reference bottom pressure. The volume conserving Boussinesq configuration uses the z^* vertical coordinate from Stacey et al. (1995) and Adcroft and Campin (2004) (see also the appendix to Griffies et al. (2011)), defined as

$$z^* = H\left(\frac{z - \eta}{H + \eta}\right), \tag{195}$$

where $z = -H(x,y)$ is the ocean bottom.

- The surface boundary conditions are given by the Coordinated Ocean–ice Reference Experiments (CORE) protocol as detailed by Griffies et al. (2009), which uses the Normal Year Forcing dataset from Large and Yeager (2009) with a monthly mean river runoff updated from Dai et al. (2009). Sea surface salinity is restored to climatology using a restoring time scale of 60 days over a 10 m top model grid cell, and the global mean of this restoring is normalized to zero at each model time step. Sea surface salinity restoring is an artefact of running an ocean–ice model decoupled from an interactive atmosphere, and it is required to maintain a stable simulation over the centennial time scale considered in this paper (Griffies et al., 2009). Additionally, the global mean of precipitation, evaporation, and runoff is set to zero at each model time step to help remove tendencies for long-term drift, with this approach also commonly used for simulations in Griffies et al. (2009).

B.2. Terms affecting the buoyancy budget

In addition to the boundary fluxes of heat and salt detailed in Section 3.4, we expose here details of certain ocean processes that impact on the budget for buoyancy within the ocean model, and thus impact on the sea level budget.

- Shortwave radiation is allowed to penetrate through the water column using a climatological chlorophyll field as updated from the methods detailed in Sweeney et al. (2005). The shortwave attenuation with ocean depth is based on the seawater optics of Manizza et al. (2005).
- Geothermal heating is introduced at the ocean bottom. The geothermal heat flux was generated from spherical harmonic coefficients given by Hamza et al. (2008). In their analysis the global averaged geothermal heating of the ocean is approximately $0.062\ \mathrm{W\,m^{-2}}$. In contrast, the work of Emile-Geay and Madec (2009) chose a different product that leads to an averaged heating of $0.086\ \mathrm{W\,m^{-2}}$, though the shape of their heat flux is similar to that used here.
- Neutral diffusion (Section 6) is based on Griffies et al. (1998) with a constant diffusivity of $600\ \mathrm{m^2\,s^{-1}}$ and the neutral slope tapering scheme of Danabasoglu and McWilliams (1995) using 1/200 for the maximum slope.
- Following the recommendations from Treguier et al. (1997), Ferrari et al. (2008), and Ferrari et al. (2010), neutral diffusion is exponentially transitioned to horizontal diffusion in those regions where the surface boundary layer is encountered. Furthermore, following from the recommendations of Gerdes et al. (1991), neutral diffusive fluxes are converted to horizontal diffusion next to solid walls. Fig. 12 shows the contribution to the non-Boussinesq steric effect from such boundary mixing processes.
- The quasi-Stokes transport from mesoscale eddies (Section 7) is implemented using the skew flux approach of Griffies (1998). The quasi-Stokes streamfunction is computed via a boundary value problem extending across the full ocean column according to Ferrari et al. (2010), which contrasts to the the local approach of Gent and McWilliams (1990) and Gent et al. (1995). The horizontal variation of the eddy diffusivity is based on vertically averaged flow properties (Griffies et al., 2005), with an allowable range of values specified at $100\ \mathrm{m^2\,s^{-1}} - 800\ \mathrm{m^2\,s^{-1}}$.
- The parameterization of submesoscale eddy induced mixed layer restratification (Section 7) is based on Fox-Kemper et al. (2011).
- Ocean vertical mixing is parameterized using the KPP scheme from Large et al. (1994); parameterizations of tide mixing from Simmons et al. (2004) and Lee et al. (2006); enhanced vertical diffusivity in regions of gravitationally unstable stratification; and a specified background diffusivity $\approx 10^{-5}\ \mathrm{m^2\,s^{-1}}$. The net effect from these schemes is a total vertical tracer diffusivity, whose impact on the non-Boussinesq steric effect is discussed in Section 5.1. The KPP scheme also provides a non-local mixing term that appears as a source in the temperature and salinity equations (21) and (22). The non-local KPP contribution to the non-Boussinesq steric effect is discussed in Section 5.2.
- There is tracer mixing due to parameterizations of overflow processes and inland sea exchange, with details given in Griffies et al. (2005). These processes contribute a negligible effect to global mean sea level (see Table 1).
- As river water enters the ocean, it is mixed into the upper four grid cells with the ambient water. The river water is assumed to have zero salinity and have the same temperature as the sea surface. This mixing generally increases the seawater buoyancy, and so provides a positive contribution to sea level (see Table 1).
- Due to the computational null-mode present on a B-grid (Mesinger, 1973; Killworth et al., 1991), the bottom pressure is smoothed using a Laplacian filter. This smoothing necessitates a corresponding flux of buoyancy in order to conserve tracer (see Section 12.9 of Griffies (2004)). This smoothing contributes a relatively small effect to global mean sea level (see Table 1).
- The sea ice model assumes a uniform salinity of five parts per thousand (see the Appendix toDelworth et al. (2006)) (Section 3.4.2).

B.3. Experimental design

The ocean–ice model simulation was extended for 600 years using the volume conserving Boussinesq version with z^* as the vertical coordinate. It was then re-initialized at year 600 with zero velocity and zero sea level for both the mass conserving non-Boussinesq version using the vertical coordinate p^*, and the volume conserving Boussinesq version using z^*. The 600 year spin-up allows for certain of the ocean features to reach quasi-equilibrium over a multi-centennial time scale, and the reinitialization provides for a clear comparison of the non-Boussinesq and Boussinesq sea level patterns shown in Fig. 3.

The results shown in this paper are taken as 20 year means from years 141–160 after the re-initialization. The qualitative features of the patterns are reasonably stationary even with single year means, since the Normal Year Forcing from Large and Yeager (2009) uses a repeating annual cycle. Furthermore, we found no significant differences between all patterns and their global means whether diagnosed from the volume conserving Boussinesq or mass conserving non-Boussinesq simulations. Finally, note that initialization of the p^* simulation from year 600 of the z^* simulation leads to a slight warm drift in the p^* simulation.

B.4. Caveats on water fluxes in the ocean–ice simulation

As detailed in Griffies et al. (2009), ocean–ice simulations have nontrivial limitations, many of which relate to the surface hydrological forcing. These limitations are summarized here.

- The global mean precipitation minus evaporation plus river runoff is normalized to zero at each time step to reduce long term drift arising in a model absent an interactive atmosphere and land model (Griffies et al., 2009). So the only means for net liquid water to enter the ocean is through exchange with the sea ice model.
- The river runoff dataset from Large and Yeager (2009) is an annual mean, with no seasonal cycle.
- There is no solid runoff from calving land ice.

- Sea surface salinity was restored to climatology using a restoring time scale of 60 days over a 10 m top model grid cell. The net salt transport from the restoring is normalized to zero at each model time step. The only means for the restoring salt term to contribute to the non-Boussinesq steric effect is through the weak spatial dependence of the haline contraction coefficient, β, and the surface density, $\rho(\eta)$ (see Eq. (46)). The net contribution to global mean sea level from this term remains small relative to the more physically relevant terms (see Table 1).

Appendix C. Inverse barometer sea level responses

Sea level is depressed in response to applied surface loading. An *inverse barometer* response of sea level is characterized by an exact compensation for the surface loading, so that there is no signal in the horizontal pressure gradient nor in the bottom pressure. That is, the sea level depresses by just the amount needed to compensate for the added loading. We describe in this section two such responses that are commonly encountered in ocean climate studies: one due to atmospheric loading, and one due to sea ice loading. These responses of sea level to applied forcing are important when making statements about the effective mean sea level impacting coastlines.

C.1. Inverse barometer response to atmospheric loading

Hydrostatic pressure at the ocean bottom can be written

$$p_b = p_a + g\int_{-H}^{\eta}\rho\,dz = p_a + g\int_{0}^{\eta}\rho\,dz + g\int_{-H}^{0}\rho\,dz$$
$$= p_a + g\eta\bar{\rho}^{\eta} + gH\bar{\rho}^{H}, \tag{196}$$

where we introduced the resting-column averaged density

$$H\bar{\rho}^{H} = \int_{-H}^{0}\rho\,dz, \tag{197}$$

and near-surface averaged density

$$\eta\bar{\rho}^{\eta} = \int_{0}^{\eta}\rho\,dz. \tag{198}$$

For convenience, assume the surface height η to be nonzero in the following, thus ensuring $\bar{\rho}^{\eta} > 0$. Furthermore, for those cases where $\eta < 0$, we set density in the region between $z = 0$ and η equal to $\rho(\eta)$ so that the formalism holds for both $\eta > 0$ and $\eta < 0$.

At any instance in time, the applied pressure consists of a global mean, $\overline{p_a}$, plus a fluctuation about the mean, so that the bottom pressure can be written as

$$p_b = \overline{p_a} + g\bar{\rho}^{\eta}\left(\eta + \frac{p_a - \overline{p_a}}{g\bar{\rho}^{\eta}}\right) + gH\bar{\rho}^{H}$$
$$= \overline{p_a} + g\bar{\rho}^{\eta}(\eta - \eta^{ib}) + gH\bar{\rho}^{H}, \tag{199}$$

where we introduced the *inverse barometer* surface height (see, e.g., Eq. (9.9.4) in Gill, 1982)[4]

$$\eta^{ib} = \frac{\overline{p_a} - p_a}{g\bar{\rho}^{\eta}}. \tag{200}$$

In the general case, the ocean sea level can be written

$$\eta = \eta' + \eta^{ib} \tag{201}$$

so that

$$p_b = \overline{p_a} + g\bar{\rho}^{\eta}\eta' + gH\bar{\rho}^{H}. \tag{202}$$

[4] As noted on p. 337 of Gill (1982), for an ocean surface respecting the inverse barometer sea level, there is about 1 cm of sea level depression per millibar of atmospheric pressure increase.

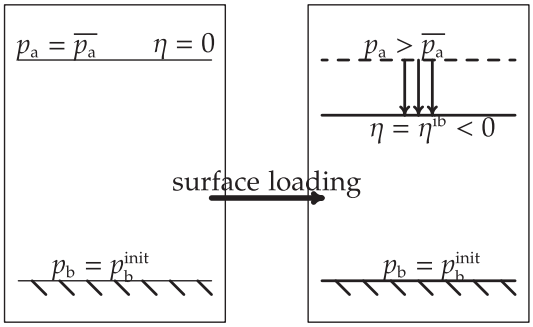

Fig. 15. An illustration of the inverse barometer response of sea level to an anomalous applied pressure. The initial condition is depicted on the left, with sea level $\eta = 0$ and zero anomalous applied pressure $p_a = \overline{p_a}$. As the applied pressure develops an anomaly, here shown for $p_a > \overline{p_a}$, the sea level is depressed. If the depression is equal to the inverse barometer value, $\eta = \eta^{ib}$, then the bottom pressure remains unchanged between the initial and the final configuration. That is, the mass per area of the total column, including the atmosphere and sea ice, remains unchanged when the sea level responds as in inverse barometer.

The special case of $\eta = \eta^{ib}$, in which $\eta' = 0$, is known as an inverse barometer response of the ocean surface to area anomalies in the applied forcing. For example, if the applied pressure has a positive anomaly, then the inverse barometer surface height η^{ib} is negative (Eq. (200)). This situation is depicted in Fig. 15. For an inverse barometer response, the bottom pressure only feels the global mean applied pressure, plus pressure from the weight of the resting ocean liquid

$$p_b^{ib} = \overline{p_a} + gH\bar{\rho}^{H}. \tag{203}$$

An inverse barometer response of the sea level thus represents an exact compensation by the ocean surface to areal anomalies in the applied pressure. That is, the mass per area below the resting ocean at $z = 0$ is the same whether or not there is an anomalous applied pressure.

There are cases where an inverse barometer response is roughly satisfied, such as for large-scale atmospheric anomalies occurring on time scales beyond a few days. Fu (2001) provides a more detailed summary with references.

C.2. Inverse barometer response to sea ice loading

The liquid seawater surface is depressed under the weight of sea ice. To extract the dynamically relevant sea surface fluctuations in the presence of sea ice loading, we pursue the same formulation as in Section C.1 for an inverse barometer response to atmospheric loading. Here, define an inverse barometer surface height associated with fluctuations in the sea ice pressure loading on the liquid ocean. It is convenient to compute this inverse barometer response relative to the case of zero sea ice, so that

$$\eta_{ice}^{ib} = -\left(\frac{p_{ice}}{g\bar{\rho}^{\eta}}\right) \tag{204}$$

with p_{ice} the pressure loading on the liquid ocean due to sea ice. With the inverse barometer sea surface defined as such, the bottom pressure takes the form

$$p_b^{ib} = g\bar{\rho}^{\eta}\eta' + g\bar{\rho}^{H}H, \tag{205}$$

where

$$\eta' = \eta - \eta_{ice}^{ib} = \eta + \frac{p_{ice}}{g\bar{\rho}^{\eta}} \tag{206}$$

is an effective sea level. That is, only fluctuations in surface height relative to the sea ice inverse barometer η_{ice}^{ib} impact bottom pressure.

As sea ice forms, there is a transfer of mass (freshwater, salt, and other tracers) between the liquid phase and solid phase. The total mass in the two phases within a vertical column remains unaffected by the phase change. The bottom pressure therefore remains unchanged as sea ice forms. The liquid sea surface is thus depressed by an amount equal to the inverse barometer $\eta^{\rm ib}_{\rm ice}$. Hence, when measuring sea level in regions including sea ice, the effective sea level

$$\eta^{\rm effective} = \eta' \tag{207}$$

is relevant for determining the effects of sea level on coastlines. That is, as sea ice melts or forms, only those sea level fluctuations relative to $\eta^{\rm effective}$ impact coastlines. Furthermore, as noted by Campin et al. (2008), $\eta^{\rm effective}$ is roughly that level to which liquid water would rise upon drilling a hole through the sea ice.

What is the thickness of sea ice in relation to the depression of the sea level? To answer this question, assume sea ice pressure satisfies the hydrostatic balance, in which case the applied pressure on the liquid seawater arising from the floating sea ice is

$$p_{\rm ice} = \frac{g M_{\rm ice}}{A_{\rm ice}}, \tag{208}$$

with $M_{\rm ice}$ the ice mass and $A_{\rm ice}$ the sea ice area in contact with the liquid seawater. Furthermore, let the mass of ice be given by

$$M_{\rm ice} = \rho_{\rm ice} A_{\rm ice} h_{\rm ice}, \tag{209}$$

where $\rho_{\rm ice}$ is the ice density, and $h_{\rm ice}$ defines the ice thickness. Use of this relation for a sea level equal to its inverse barometer value (204) leads to

$$h_{\rm ice} = |\eta^{\rm ib}_{\rm ice}| \frac{\bar\rho^{\eta}}{\rho_{\rm ice}}. \tag{210}$$

Since the density of ice is about 90% of liquid seawater, the thickness of sea ice is about 10/9 times larger than the sea level depression. The extra sea ice thickness will rise above the sea surface, with the majority (about 90%) of the sea ice sitting beneath the liquid surface.

We close this subsection by making a connection between Archimedes' Principle and the inverse barometer response to sea ice loading. For this purpose, again assume sea ice pressure satisfies the hydrostatic balance, so that the inverse barometer surface height is then given by

$$\eta^{\rm ib}_{\rm ice} = -\left(\frac{M_{\rm ice}}{A_{\rm ice}\bar\rho^{\eta}}\right). \tag{211}$$

The volume of liquid seawater displaced by the floating sea ice is then given by

$$V^{\rm displace} = |\eta^{\rm ib}_{\rm ice}| A_{\rm ice} = \frac{M_{\rm ice}}{\bar\rho^{\eta}} = \frac{p_{\rm ice} A_{\rm ice}}{g\bar\rho^{\eta}} = \frac{F_{\rm ice}}{g\bar\rho^{\eta}}. \tag{212}$$

In the last step, we introduced the force $F_{\rm ice} = p_{\rm ice} A_{\rm ice}$ exerted on the liquid seawater from the floating ice. Through Newton's Third Law, this force is equal in magnitude to that exerted by the liquid seawater on the ice, which identifies it as the buoyancy force that keeps the sea ice floating

$$F_{\rm ice} = g\bar\rho^{\eta} V^{\rm displace}. \tag{213}$$

This relation is an expression of Archimedes' Principle, which states that the buoyancy force exerted on a body within a liquid is given by the weight of the liquid displaced by the body. The presence of an averaged density $\bar\rho^{\eta}$ reflects the generally nonuniform density of the liquid displaced by the sea ice. For most purposes, however, this density can be equated to the ocean surface density $\rho(z = \eta)$. For an analysis with volume conserving Boussinesq fluids, $\bar\rho^{\eta}$ is replaced by ρ_o.

Appendix D. Sea level in volume conserving Boussinesq fluids

The kinematics of Boussinesq fluids are based on volume conservation rather than mass conservation. Consequently, Boussinesq fluids omit the non-Boussinesq steric effect and the global steric effect. As shown in Figs. 2 and 3, the non-Boussinesq steric effect has little impact on the large-scale patterns of sea level. However, as noted by Greatbatch (1994), volume conserving Boussinesq models fail to capture a proper representation of global mean sea level. The purpose of this appendix is to detail diagnostic corrections that allow volume conserving Boussinesq models to account for the missing non-Boussinesq steric effect in their global mean sea level. The presentation is aimed at exposing details, unavailable in the literature, of use for practical calculations with volume conserving Boussinesq ocean climate models.

D.1. Global ocean volume and mass

To develop a basic understanding of Boussinesq fluid kinematics, reconsider the discussion of global mean sea level given in Section 4.5. The key difference here is that rather than conserving mass, the Boussinesq fluid conserves volume, which is realized by introducing a nonzero mass source/sink to the Boussinesq fluid. That is, for a volume conserving Boussinesq ocean, $\partial_t \mathcal{V} = 0$ in the absence of surface boundary fluxes, so that seawater mass picks up a spurious source associated with changes in global mean density

$$\partial_t \mathcal{M} = \mathcal{V} \partial_t \langle \rho \rangle \quad \text{volume conserving ocean.} \tag{214}$$

Consequently, if the density changes, the Boussinesq mass changes, even when there are zero fluxes of mass across the ocean boundaries. For example, when the ocean warms with a positive thermal expansion coefficient, then density decreases. In order to maintain a constant volume for the Boussinesq fluid, there must in turn be a decrease in ocean mass when density decreases. We consider this change in mass to be physically spurious, since it is not a process that appears in the real ocean. Nonetheless, it is a process that occurs in Boussinesq ocean models, and must be considered when examining their mass budget. In particular, if interested in the mass distribution of seawater, such as needed for angular momentum (Bryan, 1997), bottom pressure (Ponte, 1999), or geoid perturbations (Kopp et al., 2010), one must account for this spurious mass change that arises due to the oceanic Boussinesq approximation. Section D.3 presents the global correction commonly used to partially correct for the spurious mass source.

D.2. Evolution of Boussinesq sea level

Volume conservation for a fluid parcel means the three-dimensional velocity field is non-divergent: $\nabla \cdot \mathbf{v} = 0$. Integrating this expression over the depth of the ocean, and using the surface and bottom kinematic boundary conditions

$$(\partial_t + \mathbf{u} \cdot \nabla)\eta^{\rm B} = Q_{\rm m}/\rho_o + w \quad \text{at } z = \eta^{\rm B}, \tag{215}$$

$$w + \mathbf{u} \cdot \nabla H = 0 \quad \text{at } z = -H \tag{216}$$

leads to the evolution equation for the volume conserving Boussinesq surface height

$$\frac{\partial \eta^{\rm B}}{\partial t} = Q_{\rm m}/\rho_o - \nabla \cdot \mathbf{U}. \tag{217}$$

In this equation, ρ_o is a constant reference density typically taken as a representative mean value for the ocean domain. The Boussinesq sea level equation (217) is isomorphic to the hydrostatic non-Boussinesq bottom pressure equation (11). More complete relations between hydrostatic Boussinesq and hydrostatic

non-Boussinesq fluids have been discussed by Huang et al. (2001), DeSzoeke and Samelson (2002), Marshall et al. (2004), and Losch et al. (2004).

Eq. (217) indicates that the Boussinesq surface height is affected by two physical processes.

1. *Boundary fluxes*: The introduction of volume through the ocean boundaries, with the mass flux converted to a volume flux via the constant reference density ρ_o.
2. *Ocean dynamics*: The convergence of vertically integrated velocity.

The Boussinesq sea level in Eq. (217) is not impacted by a non-Boussinesq steric effect (Section 3). Herein lies the reason that volume conserving Boussinesq models do not account for changes in global mean sea level associated with changes in global mean buoyancy forcing.

D.3. Diagnostic corrections used for Boussinesq fluids

We now present diagnostic adjustments made to the Boussinesq sea level and bottom pressure to partially correct for the missing non-Boussinesq steric effect.

D.3.1. Adjusting for the missing global steric sea level

For the diagnosis of sea level in a volume conserving Boussinesq model, Greatbatch (1994) argued for the introduction of a globally uniform time dependent correction to be added to the Boussinesq sea level at each grid point. In effect, the "corrected" sea level to be diagnosed from a Boussinesq model evolves according to the following equation

$$\frac{\partial \eta^{\mathrm{B}}_{\mathrm{diag}}}{\partial t} = \frac{\partial \eta^{\mathrm{B}}}{\partial t} + \frac{\partial \bar{\eta}_{\text{non-bouss steric}}}{\partial t}, \tag{218}$$

where the prognostic surface height η^{B} evolves according to $\partial \eta^{\mathrm{B}}/\partial t = \mathrm{Q_m}/\rho_o - \nabla \cdot \mathbf{U}$ as in Eq. (217). To account for the global steric effect missing from the Boussinesq model, the new term in the diagnostic equation (218) is given by

$$\frac{\partial \bar{\eta}_{\text{non-bouss steric}}}{\partial t} = -\frac{\mathcal{V}}{\mathcal{A}} \left\langle \frac{1}{\rho} \frac{\mathrm{d}\rho}{\mathrm{d}t} \right\rangle \approx -\frac{\mathcal{V}}{\mathcal{A}} \frac{\partial_t \langle \rho \rangle}{\langle \rho \rangle}. \tag{219}$$

The approximation in this equation follows from the discussion surrounding equation (77), where it was noted that the global mean non-Boussinesq steric effect corresponds to the global steric effect, with the correspondence exact in the case of zero water fluxes. It is at the same level as the approximation

$$\overline{\left(\frac{\mathrm{Q_m}}{\rho(\eta)} \right)} \approx \frac{1}{\rho_o} \overline{\mathrm{Q_m}} \tag{220}$$

commonly used in Boussinesq models. The global steric effect involves the time tendency of the global mean *in situ* density $\langle \rho \rangle$, with this term readily diagnosed from model output. It is therefore the global steric effect that is commonly diagnosed to adjust sea level in volume conserving Boussinesq ocean models, rather than the non-Boussinesq steric effect. Again, adjusting with the global steric effect ensures that the diagnosed global mean sea level in the Boussinesq model better emulates the sea level in the non-Boussinesq model, and it does so by introducing to the volume conserving Boussinesq model the impact of global mass conservation.

We now discuss how to evaluate the diagnosed sea level $\eta^{\mathrm{B}}_{\mathrm{diag}}$ at any particular discrete model time step. For this purpose, start by noting that a discrete time step of the global steric sea level equation (219) can be written

$$\bar{\eta}_{\text{non-boussteric}}(\tau_{n+1}) = \bar{\eta}_{\text{non-bouss steric}}(\tau_n) + \frac{\mathcal{V}(\tau_{n+1/2})}{\mathcal{A}} \ln \left(\frac{\langle \rho(\tau_n) \rangle}{\langle \rho(\tau_{n+1}) \rangle} \right), \tag{221}$$

where the ocean volume can be approximated as $\mathcal{V}(\tau_{n+1/2}) = (\mathcal{V}(\tau_{n+1}) + \mathcal{V}(\tau_n))/2$. We are often interested in the global steric sea level relative to an initial condition or reference state where it is assumed to be zero. Correspondingly, the initial value for the diagnosed sea level $\eta^{\mathrm{B}}_{\mathrm{diag}}(\tau_{n=0})$ is the same as the initial Boussinesq sea level $\eta^{\mathrm{B}}(\tau_{n=0})$. These initial conditions allow us to update $\eta^{\mathrm{B}}_{\mathrm{diag}}$ according to the trivial diagnostic equation

$$\eta^{\mathrm{B}}_{\mathrm{diag}}(\tau_{n+1}) = \eta^{\mathrm{B}}(\tau_{n+1}) + \bar{\eta}_{\text{non-bouss steric}}(\tau_{n+1}), \tag{222}$$

where the Boussinesq sea level $\eta^{\mathrm{B}}(\tau_{n+1})$ is updated according to a discretized version of Eq. (217)

$$\frac{\eta^{\mathrm{B}}(\tau_{n+1}) - \eta^{\mathrm{B}}(\tau_n)}{\Delta \tau} = \frac{\mathrm{Q_m}(\tau_n)}{\rho_o} - \nabla \cdot \mathbf{U}(\tau_n), \tag{223}$$

and the global mean steric sea level $\bar{\eta}_{\text{non-bouss steric}}(\tau_{n+1})$ is updated according to Eq. (221).

D.3.2. Approximating the global steric sea level correction

In practice, there are various approximations made when evaluating the global steric sea level correction from a volume conserving Boussinesq ocean climate model simulation, and we outline here three common approximations. For many purposes, the resulting global mean sea levels resulting from these approximations are nearly identical.

1. *Approximation A*: The first approximation considers the leading order expansion of the natural logarithm in Eq. (221), so that
$$\ln \left(\frac{\langle \rho(\tau_n) \rangle}{\langle \rho(\tau_{n+1}) \rangle} \right) = \ln \left(1 - \frac{\langle \rho(\tau_{n+1}) \rangle - \langle \rho(\tau_n) \rangle}{\langle \rho(\tau_{n+1}) \rangle} \right) \approx -1 + \frac{\langle \rho(\tau_n) \rangle}{\langle \rho(\tau_{n+1}) \rangle}. \tag{224}$$
2. *Approximation B*: The next approximation is to note that the global ocean volume $\mathcal{V}$ changes only by a tiny fractional amount during the course of a centennial scale climate simulation. Hence, it is common to keep the volume appearing in the steric correction equal to its initial value $\mathcal{V}(\tau) = \mathcal{V}^0$, in which case
$$\eta^{\mathrm{B}}_{\mathrm{diag}}(\tau_N) \approx \eta^{\mathrm{B}}(\tau_N) + \frac{\mathcal{V}^0}{\mathcal{A}} \ln \left(\frac{\langle \rho \rangle^0}{\langle \rho(\tau_N) \rangle} \right), \tag{225}$$
where $\langle \rho \rangle^0$ is the global mean density for the initial state. For a rigid lid model, or a model that uses virtual salt fluxes, the ocean model volume is indeed held constant. This approximation breaks down when the ocean volume changes by a sizable amount, as may occur for studies of massive land ice melting.
3. *Approximation C*: The final approximation uses time mean density fields to compute the time tendency, and the corresponding use of either a time mean volume (or a constant volume as in Approximation B). This approximation is generally used when examining the output of many different climate models, in which it is typical that the analyst only has access to the time mean (monthly or annual) density field (e.g.,Yin et al., 2010). This approximation is the *de facto* method for quantifying sea level rise in Boussinesq ocean climate simulations.

D.3.3. Adjusting for the spurious mass source

The spurious mass source appearing in Eq. (214) provides a spurious tendency for the evolution of mass in each grid cell of a volume conserving Boussinesq model; e.g., in columns where density is reduced, mass is also spuriously reduced. Following the above approach used to adjust the Boussinesq sea level, it is

common to adjust the mass of a column of Boussinesq fluid to counteract this spurious mass source/sink. The form of the area weighted adjustment is given by

$$m^{\mathrm{B}}_{\mathrm{diag}}(x,y,\tau) = m^{\mathrm{B}}(x,y,\tau) - \frac{\mathrm{d}A}{\mathcal{A}}\mathcal{V}(\tau)(\langle\rho(\tau)\rangle - \langle\rho(\tau-1)\rangle), \tag{226}$$

where $\mathrm{d}A$ is the horizontal area for a grid cell, and

$$m^{\mathrm{B}}(x,y,\tau) = \mathrm{d}A\int_{-H}^{\eta^{\mathrm{B}}}\rho\,\mathrm{d}z \tag{227}$$

is the mass in a column of Boussinesq seawater. The corresponding correction to the Boussinesq bottom pressure takes the form

$$\frac{\partial(p_{\mathrm{b}}-p_{\mathrm{a}})^{\mathrm{B}}_{\mathrm{diag}}}{\partial t} = \frac{\partial(p_{\mathrm{b}}-p_{\mathrm{a}})^{\mathrm{B}}}{\partial t} - \frac{g\mathcal{V}\partial_t\langle\rho\rangle}{\mathcal{A}}, \tag{228}$$

which is discretized as

$$(p_{\mathrm{b}}-p_{\mathrm{a}})^{\mathrm{B}}_{\mathrm{diag}} = (p_{\mathrm{b}}-p_{\mathrm{a}})^{\mathrm{B}} - g\frac{\mathcal{V}(\tau)}{\mathcal{A}}(\langle\rho(\tau)\rangle - \langle\rho(\tau-1)\rangle). \tag{229}$$

In this equation,

$$(p_{\mathrm{b}}-p_{\mathrm{a}})^{\mathrm{B}} = \frac{gm^{\mathrm{B}}}{\mathrm{d}A} = g\int_{-H}^{\eta^{\mathrm{B}}}\rho\,\mathrm{d}z \tag{230}$$

is the weight per area in a column of Boussinesq seawater. This adjustment to the bottom pressure was used by Bryan (1997), Ponte (1999), and Kopp et al. (2010) for their studies of angular momentum, bottom pressure, and geoid, respectively, using volume conserving Boussinesq ocean models.

Appendix E. Details of the cabbeling and thermobaricity calculation

We provide here details for the derivation of the non-Boussinesq steric effect arising from cabbeling and thermobaricity given by Eq. (102) in Section 6.5. Following from McDougall (1987b), this approach is based on working with the coarse-grained or averaged equations of an ocean model, where averaging has been applied over the mesoscales. To streamline the notation in the following manipulations, we introduce a comma notation to signify partial derivatives, in which case, for example,

$$v_{,\Theta} = \frac{\partial v}{\partial\Theta} \tag{231}$$

and

$$v_{,\Theta p} = \frac{\partial^2 v}{\partial\Theta\,\partial p} \tag{232}$$

where $v = \rho^{-1}$ is the specific volume.

As a first step, eliminate the salt flux by using Eq. (101) to write

$$\mathbf{J}^{(\Theta)}\cdot\nabla(\alpha/\rho) - \mathbf{J}^{(S)}\cdot\nabla(\beta/\rho) = \mathbf{J}^{(\Theta)}\cdot[v_{,S}\nabla v_{,\Theta} - v_{,\Theta}\nabla v_{,S}]/v_{,S}. \tag{233}$$

Next, expand the gradients of the specific volume to write

$$\nabla v_{,\Theta} = v_{,\Theta\Theta}\nabla\Theta + v_{,\Theta S}\nabla S + v_{,\Theta p}\nabla p, \tag{234}$$

$$\nabla v_{,S} = v_{,SS}\nabla S + v_{,\Theta S}\nabla\Theta + v_{,Sp}\nabla p, \tag{235}$$

so that

$$\begin{aligned} v_{,S}\nabla v_{,\Theta} - v_{,\Theta}\nabla v_{,S} &= \nabla\Theta(v_{,S}v_{,\Theta\Theta} - v_{,\Theta}v_{,\Theta S}) + \nabla S(v_{,S}v_{,\Theta S} - v_{,\Theta}v_{,SS}) \\ &\quad + \nabla p(v_{,S}v_{,\Theta p} - v_{,\Theta}v_{,Sp}). \end{aligned} \tag{236}$$

Next make use of the identity (101), as well as the following expression holding true for neutral diffusive fluxes

$$\nabla S\cdot\mathbf{J}^{(\Theta)} = \nabla\Theta\cdot\mathbf{J}^{(S)}, \tag{237}$$

in order to write

$$\mathbf{J}^{(\Theta)}\cdot\nabla S(v_{,S}v_{,\Theta S} - v_{,\Theta}v_{,SS}) = -\mathbf{J}^{(\Theta)}\cdot\nabla\Theta\left(v_{,\Theta}v_{,\Theta S} - v_{,SS}\frac{(v_{,\Theta})^2}{v_{,S}}\right). \tag{238}$$

Bringing these results together leads to

$$\begin{aligned} \mathbf{J}^{(\Theta)}\cdot\nabla v_{,\Theta} + \mathbf{J}^{(S)}\cdot\nabla v_{,S} &= \mathbf{J}^{(\Theta)}\cdot\nabla p\left[v_{,\Theta p} - v_{,pS}\left(\frac{v_{,\Theta}}{v_{,S}}\right)\right] \\ &\quad + \mathbf{J}^{(\Theta)}\cdot\nabla\Theta\left[v_{,\Theta\Theta} - 2v_{,\Theta S}\left(\frac{v_{,\Theta}}{v_{,S}}\right) + v_{,SS}\left(\frac{v_{,\Theta}}{v_{,S}}\right)^2\right] \\ &= -\rho^{-2}\mathbf{J}^{(\Theta)}\cdot\nabla p\left[\rho_{,\Theta p} - \rho_{,pS}\left(\frac{\rho_{,\Theta}}{\rho_{,S}}\right)\right] - \rho^{-2}\mathbf{J}^{(\Theta)} \\ &\quad\cdot\nabla\Theta\left[\rho_{,\Theta\Theta} - 2\rho_{,\Theta S}\left(\frac{\rho_{,\Theta}}{\rho_{,S}}\right) + \rho_{,SS}\left(\frac{\rho_{,\Theta}}{\rho_{,S}}\right)^2\right]. \end{aligned} \tag{239}$$

We next write the terms in brackets in forms consistent with those introduced by McDougall (1987b). For that purpose, introduce the *cabbeling* parameter (units of squared inverse temperature)

$$\begin{aligned} \mathcal{C} &= \frac{\partial\alpha}{\partial\Theta} + 2\frac{\alpha}{\beta}\frac{\partial\alpha}{\partial S} - \left(\frac{\alpha}{\beta}\right)^2\frac{\partial\beta}{\partial S} \\ &= -\rho^{-1}\left[\rho_{,\Theta\Theta} - 2\rho_{,\Theta S}\left(\frac{\rho_{,\Theta}}{\rho_{,S}}\right) + \rho_{,SS}\left(\frac{\rho_{,\Theta}}{\rho_{,S}}\right)^2\right] \\ &= \rho\left[v_{,\Theta\Theta} - 2v_{,\Theta S}\left(\frac{v_{,\Theta}}{v_{,S}}\right) + v_{,SS}\left(\frac{v_{,\Theta}}{v_{,S}}\right)^2\right] \end{aligned} \tag{240}$$

and *thermobaricity* parameter (units of inverse temperature times inverse pressure)

$$\begin{aligned} \mathcal{T} &= \beta\partial_p\left(\frac{\alpha}{\beta}\right) = \frac{\partial\alpha}{\partial p} - \frac{\alpha}{\beta}\frac{\partial\beta}{\partial p} = \rho v_{,S}\partial_p\left(\frac{v_{,\Theta}}{v_{,S}}\right) \\ &= -\rho^{-1}\rho_{,S}\partial_p\left(\frac{\rho_{,\Theta}}{\rho_{,S}}\right) = -\rho^{-1}\left[\rho_{,\Theta p} - \rho_{,pS}\left(\frac{\rho_{,\Theta}}{\rho_{,S}}\right)\right], \end{aligned} \tag{241}$$

to render the desired result

$$\begin{aligned} &(\mathbf{J}^{(\Theta)}\cdot\nabla(\alpha/\rho) - \mathbf{J}^{(S)}\cdot\nabla(\beta/\rho))_{\text{neutral diffusion}} \\ &\quad = \rho^{-1}\mathbf{J}^{(\Theta)}\cdot(\mathcal{T}\nabla p + \mathcal{C}\nabla\Theta). \end{aligned} \tag{242}$$

References

Adcroft, A., Campin, J.-M., 2004. Rescaled height coordinates for accurate representation of free-surface flows in ocean circulation models. Ocean Modelling 7, 269–284.

Adcroft, A., Scott, J.R., Marotzke, J., 2001. Impact of geothermal heating on the global ocean circulation. Geophysical Research Letters 28, 1735–1738.

Batchelor, G.K., 1967. An Introduction to Fluid Dynamics. Cambridge University Press, Cambridge, England.

Bleck, R., 1978. Finite difference equations in generalized vertical coordinates. Part I: Total energy conservation. Contributions to Atmospheric Physics 51, 360–372.

Bryan, F.O., 1997. The axial angular momentum balance of a global ocean general circulation model. Dynamics of Atmospheres and Oceans 25, 191–216.

Bryan, K., 1996. The steric component of sea level rise associated with enhanced greenhouse warming: a model study. Climate Dynamics 12, 545–555.

Campin, J.-M., Marshall, J., Ferreira, D., 2008. Sea ice–ocean coupling using a rescaled vertical coordinate z*. Ocean Modelling 24, 1–14.

Chaikin, P.M., Lubensky, T.C., 1995. Principles of Condensed Matter Physics. Cambridge University Press, Cambridge, United Kingdom.

Church, J., Gregory, J., 2001. Changes in sea level. In: Climate Change 2001: The Scientific Basis. Cambridge University Press, Cambridge, UK, pp. 639–693.

Cox, M.D., 1987. Isopycnal diffusion in a z-coordinate ocean model. Ocean Modelling 74, 1–5.

Dai, A., Qian, T., Trenberth, K., Milliman, J., 2009. Changes in continental freshwater discharge from 1948–2004. Journal of Climate 22, 2773–2791.

Danabasoglu, G., Large, W., Briegleb, B., 2010. Climate impacts of parameterized nordic sea overflows. Journal of Geophysical Research 115, C11005. http://dx.doi.org/10.1029/2010JC006243.

Danabasoglu, G., McWilliams, J.C., 1995. Sensitivity of the global ocean circulation to parameterizations of mesoscale tracer transports. Journal of Climate 8, 2967–2987.

Davis, R.E., 1994a. Diapycnal mixing in the ocean: equations for large-scale budgets. Journal of Physical Oceanography 24, 777–800.
Davis, R.E., 1994b. Diapycnal mixing in the ocean: the Osborn-Cox model. Journal of Physical Oceanography 24, 2560–2576.
DeGroot, S.R., Mazur, P., 1984. Non-Equilibrium Thermodynamics. Dover Publications, New York, 510 pp.
Delworth, T.L., Broccoli, A.J., Rosati, A., Stouffer, R.J., Balaji, V., Beesley, J.A., Cooke, W.F., Dixon, K.W., Dunne, J., Dunne, K.A., Durachta, J.W., Findell, K.L., Ginoux, P., Gnanadesikan, A., Gordon, C., Griffies, S.M., Gudgel, R., Harrison, M.J., Held, I.M., Hemler, R.S., Horowitz, L.W., Klein, S.A., Knutson, T.R., Kushner, P.J., Langenhorst, A.L., Lee, H.-C., Lin, S., Lu, L., Malyshev, S.L., Milly, P., Ramaswamy, V., Russell, J., Schwarzkopf, M.D., Shevliakova, E., Sirutis, J., Spelman, M., Stern, W.F., Winton, M., Wittenberg, A.T., Wyman, B., Zeng, F., Zhang, R., 2006. GFDL's CM2 global coupled climate models – Part 1: Formulation and simulation characteristics. Journal of Climate 19, 643–674.
DeSzoeke, R.A., 2009. Isentropic averaging. Journal of Marine Research 67, 533–567.
DeSzoeke, R.A., Bennett, A.F., 1993. Microstructure fluxes across density surfaces. Journal of Physical Oceanography 23, 2254–2264.
DeSzoeke, R.A., Samelson, R.M., 2002. The duality between the Boussinesq and non-Boussinesq hydrostatic equations of motion. Journal of Physical Oceanography 32, 2194–2203.
Dunne, J.P., John, J.G., Hallberg, R.W., Griffies, S.M., Shevliakova, E.N., Stouffer, R.J., Krasting, J.P., Sentman, L.A., Milly, P.C.D., Malyshev, S.L., Adcroft, A.J., Cooke, W., Dunne, K.A., Harrison, M.J., Levy, H., Samuels, B.L., Spelman, M., Winton, M., Wittenberg, A.T., Phillips, P.J., Zadeh, N., in revision. GFDLs ESM2 global coupled climate-carbon Earth System Models. Part I: Physical formulation and baseline simulation characteristics. Journal of Climate.
Eden, C., 2012. Relating Lagrangian, residual, and isopycnal means. Journal of Physical Oceanography. http://dx.doi.org/10.1175/JPO-D-11-068.1.
Eden, C., Greatbatch, R., Olbers, D., 2007. Interpreting eddy fluxes. Journal of Physical Oceanography 37, 1282–1296.
Emile-Geay, J., Madec, G., 2009. Geothermal heating, diapycnal mixing and the abyssal circulation. Ocean Science 5 (2), 203–217.
Ferrari, R., Griffies, S.M., Nurser, A., Vallis, G., 2010. A boundary-value problem for the parameterized mesoscale eddy transport. Ocean Modelling 32, 143–156.
Ferrari, R., McWilliams, J., Canuto, V., Dubovikov, M., 2008. Parameterization of eddy fluxes near oceanic boundaries. Journal of Climate 21, 2770–2789.
Fox-Kemper, B., Danabasoglu, G., Ferrari, R., Griffies, S.M., Hallberg, R.W., Holland, M., Peacock, S., Samuels, B., 2011. Parameterization of mixed layer eddies. III: Global implementation and impact on ocean climate simulations. Ocean Modelling 39, 61–78.
Fox-Kemper, B., Ferrari, R., Hallberg, R., 2008. Parameterization of mixed layer eddies. I: Theory and diagnosis. Journal of Physical Oceanography 38, 1145–1165.
Fu, L.-L., 2001. Ocean circulation and variability from satellite altimetry. In: Seidler, G., Church, J., Gould, J. (Eds.), Ocean Circulation and Climate, International Geophysics Series, vol. 77. Academic Press, San Diego, pp. 141–172.
Gent, P.R., McWilliams, J.C., 1990. Isopycnal mixing in ocean circulation models. Journal of Physical Oceanography 20, 150–155.
Gent, P.R., Willebrand, J., McDougall, T.J., McWilliams, J.C., 1995. Parameterizing eddy-induced tracer transports in ocean circulation models. Journal of Physical Oceanography 25, 463–474.
Gerdes, R., Köberle, C., Willebrand, J., 1991. The influence of numerical advection schemes on the results of ocean general circulation models. Climate Dynamics 5, 211–226.
Gill, A., 1982. Atmosphere–Ocean Dynamics. International Geophysics Series, Vol. 30. Academic Press, London, p. 62 + xv pp.
Gill, A.E., Niiler, P., 1973. The theory of the seasonal variability in the ocean. Deep-Sea Research 20 (9), 141–177.
Gnanadesikan, A., Dixon, K.W., Griffies, S.M., Balaji, V., Beesley, J.A., Cooke, W.F., Delworth, T.L., Gerdes, R., Harrison, M.J., Held, I.M., Hurlin, W.J., Lee, H.-C., Liang, Z., Nong, G., Pacanowski, R.C., Rosati, A., Russell, J., Samuels, B.L., Song, S.M., Spelman, M.J., Stouffer, R.J., Sweeney, C.O., Vecchi, G., Winton, M., Wittenberg, A.T., Zeng, F., Zhang, R., 2006. GFDL's CM2 global coupled climate models. Part 2: The baseline ocean simulation. Journal of Climate 19, 675–697.
Greatbatch, R.J., 1994. A note on the representation of steric sea level in models that conserve volume rather than mass. Journal of Geophysical Research 99, 12767–12771.
Greatbatch, R.J., McDougall, T.J., 2003. The non-Boussinesq temporal-residual-mean. Journal of Physical Oceanography 33, 1231–1239.
Gregg, M., Sanford, T., Winkel, D., 2003. Reduced mixing from the breaking of internal waves in equatorial waters. Nature 422, 513–515.
Griffies, S.M., 1998. The Gent-McWilliams skew-flux. Journal of Physical Oceanography 28, 831–841.
Griffies, S.M., 2004. Fundamentals of Ocean Climate Models. Princeton University Press, Princeton, USA, 518 + xxxiv pp.
Griffies, S.M., 2009. Elements of MOM4p1: GFDL Ocean Group Technical Report No. 6. NOAA/Geophysical Fluid Dynamics Laboratory, Princeton, USA, 444 pp.
Griffies, S.M., Adcroft, A.J., 2008. Formulating the equations for ocean models. In: Hecht, M., Hasumi, H. (Eds.), Eddy Resolving Ocean Models, Geophysical Monograph, vol. 177. American Geophysical Union, pp. 281–317.
Griffies, S.M., Biastoch, A., Böning, C.W., Bryan, F., Chassignet, E., England, M., Gerdes, R., Haak, H., Hallberg, R.W., Hazeleger, W., Jungclaus, J., Large, W.G., Madec, G., Samuels, B.L., Scheinert, M., Gupta, A.S., Severijns, C.A., Simmons, H.L., Treguier, A.M., Winton, M., Yeager, S., Yin, J., 2009. Coordinated ocean–ice reference experiments (COREs). Ocean Modelling 26, 1–46.
Griffies, S.M., Böning, C.W., Bryan, F.O., Chassignet, E.P., Gerdes, R., Hasumi, H., Hirst, A., Treguier, A.-M., Webb, D., 2000. Developments in ocean climate modelling. Ocean Modelling 2, 123–192.
Griffies, S.M., Gnanadesikan, A., Dixon, K.W., Dunne, J.P., Gerdes, R., Harrison, M.J., Rosati, A., Russell, J., Samuels, B.L., Spelman, M.J., Winton, M., Zhang, R., 2005. Formulation of an ocean model for global climate simulations. Ocean Science 1, 45–79.
Griffies, S.M., Gnanadesikan, A., Pacanowski, R.C., Larichev, V., Dukowicz, J.K., Smith, R.D., 1998. Isoneutral diffusion in a z-coordinate ocean model. Journal of Physical Oceanography 28, 805–830.
Griffies, S.M., Winton, M., Donner, L.J., Downes, S.M., Farneti, R., Gnanadesikan, A., Horowitz, L.W., Hurlin, W.J., Lee, H.-C., Liang, Z., Palter, J.B., Samuels, B.L., Wittenberg, A.T., Wyman, B.L., Yin, J., Zadeh, N.T., 2011. GFDL's CM3 coupled climate model: characteristics of the ocean and sea ice simulations. Journal of Climate 24, 3520–3544.
Hamza, V., Cardoso, R., Neto, C.P., 2008. Spherical harmonic analysis of the earth's conductive heat flow. International Journal of Earth Science. http://dx.doi.org/10.1007/s00531-007-0254-3.
Hesselberg, T., 1926. Die Gesetze der ausgeglichenen atmosphaerischen Bewegungen. Beiträgeder Physik der freien Atmosphere 12, 141–160.
Hsieh, W., Bryan, K., 1996. Redistribution of sea level rise associated with enhanced greenhouse warming: a simple model study. Climate Dynamics 12, 535–544.
Huang, R.X., Jin, X., Zhang, X., 2001. An oceanic general circulation model in pressure coordinates. Advances in Atmospheric Physics 18, 1–22.
IOC, SCOR, IAPSO, 2010. The international thermodynamic equation of seawater-2010: calculation and use of thermodynamic properties. Intergovernmental Oceanographic Commission, Manuals and Guides No. 56, UNESCO, 196pp. <http://www.TEOS-10.org>.
Iudicone, D., Madec, G., McDougall, T.J., 2008. Water-mass transformations in a neutral density framework and the key role of light penetration. Journal of Physical Oceanography 38, 1357–1376.
Kämpf, J., 2009. Ocean Circulation for Beginners. Springer, Verlag, Berlin, 175 pp.
Killworth, P.D., Stainforth, D., Webb, D.J., Paterson, S.M., 1991. The development of a free-surface Bryan–Cox–Semtner ocean model. Journal of Physical Oceanography 21, 1333–1348.
Klocker, A., McDougall, T.J., 2010a. Influence of the nonlinear equation of state on global estimates of dianeutral advection and diffusion. Journal of Physical Oceanography 40, 1690–1709.
Klocker, A., McDougall, T.J., 2010b. Quantifying the consequences of the ill-defined nature of neutral surfaces. Journal of Physical Oceanography 40, 1866–1880.
Kopp, R.E., Mitrovica, J.X., Griffies, S.M., Yin, J., Hay, C.C., Stouffer, R.J., 2010. The impact of Greenland melt on regional sea level: a preliminary comparison of dynamic and static equilibrium effects. Climatic Change Letters 103, 619–625.
Landau, L.D., Lifshitz, E.M., 1987. Fluid Mechanics. Pergamon Press, Oxford, UK, 539 pp.
Landerer, F., Jungclaus, J., Marotzke, J., 2007. Regional dynamic and steric sea level change in response to the IPCC-A1B scenario. Journal of Physical Oceanography 37, 296–312.
Large, W., McWilliams, J., Doney, S., 1994. Oceanic vertical mixing: a review and a model with a nonlocal boundary layer parameterization. Reviews of Geophysics 32, 363–403.
Large, W.G., Yeager, S., 2009. The global climatology of an interannually varying air–sea flux data set. Climate Dynamics 33, 341–364.
Ledwell, J.R., St.Laurent, L., Girton, J., Toole, J., 2011. Diapycnal mixing in the Antarctic circumpolar current. Journal of Physical Oceanography 41, 241–246.
Ledwell, J.R., Watson, A.J., Law, C.S., 1993. Evidence for slow mixing across the pycnocline from an open-ocean tracer-release experiment. Nature 364, 701–703.
Lee, H.-C., Rosati, A., Spelman, M., 2006. Barotropic tidal mixing effects in a coupled climate model: oceanic conditions in the northern Atlantic. Ocean Modelling 3–4, 464–477.
Lorbacher, K., Marsland, S., Church, J., Griffies, S., Stammer, D., in revision. Rapid barotropic sea-level rise from ice-sheet melting scenarios. Journal of Geophysical Research.
Losch, M., Adcroft, A., Campin, J.-M., 2004. How sensitive are coarse general circulation models to fundamental approximations in the equations of motion? Journal of Physical Oceanography 34, 306–319.
Lowe, J.A., Gregory, J.M., 2006. Understanding projections of sea level rise in a Hadley Centre coupled climate model. Journal of Geophysical Research, C11014.
Manizza, M., Le Quere, C., Watson, A., Buitenhuis, E., 2005. Bio-optical feedbacks among phytoplankton, upper ocean physics and sea–ice in a global model. Geophysical Research Letters 32. http://dx.doi.org/10.1029/2004GL020778.
Marshall, J., Adcroft, A., Campin, J.-M., Hill, C., White, A., 2004. Atmosphere–ocean modeling exploiting fluid isomorphisms. Monthly Weather Review 132, 2882–2894.
McDougall, T.J., 1983. Double diffusive convection caused by coupled molecular diffusion. Journal of Fluid Mechanics 126, 379–397.
McDougall, T.J., 1987a. Neutral surfaces. Journal of Physical Oceanography 17, 1950–1967.
McDougall, T.J., 1987b. Thermobaricity, cabbeling, and water-mass conversion. Journal of Geophysical Research 92, 5448–5464.
McDougall, T.J., 1995. The influence of ocean mixing on the absolute velocity vector. Journal of Physical Oceanography 25, 705–725.
McDougall, T.J., 2003. Potential enthalpy: a conservative oceanic variable for evaluating heat content and heat fluxes. Journal of Physical Oceanography 33, 945–963.

McDougall, T.J., Church, J.A., 1986. Pitfalls with numerical representations of isopycnal and diapycnal mixing. Journal of Physical Oceanography 16, 196–199.
McDougall, T.J., Greatbatch, R., Lu, Y., 2002. On conservation equations in oceanography: how accurate are Boussinesq ocean models? Journal of Physical Oceanography 32, 1574–1584.
McDougall, T.J., McIntosh, P.C., 2001. The temporal-residual-mean velocity. Part II: Isopycnal interpretation and the tracer and momentum equations. Journal of Physical Oceanography 31, 1222–1246.
Mesinger, F., 1973. A method for construction of second-order accurate difference schemes permitting no false two-grid-interval waves in the height field. Tellus 25, 444–457.
Milne, G., Gehrels, W., Hughes, C., Tamisiea, M., 2009. Identifying the causes of sea-level change. Nature Geosciences 2, 471–478.
Mitrovica, J.X., Tamisiea, M.E., Davis, J.L., Milne, G.A., 2001. Recent mass balance of polar ice sheets inferred from patterns of global sea-level change. Nature 409, 1026–1029.
Müller, P., 2006. The Equations of Oceanic Motions, first ed. Cambridge University Press, Cambridge, 302 pp.
Munk, W., 2003. Ocean freshening, sea level rising. Science 300, 2041–2043.
Naveira-Garabato, A., Polzin, K., King, B., Heywood, K., Visbeck, M., 2004. Widspread intense turbulent mixing in the Southern Ocean. Science 303, 210–213.
Nicholls, R., Cazenave, A., 2010. Sea-level rise and its impact on coastal zones. Science 328, 1517–1520.
Nikurashin, M., Ferrari, R., 2010. Radiation and dissipation of internal waves generated by geostrophic motions impinging on small-scale topography: application to the Southern Ocean. Journal of Physical Oceanography 40, 2025–2042.
Olbers, D.J., Wenzel, M., Willebrand, J., 1985. The inference of North Atlantic circulation patterns from climatological hydrographic data. Reviews of Geophysics 23, 313–356.
Olbers, D.J., Willebrand, J., Eden, C., 2012. Ocean Dynamics, first ed. Springer, Berlin, Germany.
Polzin, K.L., Toole, J.M., Ledwell, J.R., Schmitt, R.W., 1997. Spatial variability of turbulent mixing in the abyssal ocean. Science 276, 93–96.
Ponte, R.M., 1999. A preliminary model study of the large-scale seasonal cycle in bottom pressure over the global ocean. Journal of Geophysical Research 104, 1289–1300.
Redi, M.H., 1982. Oceanic isopycnal mixing by coordinate rotation. Journal of Physical Oceanography 12, 1154–1158.
Schmitt, R.W., 1994. Double diffusion in oceanography. Annual Review of Fluid Mechanics 26, 255–285.
Simmons, H.L., Jayne, S.R., St.Laurent, L.C., Weaver, A.J., 2004. Tidally driven mixing in a numerical model of the ocean general circulation. Ocean Modelling 6, 245–263.
Solomon, H., 1971. On the representation of isentropic mixing in ocean models. Journal of Physical Oceanography 1, 233–234.
Stacey, M.W., Pond, S., Nowak, Z.P., 1995. A numerical model of the circulation in Knight Inlet, British Columbia, Canada. Journal of Physical Oceanography 25, 1037–1062.
Stammer, D., 2008. Response of the global ocean to Greenland and Antarctic ice melting. Journal of Geophysical Research 113. http://dx.doi.org/10.1029/2006JC004079.
Starr, V.P., 1945. A quasi-Lagrangian system of hydrodynamical equations. Journal of Meteorology 2, 227–237.
Stouffer, R.J., 2004. Time scales of climate response. Journal of Climate 17, 209–217.
Sweeney, C., Gnanadesikan, A., Griffies, S.M., Harrison, M., Rosati, A., Samuels, B., 2005. Impacts of shortwave penetration depth on large-scale ocean circulation and heat transport. Journal of Physical Oceanography 35, 1103–1119.
Treguier, A.M., 1992. Kinetic energy analysis of an eddy resolving, primitive equation model of the North Atlantic. Journal of Geophysical Research 97, 687–701.
Treguier, A.M., Held, I.M., Larichev, V.D., 1997. On the parameterization of quasi-geostrophic eddies in primitive equation ocean models. Journal of Physical Oceanography 27, 567–580.
Trenberth, K.E., 2009. An imperative for climate chnage planning: tracking Earths global energy. Current Opinion in Environmental Sustainability 1, 19–27.
Yin, J., Griffies, S.M., Stouffer, R., 2010. Spatial variability of sea-level rise in 21st century projections. Journal of Climate 23, 4585–4607.
Yin, J., Schlesinger, M., Stouffer, R., 2009. Model projections of rapid sea-level rise on the northeast coast of the United States. Nature Geosciences 2, 262–266.
Young, W.R., 2012. An exact thickness-weighted average formulation of the Boussinesq equations. Journal of Physical Oceanography. http://dx.doi.org/10.1175/JPO-D-11-0102.1.